DFT Benchmarking Studies for Uranium Compounds

by

Xiaobin Zhang

A Thesis submitted to the Faculty of Graduate Studies of

The University of Manitoba

in partial fulfilment of the requirements of the degree of

MASTER OF SCIENCE

Department of Chemistry

University of Manitoba

Winnipeg, Canada

Table of Contents

List of Figures

List of Tables

List of Abbreviations

ADF	Amsterdam Density Functional
CCSD(T)	Coupled Cluster Singles and Doubles with Perturbative Triples
COSMO	Conductor -Like Screening Model
C-PCM	Conductor-Like Polarizable Continuum Model
DFT	Density Functional Theory
D-PCM	Dielectric Polarizable Continuum Model
ECP	Effective Core Potentials
ESI-MS	Electron Spray Ionization-Mass Spectrometry
EXAFS	Extended X-ray Absorption Fine Structure
GGA	Generalized Gradient Approximations
GTOs	Gaussian Type Orbitals
HF	Hartree-Fock
HFX	Hartree-Fock Exchange
HZDR	Helmholtz-Zentrum Dresden-Rossendorf
IR	Infra-Red
KS	Kohn-Sham
LCAO	Linear Combination of Atomic Orbitals
LC-ECP	Large Core Effective Core Potentials
LSD	Local Spin-Density
LDA	Local Density Approximation
LUMO	Lowest Occupied Molecular Orbitals
MAE	Mean Absolute Errors
MO	Molecular Orbital
MP2	Møller-Plesset Perturbation Theory of the 2nd Order
MSE	Mean Signed Errors
NOM	Natural Organic Matter
NMR	Nuclear Magnetic Resonance
PCM	Polarizable Continuum Model
QC	Quantum-Chemical Calculations
RECP	Relativistic Effective Core Potentials
RRT	Round-Robin Test
SC-ECP	Small-Core Effective Core Potentials
SDD	Stuttgart-Dresden
STOs	Slater Type Orbitals
TMS	Tetramethylsilane
TRLFS	Time-Resolved Laser Fluorescence Spectroscopy
UV−vis	Ultraviolet−Visible Absorption
WFT	Wave Function Theory

XAS	X-ray Absorption Structure
XC	Exchange Correlation
ZORA	Zeroth Order Regular Approximation

Abstract

Density Functional Theory (DFT) is the most widely used theoretical tool for studying actinide complexes amongst the many available computational methods. However, the best choice of functional for theoretical actinide science is still not completely clear. Thus, benchmarking studies have been performed in this thesis in order to evaluate the performance of modern DFT applied to actinide systems.

The first chapter is an introductory chapter which gives the background and the methods applied in this thesis. The second chapter is a part of the actinide spectroscopy Round-Robin test (RRT). The performance of DFT using different quantum chemistry programs with identical DFT functionals has been investigated by studying five U(VI) acetate complexes. The experimental data from the other clusters of RRT are used as reference for the quantum chemical calculations. The performance of a total of 22 different DFT functionals for small uranium complexes has been further investigated in Chapter 3. These functionals are compared by calculating geometries, vibrations frequencies, and reaction enthalpies against experimental data and high level *ab initio* CCSD(T) calculations. The last chapter presents a summary of the works in this thesis as well as directions for future studies.

Acknowledgements

I would first like to express my sincere gratitude to my supervisor, Dr Georg Schreckenbach, for the opportunity to work in his group and the continuous support of my Master's study and related research. I could not have imagined finishing this thesis without his patience, encouragement, and immense knowledge. Besides my advisor, I would like to thank the rest of members of my advisory committee, Dr. Mario Bieringer and Dr. Rebecca Davis, for their help, advice, criticism and support during the work towards this degree. I am also grateful to Dr. Johan van Lierop, Department of Physics, for willing to be the member of my thesis committee.

I would like to thank Dr. Satoru Tsushima, Dr. Ping Yang, and the rest of the coworkers in the Round-Robin test of actinide spectroscopy project. My sincere thanks also goes to Dr. Samuel Odoh, the former member of the Schreckenbach group, for his help and contributions to Chapter 3 in this thesis.

I thank my fellow labmates, Jeffery Perkins and Craig Peeples, for the stimulating discussions. Also I thank Dr. Grigory Shamov, another former member of the Schreckenbach group, for his invaluable technical support.

Finally, I would like to thank my parents, Yingui Zhang and Liqin Zhang. Without the unfailing support and continuous encouragement from them, it would be impossible to complete this thesis.

Chapter 1 : Introduction

1.1. History and Applications of Uranium

Uranium and thorium are the only two of the actinides that can be found in nature. Humanity's use of uranium compounds as colorants can be traced back to Roman times. [1] However the first time that uranium was discovered as a chemical element was in 1789 by Martin Heinrich Klaproth. He named this new element after the planet Uranus.[2] Uranium was used as a colorant for ceramics and glasses[3] after its discovery for a century until Henri Becquerel discovered that uranium emitted penetrating rays in 1896. Then Becquerel proved that these penetrating rays could discharge an electroscope. Just shortly after his discovery, Marie Curie and her husband Pierre found and named two elements, polonium and radium, in the uranium ore at trace levels. They described this new property as radioactivity.[4] In late 1938, Hahn and Strassmann discovered nuclear fission.[5] As a result, uranium plays a crucial role in the nuclear energy area. The most important isotope of uranium is ^{235}U because it can induce a chain reaction with slow neutrons. An advantage of using ^{235}U as fission fuel is that not only can it generate considerable nuclear power but it can also generate other important actinide elements by radioactive decay. The first commercial nuclear power plant has been established in the 1950s. As of January 2016,[6] there are about 440 commercial nuclear power reactors operable in 31 countries, and about 65 more are under construction. Furthermore, there are about 140 ships and submarines using nuclear power. These nuclear power stations generate 11% of the world's electricity, which is a clean energy. To study the properties of uranium and other actinides, there are 240 research reactors that have been built in 56 countries. However, after the Fukushima nuclear accident in Japan in 2011, the usage of nuclear power is encountering great resistance.

The radiation from uranium and its decay productions can result in mutation, radiation sickness, cancer, and even death. Besides radioactivity, uranium and its decay products are also very toxic. Moreover, many actinides have very long half-life, for example the half-life of ^{235}U is 703,800,000 years.[7] Thus, whether we continue or stop using nuclear power, we have to face the problem of nuclear waste.[8]

Actinides have various oxidation states. For uranium, in natural environments, the most important oxidation states are 4+ and 6+.[9] The tetravalent uranium compounds are insoluble from mildly acidic to alkaline conditions. On the other hand, the 6+ uranium compounds, usually containing the linear uranyl moiety [UO_2^{2+} or $(O=U=O)^{2+}$], are highly soluble and mobile.[10] In solution, UO_2^{2+} not only forms soluble complexes with inorganics such as carbonate, oxalate and hydroxide etc., but also can react with organic matter.[4] When an effective reductant is present, U(VI) can be reduced to U(IV). The reductants can be H_2S, fossil plants, methane or transported humic material. Better understanding of these uranium oxides can help us to control nuclear pollution in natural environments. Uranium halides comprise one of the most popular research topics in uranium chemistry because they have a wide range of applications in uranium industries. For example, uranium tetrafluoride can be used as molten-salt reactor fuel or for the preparation of enriched uranium metal; uranium hexafluoride is used for centrifuge separations in uranium enrichment. Although the data of uranium complexes are relatively rare, the uranium halides are the one actinide molecule series most studied both experimentally and theoretically.[11—20] These well-established experimental data give us a good data set for theoretical benchmarking studies.

Because of the toxicity and radioactivity of uranium and related compounds, the laboratories that want to investigate them experimentally need to follow strict procedures. This

usually requires special equipment and protections. By contrast, computational studies are a relatively cheap and safe tool. They are easy to perform and can be applied to systems even without available experimental data. What is more, computational calculations can give us the chance to better understand the properties of these uranium compounds on the atomic level.

1.2. The Schrödinger Equation and Approximation Methods

1.2.1. Schrödinger Equation.

The fundamental goal of quantum chemistry is to solve the Schrödinger Equation[21]. Wave functions are the solutions to the Schrödinger Equation. They are descriptions of the quantum states of a system in quantum mechanics.

The non-relativistic wave function evolves in time, for example in an excited state, according to the time-dependent Schrödinger Equation.

$$\hat{\mathrm{H}}\psi(x,t) = i\hbar\frac{\partial\psi}{\partial t} \qquad (1.1)$$

Where i is the imaginary unit, $\hbar$ is the Planck constant divided by 2π, the symbol ∂/∂t indicates a partial derivative with respect to time t, Ψ is the wave function of the quantum system, and $\hat{\mathrm{H}}$ is the Hamiltonian operator.

The wave functions, which form standing waves known as stationary states such as atomic orbitals or molecular orbitals, can be determined by the time-independent Schrödinger Equation.

$$\hat{\mathrm{H}}\psi = E\psi \qquad (1.2)$$

Where $\hat{\mathrm{H}}$ is Hamiltonian operator, Ψ is a certain wave function, and E is the energy of the state Ψ.

There are five contributions to the Hamiltonian of a molecular system:

$$\hat{\mathrm{H}} = -\sum \frac{\hbar^2}{2m_e}\nabla_i^2 - \sum_k \frac{\hbar^2}{2m_k}\nabla_k^2 - \sum_i \sum_k \frac{e^2 Z_k}{r_{ik}} + \sum_{i<j} \frac{e^2}{r_{ij}} + \sum_{k<l} \frac{e^2 Z_k Z_l}{r_{kl}} \qquad (1.3)$$

Where *i* and *j* run over electrons, *k* and *l* run over nuclei, m_e is the mass of electron, m_k is the mass of nucleus *k*, ∇^2 is the Laplacian operator, *e* is the charge on the electron, *Z* is the atomic number, and r_{ab} is the distance between particles *a* and *b*. The first term in Eq. 1.3 is the kinetic energy operator for each electron in the system. The second term is the kinetic energy operator for each nucleus in the system. The third term is the total electron-nucleus Coulombic attraction in the molecule. The fourth term is the potential energy from Coulombic electron-electron repulsions. The last term is the potential energy of Coulombic nuclei-nuclei repulsions.

1.2.2. Born-Oppenheimer approximation[22]

For many-particle molecular systems, it is extremely difficult to solve the Schrödinger Equation to determine the accurate wave functions due to the correlated motions of particles. In order to simplify this problem, we can include the Born-Oppenheimer approximation which assumes that the motion of atomic nuclei and electrons in a molecule can be separated because the nuclei of the molecular systems are moving much slower than the electrons. The resulting electronic Schrödinger Equation is:

$$(\hat{H}_{el} + \hat{V}_N)\psi_{el}(q_i; q_k) = E_{el}\psi_{el}(q_i; q_k) \qquad (1.4)$$

Where the subscript '*el*' emphasizes the invocation of the Born-Oppenheimer approximation. H_{el} includes the first, third, and fourth terms of Equation 1.3, V_N is the nuclear-nuclear repulsion energy which is the last term in Equation 1.3, q_i are independent variables (electronic coordinates), and q_k are parameters (nuclear coordinates). Because of the Born-Oppenheimer approximation, V_N is a constant that represents a given set of fixed nuclear coordinates q_k. So when solving Equation 1.4 the V_N term can always be ignored. Generally speaking, the Born-

Oppenheimer approximation can be very accurate in most cases and significantly improves computational efficiency. However, the Born-Oppenheimer approximation becomes problematic near Level Crossings.[23] Moreover, Waschewsky et al.[24] proved that in the class of reactions known as Woodward-Hoffmann forbidden reactions, the Born-Oppenheimer approximation fails and can result in a marked reduction in the reaction rate.

The Schrödinger Equation cannot be solved exactly except for a hydrogen atom and H_2^+ cation. In order to solve Equation 1.4, there are two principal approximation methods in quantum chemistry: variational method and perturbation theory.

1.2.3. Variational Method[25]

Assuming that we are solving for a ground-state wave function ψ_{el} and energy E_{el} which satisfy the Schrödinger Equation including Born-Oppenheimer approximation:

$$\hat{H}_{el}\psi_{el} = E_{el}\psi_{el} \qquad (1.5)$$

Then multiply Equation 1.5 from the left by ψ_{el}^* and integrate over all space:

$$E_{el} = \frac{\int \psi_{el}^* \hat{H}_{el}\psi_{el} d\tau}{\int \psi_{el}^* \psi_{el} d\tau} = \frac{<\psi_{el}|\hat{H}_{el}|\psi_{el}>}{<\psi_{el}|\psi_{el}>} \qquad (1.6)$$

Where $d\tau$ is the appropriate volume element.

If we substitute any other function ϕ instead of ψ_{el}:

$$E_{\varphi} = \frac{\int \phi^* \hat{H} \phi d\tau}{\int \phi^* \phi d\tau} = \frac{<\phi|\hat{H}|\phi>}{<\phi|\phi>} \qquad (1.7)$$

The ground-state energy E_{el} will be smaller than E_ϕ. This is the variational principle:

$$E_{el} \leq E_{\phi} \qquad (1.8)$$

Then we can use any trial function to calculate an upper bound to E_0. If we choose a trial function with some arbitrary variational parameters, such as α, β, γ …:

$$E_{el} \leq E_{\phi}(\alpha, \beta, \gamma, \ldots) \qquad (1.9)$$

Then we can optimize these parameters to approach the exact ground-state energy E_0.

1.2.4. Perturbation Theory.[26]

Suppose we are solving the Schrödinger Equation using perturbation theory. We can rewrite the Hamiltonian operator as the sum of the unperturbed Hamiltonian operator and a perturbation:

$$\hat{H} = \hat{H}^{(0)} + \hat{H}^{(1)} \qquad (1.10)$$

This approximation can describe a complex system by starting with a simple system which is known ($\hat{H}^{(0)}$); then add an additional perturbation Hamiltonian for the weak disturbances if the disturbances are not too large.

Take the one-dimensional anharmonic oscillator as an example

$$\hat{H} = -\frac{\hbar^2}{2m}\frac{d^2}{dx^2} + \frac{1}{2}kx^2 + cx^3 + dx^4 \qquad (1.11)$$

The Hamiltonian 1.11 is related to the Hamiltonian of the harmonic oscillator

$$\hat{H}^0 = -\frac{\hbar^2}{2m}\frac{d^2}{dx^2} + \frac{1}{2}kx^2 \qquad (1.12)$$

If the constants c and d in Hamiltonian 1.11 are small, then the eigenfunctions and eigenvalues of the anharmonic oscillator are expected to be closely related to those of the harmonic oscillator. Thus, the system with $\hat{H}^0$ is the unperturbed system and the system with $\hat{H}$ is the perturbed system. The difference between these two Hamiltonians is the perturbation $\hat{H}^{(0)}$. Thus we got Equation 1.10, where $\hat{H}^{(1)} = cx^3 + dx^4$.

For a nondegenerate system, the first-order energy correction is given by

$$E_n^{(1)} = \left\langle \psi_n^{(0)} \middle| \hat{H}' \middle| \psi_n^{(0)} \right\rangle = \int \psi_n^{(0)*} \hat{H}' \psi_n^{(0)} d\tau \qquad (1.13)$$

The ground state wave function for the harmonic oscillator is

$$\psi_0^{(0)} = \left(\frac{\alpha}{\pi}\right)^{\frac{1}{4}} e^{-\frac{\alpha x^2}{2}} \qquad (1.14)$$

Thus, the first-order energy correction for the ground state of anharmonic oscillator is

$$E_0^{(1)} = \left\langle \psi_0^{(0)} \middle| cx^3 + dx^4 \middle| \psi_0^{(0)} \right\rangle = \left(\frac{\alpha}{\pi}\right)^{\frac{1}{2}} \int_{-\infty}^{+\infty} e^{-\alpha x^2} (cx^3 + dx^4) dx = \frac{3d}{4\alpha^2} = \frac{3dh^2}{64\pi^4 \nu^2 m^2} \qquad (1.15)$$

where $\alpha \equiv 2\pi\nu m/\hbar = 4\pi^2 \nu m/h$ for the oscillator, m is the particle's mass, and ν is the angular frequency of the oscillator. Higher order corrections can be calculated in a similar fashion.

1.2.5. Approximations for Calculating Vibrational Frequencies

Quantum chemistry calculations usually overestimate vibrational frequencies compared to the experimental fundamental frequencies. Thus the calculated vibrational frequencies are often multiplied by a scale factor which is typically in the range from 0.8 to 1.0.[27] These differences are due to three factors: [28] 1) The overall neglect of the effect of anharmonicity. 2) Using incomplete basis sets. 3) The approximations of the method used to solve the Schrödinger equation.

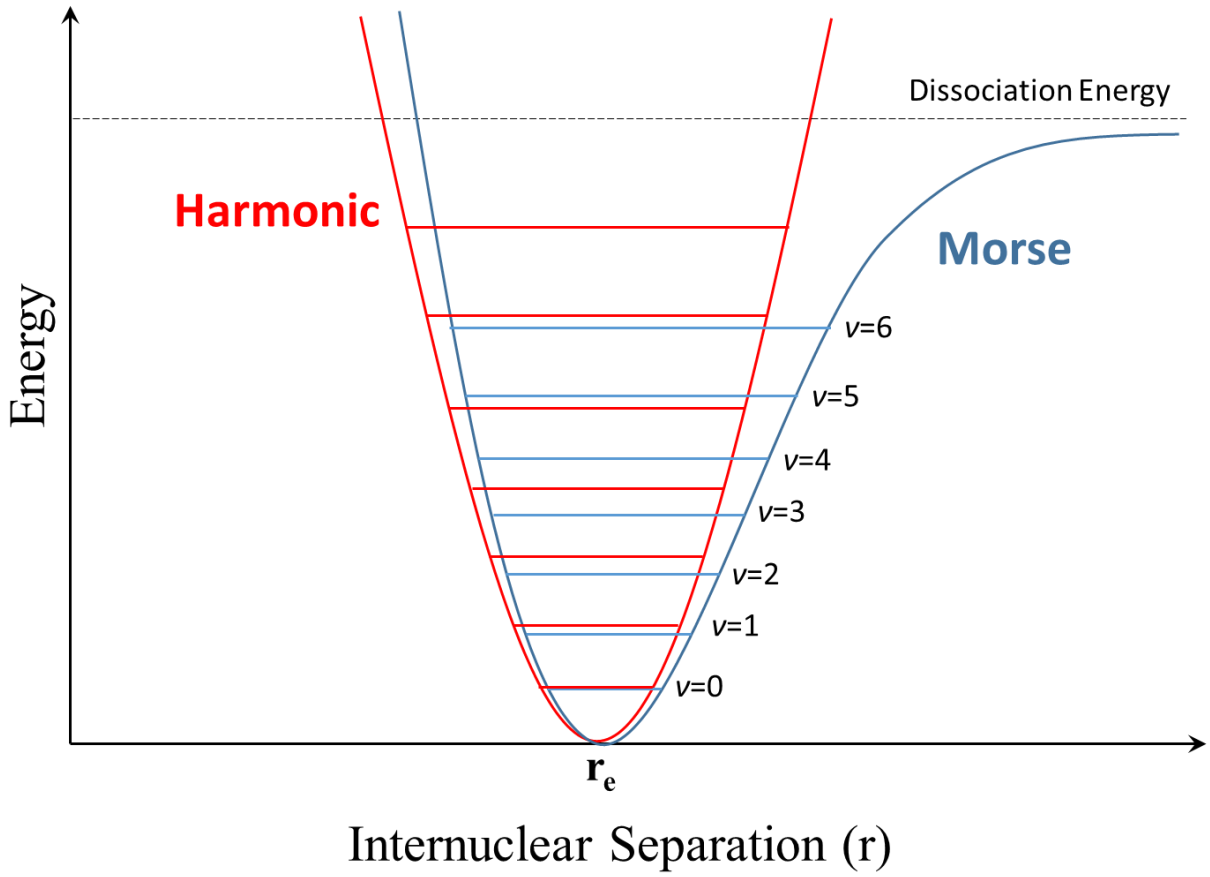

Figure 1.1 A comparison of harmonic oscillator potential (red) and Morse potential (blue).

The vibrational frequencies predict by quantum-chemical programs usually apply the harmonic approximation. However, the real potential energy surface is not harmonic. **Figure 1.1** illustrates the internuclear potential for a diatomic molecule. The harmonic oscillator potential is

a good approximation near the region of the bottom, which is the minimum. In experiment, especially for polyatomic molecules, usually only the fundamental frequencies, which are the transitions from v=0 to v=1, are measured. Thus, there are differences between harmonic oscillator approximation and real potential energy surface. The second factor arises when calculating the real chemical systems, which have large number of atoms, not only because the number of basis functions increases rapidly with the size of the molecules, but also the cost of computations with electron correlation will rise very quickly when the molecular size becomes larger. These prevent the application of advanced theoretical treatments for large systems and bring errors to the calculated vibrational frequencies. The third factor comes from the approximation of the method to the Schrödinger equation. For DFT, this usually comes from the approximate exchange-correlation functional.

1.3. Electronic Basis Sets

A basis set is the set of mathematical functions which are used to construct a wave function. In Hartree-Fock (HF) theory, we can use a linear combination of basis set functions to express the molecular orbitals. When we use a complete basis set the HF limit has been reached. However, using an infinite basis set is impossible. So it is very important to balance efficiency and accuracy of the calculations when choosing a basis set.

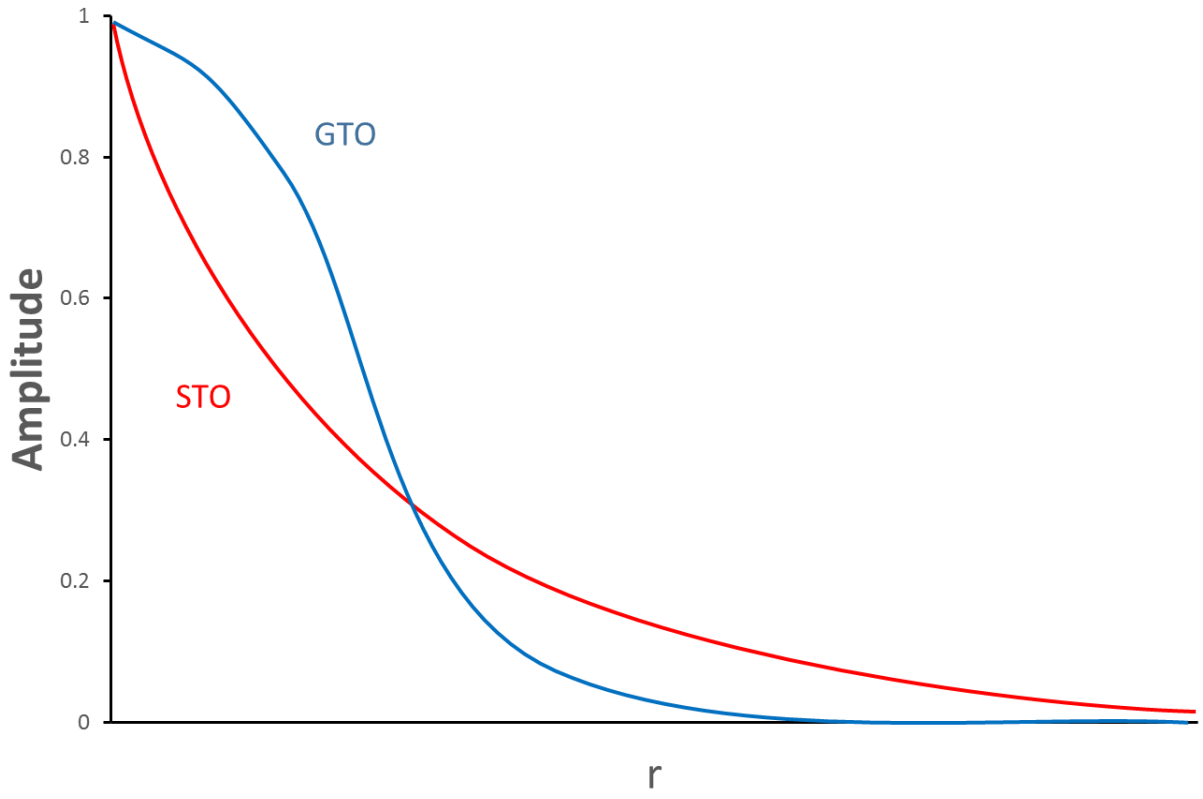

Figure 1.2 Behavior of e^x where x = r (Red line, STO) and x = r^2 (Blue line, GTO)

There are two principal types of basis functions that are used in modern quantum chemistry. One is Slater-type orbitals (STOs), another one is Gaussian-type orbitals (GTOs). STOs use the exponentially decaying electronic distribution ($e^{-\xi r}$) of the hydrogen atom:

$$\varphi(r,\theta,\varphi;\ \xi,n,l,m) = \frac{(2\xi)^{n+\frac{1}{2}}}{[(2n)!]^{\frac{1}{2}}} r^{n-1} e^{-\xi r} Y_l^m(\theta,\varphi) \qquad (1.16)$$

Where ξ is an exponent that can be chosen according to a simple set of rules developed by Slater,[29] n is the principal quantum number for the orbital, Y^l_m (θ,φ) is a spherical harmonic function where l and m are angular momentum quantum numbers. As **Figure 1.2** shows, STOs can correctly describe the cusp at the nucleus.

A disadvantage of STOs is the fact that most of the required integrals of the STOs which are needed in the SCF procedure have to be calculated numerically, and this reduces the speed of computations. Thus, in 1950, Boys[30] suggested to change the radial decay of the STOs from e^{-r} to e^{-r^2}. In this way, the Atomic-Orbital-like basis function takes on the form of a Gaussian function:

$$\varphi(\mathrm{x,y,z};\alpha,\mathrm{i,j,k}) = (\frac{2\alpha}{\pi})^{3/4}[\frac{(8\alpha)^{i+j+k} i!\,j!\,k!}{(2i)!(2j)!(2k)!}]^{1/2} x^i y^j z^k e^{-\alpha(x^2+y^2+z^2)} \qquad (1.17)$$

Where α is an exponent controlling the width of the GTO; i, j and k are non-negative integers which define the nature of the orbital in a Cartesian sense.

The reason for using GTOs is the so called 'Gaussian Product Theorem'. This theorem guarantees that the product of two GTOs centered on two different atoms can be present as a finite sum of Gaussians centered on a point along the line across these two atoms. Thus, four-center integrals can be reduced to the finite sums of two-center integrals. Then these two-center integrals can be further reduced to one-center integrals. In this way, using GTOs will be much faster than using STOs. However, GTOs give the wrong cusp and decay much faster than STOs in the long range, as **Figure 1.2** shows.

In order to combine the computational efficiency of GTOs and the proper "shape" of STOs, we can use several GTOs within one basis function to approximate GTOs, as so-called contracted Gaussian functions: [31]

$$\Phi(x,y,z;\{\alpha\},I,j,k) = \sum_{a=1}^{M} c_a \phi(x,y,z;\alpha_a,i,j,k) \qquad (1.18)$$

Where M is the number of Gaussians in the linear combination. The shape of the basis function is controlled by the coefficients c_a. Nowadays, most quantum chemistry programs use GTOs, just a few are still using STOs, such as ADF[32].

1.4. The Hartree-Fock Method[33,34] and Post Hartree-Fock Approaches

The Hartree-Fock (HF) method is a milestone in modern quantum chemistry because it is the first approximation for all atomic and molecular calculations. In the Hartree-Fock method, MOs can be determined as eigenfunctions of a set of one-electron operators individually. However, each electron can be treated as moving in the static field of all the other electrons which includes exchange effects on the Coulomb repulsion.

After applying the Born-Oppenheimer approximation, for a system with 2N electrons and M nuclei Equation 1.3 can be written as

$$\widehat{H}_{el} = -\frac{1}{2}\sum_{i=1}^{2N} \nabla_i^2 - \sum_{i=1}^{2N}\sum_{A=1}^{M} \frac{Z_A}{r_{iA}} + \sum_{i=1}^{2N}\sum_{j>i} \frac{1}{r_{ij}} + \sum_{A}^{M}\sum_{B<A}^{M} \frac{Z_A Z_B}{R_{AB}} \qquad (1.19)$$

Where the four terms represent the kinetic energy of the electrons, the interaction of each electron with each nucleus, electron-electron interactions, and inter-nuclear interactions, respectively. Note that now Equation 1.19 uses atomic units.

The Hartree-Fock wave function can be given by the Slater determinant

$$\psi(1,2,\dots,2\mathrm{N}) = \frac{1}{\sqrt{(2N)!}} \begin{vmatrix} \psi_1\alpha(1) & \psi_1\beta(1) & \cdots & \psi_N\alpha(1) & \psi_N\beta(1) \\ \psi_1\alpha(2) & \psi_1\beta(2) & \cdots & \psi_N\alpha(2) & \psi_N\beta(2) \\ \vdots & \vdots & \ddots & \vdots & \vdots \\ \psi_1\alpha(2\mathrm{N}) & \psi_1\beta(2\mathrm{N}) & \cdots & \psi_N\alpha(2\mathrm{N}) & \psi_N\beta(2\mathrm{N}) \end{vmatrix} \qquad (1.20)$$

The energy is

$$E_{el} = \langle \psi^*(1,2,\ldots,2N) | \widehat{H} | \psi(1,2,\ldots,2N) \rangle \quad (1.21)$$

The Equation 1.21 can be rewritten as

$$E_{el} = 2\sum_{j=1}^{N} I_j + \sum_{i=1}^{N}\sum_{j=1}^{N}(2J_{ij} - K_{ij}) \quad (1.22)$$

Where

$$I_j = \int d\, r_j \psi_j^*(r_j)(-\tfrac{1}{2}\nabla_j^2 - \sum_N^M \tfrac{Z_A}{r_{jA}})\psi_j(r_j) \quad (1.23)$$

$$J_{ij} = \int\int d\, r_1 d\, r_2 \psi_i^*(r_1)\psi_j^*(r_2)\tfrac{1}{r_{12}}\psi_i(r_1)\psi_j(r_2) \quad (1.24)$$

$$K_{ij} = \int\int d\, r_1 d\, r_2 \psi_i^*(r_1)\psi_j^*(r_2)\tfrac{1}{r_{12}}\psi_i(r_2)\psi_j(r_1) \quad (1.25)$$

After applying the variational principle to Equation 1.22, the spatial orbitals that minimize the energy E satisfy the equations

$$\hat{F}(r_1)\psi_i(r_1) = \varepsilon_i\psi_i(r_1) \qquad i = 1,2,\ldots,N \quad (1.26)$$

Where $\hat{F}(r_1)$is the Fock operator

$$\hat{F}(r_1) = \hat{f}(r_1) + \sum_{j=1}^{N}[2\hat{J}_j(r_1) - \hat{K}_j(r_1)] \quad (1.27)$$

Where

$$\hat{f}(r_1) = -\tfrac{1}{2}\nabla_1^2 - \sum_A \tfrac{Z_A}{r_{1A}} \quad (1.28)$$

$\hat{J}_j(r_1)$ is the Coulomb operator

$$\hat{J}_j(r_1)\psi_i(r_1) = \psi_i(r_1)\int d\, r_2 \psi_j^*(r_2)\tfrac{1}{r_{12}}\psi_j(r_2) \quad (1.29)$$

$\widehat{K}_j(r_1)$ is the exchange operator

$$\hat{K}_j(r_1)\psi_i(r_1) = \psi_j(r_1)\int d\, r_2 \psi_j^*(r_2)\frac{1}{r_{12}}\psi_i(r_2) \qquad (1.30)$$

An expression for the energy of the i^{th} molecular orbital can be obtain by multiplying Equation 1.30 from the left by $\psi_i^*(r_1)$ and integrating over r_1

$$\varepsilon_i = \int dr_1\, \psi_i^*(r_1)\hat{F}(r_1)\psi_i(r_1) \qquad (1.31)$$

Using the Fock operator, Equation 1.31 becomes

$$\varepsilon_i = I_j \sum_{j=1}^{N}(2J_{ij} - K_{ij}) \qquad (1.32)$$

Comparing with 1.22, we get

$$E = \sum_{i=1}^{N}(I_i + \varepsilon_i) \qquad (1.33)$$

Clemens Roothaan[35] expressed the molecular orbitals as linear combinations of basis functions

$$\psi = \sum_{v=1}^{K} c_v \phi_v \qquad (1.34)$$

Thus, the Hartree-Fock-Roothaan Equations are

$$\sum_v F_{\mu v} c_v = \varepsilon \sum_v S_{\mu v} c_v \qquad \mu = 1,2,\ldots,K \qquad (1.35)$$

Where $F_{\mu v}$ is the Fock matrix Clements

$$F_{\mu v} = \int dr_1 \phi_\mu^*(r_1)\hat{F}(r_1)\phi_v(r_1) \qquad (1.36)$$

And $S_{\mu v}$ is the overlap matrix elements

$$S_{\mu v} = \int dr_1 \phi_\mu^*(r_1)\phi_v(r_1) \qquad (1.37)$$

The set of algebraic equations for the c_v in Equation 1.35 are the Hartree–Fock–Roothaan equations. We can further write them in matrix notation

$$\mathrm{Fc} = \varepsilon \mathrm{Sc} \qquad (1.38)$$

Where F and S are K × K matrices and c is a K × 1 column vector. This equation can be solved through a self-consistent procedure known as the SCF.[25]

In spite of many successes of the HF method, there are two deficiencies of it because HF uses a single Slater determinant to describe the system, Equation 1.20. These deficiencies are the so-called non-dynamical and dynamical electron correlation, respectively.

$$E_{correlation} = E_0 - E_{HF} = E_{non-dynamical\ correlation} + E_{dynamical\ correlation} \quad (1.39)$$

Where $E_{correlation}$ is the correlation energy as the difference between the ground state electronic energy and the HF energy, $E_{non-dynamical\ correlation}$ is the non-dynamical correlation, and $E_{dynamical\ correlation}$ is the dynamical correlation.

The contributions of electron correlation are relative small (~1%) compared to the total energy. However they will induce large errors in property calculations and reaction energies. There are various approaches to improve upon the HF method, the so-called post Hartree-Fock approaches. Of those, only second-order Møller-Plesset perturbation theory (MP2)[36,37] and the coupled cluster singles and doubles and perturbatively included triples [CCSD(T)][38,39] methods are employed in this work.

1.5. Density Functional Theory

Kohn-Sham spin-density functional theory (DFT) is the most popular method both in quantum chemistry and condensed matter physics, not only because of its accuracy, but also its efficiency. An electron density depending on only three spatial coordinates. By contrast, the many-body problem of N electrons depend on 3N spatial coordinates. Thus, DFT is much faster than the HF and especially post-HF methods. The Thomas-Fermi model[40] and Slater's X_α exchange functional[41,42]are the predecessors of modern Density Functional Theory. There are two fundamental Hohenberg-Kohn theorems[43] which are the foundation stones of modern density functional theory. The first one states that the external potential V(r) is a unique functional of the electron density ρ(r). The second Hohenberg-Kohn theorem states that the ground state energy can be obtained variationally, which means that the density that minimizes the total energy is the exact ground state density. The Kohn-Sham equations are:

$$\widehat{H}_{ks}\phi_i \equiv \left[-\frac{1}{2}\nabla^2 + V_{\text{eff}}(r)\right]\phi_i(r) = \varepsilon_i\phi_i(r) \qquad (1.40)$$

Where $\{\phi_i\}$ are the Kohn-Sham one-electron orbitals. Thus, the electron density is

$$\rho(r) = \sum_{i=1}^{N}|\phi_i|^2 \qquad (1.41)$$

$V_{\text{eff}}(r)$ is effective potential

$$V_{\text{eff}}(r) = V(r) + \int \frac{\rho(r\prime)}{|r-r\prime|}dr' + V_{xc}(r) \qquad (1.42)$$

Where $V(r)$ is external potential, $\rho(r')$ is electron density, and $V_{xc}(r)$ is the exchange-correlation potential defined as

$$V_{xc}(r) = \frac{\delta E_{xc}[\rho]}{\delta\rho(r)} \qquad (1.43)$$

The problem of DFT is that the exact exchange-correlation energy functional is unknown. However, different approximations have been developed in order to overcome this problem. These include:

1) The local spin-density (LSD) approximation

$$E_{xc}^{LSD}[n_\uparrow, n_\downarrow] = \int d^3r\, n\, \varepsilon_{xc}^{unif}(n_\uparrow, n_\downarrow) \quad (1.44)$$

Where $\varepsilon_{xc}^{unif}(n_\uparrow, n_\downarrow)$ is the exchange-correlation energy per particle of an electron gas with uniform spin densities $n_\uparrow$ and $n_\downarrow$.

2) Generalized gradient approximation (GGA)

$$E_{xc}^{GGA}[n_\uparrow, n_\downarrow] = \int d^3r\, n\, \varepsilon_{xc}^{GGA}(n_\uparrow, n_\downarrow, \nabla n_\uparrow, \nabla n_\downarrow) \quad (1.45)$$

Which introduces the density gradients $\nabla n_\uparrow$ and $\nabla n_\downarrow$.

3) Meta-GGA

$$E_{xc}^{MGGA}[n_\uparrow, n_\downarrow] = \int d^3r\, n\, \varepsilon_{xc}^{MGGA}(n_\uparrow, n_\downarrow, \nabla n_\uparrow, \nabla n_\downarrow, \nabla^2 n_\uparrow, \nabla^2 n_\downarrow, \tau_\uparrow, \tau_\downarrow) \quad (1.46)$$

Where $\nabla^2 n_\sigma(r)$ is the Laplacian of the density, and τ_σ is the so-called kinetic energy density:

$$\tau_\sigma(r) = \frac{1}{2}\sum_u^{occ.} |\nabla \varphi_{i\sigma}(r)|^2 \quad (1.47)$$

4) Hyper-GGAs which include the widely used hybrid functionals

$$E_{xc}^{HGGA}[n_\uparrow, n_\downarrow] = \int d^3r\, n\, \varepsilon_{xc}^{HGGA}(n_\uparrow, n_\downarrow, \nabla n_\uparrow, \nabla n_\downarrow, \nabla^2 n_\uparrow, \nabla^2 n_\downarrow, \tau_\uparrow, \tau_\downarrow, \varepsilon_{x\uparrow}, \varepsilon_{x\downarrow}) \quad (1.48)$$

Where ε_x is the exact exchange energy density

$$\varepsilon_{x\sigma}(r) = \frac{1}{2}\int d^3r' \frac{n_x^\sigma(r,r')}{|r'-r|} = -\frac{1}{2n_\sigma(r)}\int d^3r' \frac{\left|\sum_i^{occ.} \phi_{i\sigma}^*(r)\phi_{i\sigma}(r')\right|^2}{|r'-r|} \quad (1.49)$$

The functional including Hartree-Fock exchange is called hybrid GGA.

The fifth rung of the ladder **(Figure 1.3)** contains all the Kohn-Sham orbitals, both unoccupied and occupied. At this level, the adiabatic connection

$$E_{xc}[n_\uparrow, n_\downarrow] = \frac{1}{2}\int d^3r n(\boldsymbol{r}) \int d^3r' \int_0^1 d\lambda \frac{n_{xc}^{\lambda}([n_\uparrow, n_\downarrow]; \boldsymbol{r}, \boldsymbol{r'})}{|\boldsymbol{r'} - \boldsymbol{r}|} \quad (1.50)$$

leads to generalizations of the random phase approximation (RPA). Where $n(\boldsymbol{r})$ is the ground state density, $\lambda/|\mathbf{r'}\text{-}\mathbf{r}|$ is the strength of the electron-electron repulsions ($0 \leq \lambda \leq 1$), and $n_{xc}^{\lambda}([n_\uparrow, n_\downarrow]; \boldsymbol{r}, \boldsymbol{r'})$ is the density at **r'** of the exchange-correlation hole surrounding an electron at **r**,

$$n_{xc}^{\lambda} = n_x + n_c^{\lambda} \quad (1.51)$$

Where n_c is the correlation hole density and n_x is the exchange hole density which is independent of λ.

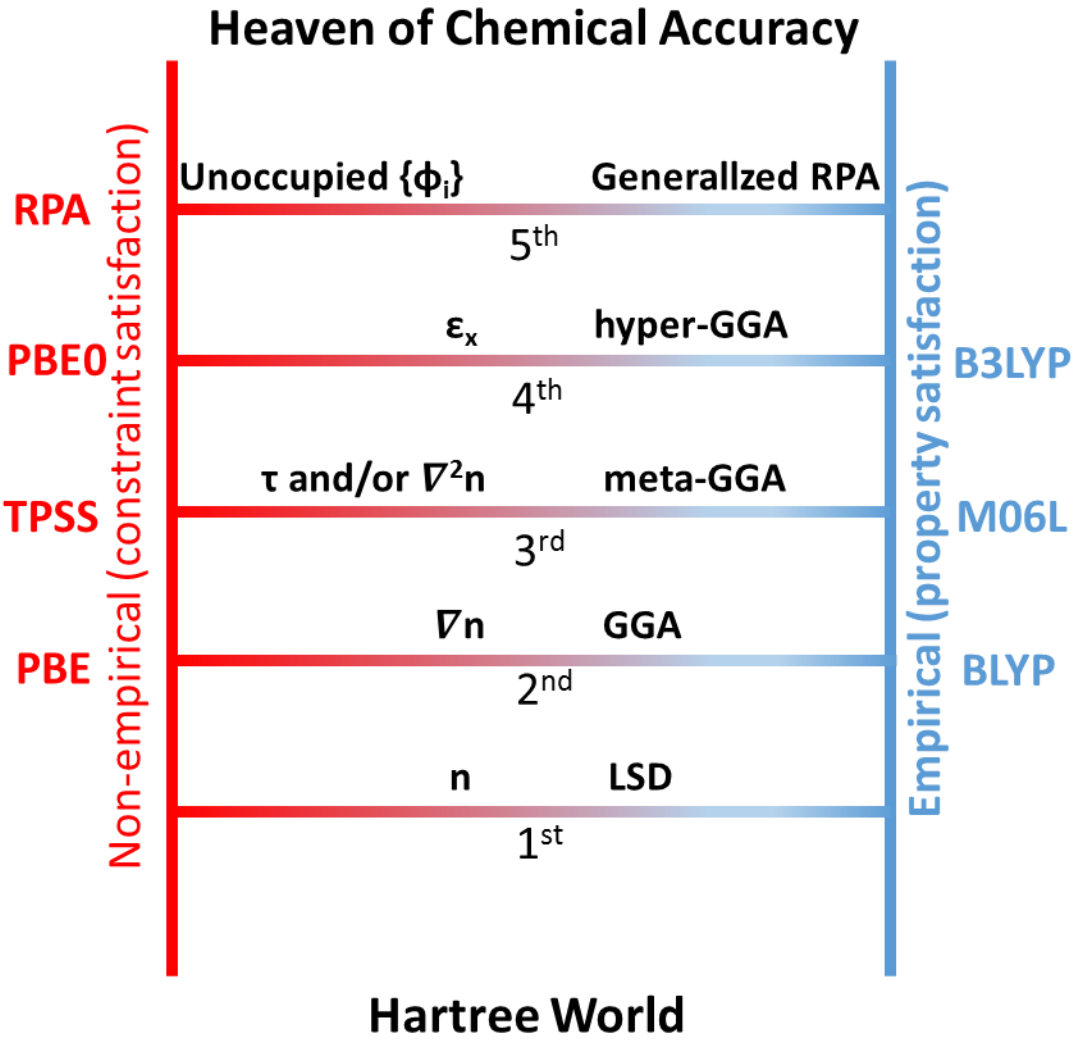

Figure 1.3 Jacob's ladder of density functional approximations to the exchange-correlation energy proposed by J. P. Perdew. Some examples of actual approximate XC functionals are included.

Figure 1.3 shows Jacob's ladder of DFT approximations.[44,45,46] Each rung in **Figure 1.3** incorporates the design elements from lower rungs. For example, PBE[47,48] and BLYP[49,50] are GGA functionals, TPSS[51] and M06L[52] are meta-GGA, and PBE0[53,54,55] and B3LYP[56,57] are hybrid functionals belonging to the class of hyper-GGA. The lower rungs may be not as accurate as the higher ones. On the other hand, they require less computation time and are easier to

understand. So the user should choose the appropriate approximation which can balance accuracy and efficiency.

1.6. Relativistic Effects

The Dirac Equation[58] was put forward in 1929. It is usually considered as giving the best description for relativistic effects on the electronic structure. The particles can have positive or negative energies in Dirac theory. In this thesis, only the positive states of the electrons are considered.

The four-component Dirac equation is given by:

$$\hat{H}_d \psi = E\psi \tag{1.52}$$

Where:

$$\hat{H}_d = c \cdot \alpha \cdot p + \beta c^2 + V \tag{1.53}$$

Where c is the speed of light, p is the momentum, V is the external potential, and α (x, y, z-components) and β are the 4 × 4 Dirac matrices:

$$\alpha = \begin{bmatrix} 0 & \sigma \\ \sigma & 0 \end{bmatrix} \tag{1.54}$$

$$\sigma_x = \begin{bmatrix} 0 & 1 \\ 1 & 0 \end{bmatrix}, \sigma_y = \begin{bmatrix} 0 & -i \\ i & 0 \end{bmatrix}, \sigma_z = \begin{bmatrix} 1 & 0 \\ 0 & -1 \end{bmatrix} \tag{1.55}$$

$$\beta = \begin{bmatrix} I & 0 \\ 0 & I \end{bmatrix} \tag{1.56}$$

Where *I* is the two-dimensional identity matrix and σ are the 2 × 2 Pauli spin matrices.

The equation contains large component ψ_L and small component ψ_s. ψ_L is much larger than ψ_s for positive energy states.

$$\psi = \begin{bmatrix} \psi_L \\ \psi_s \end{bmatrix} = \begin{bmatrix} \psi_L \uparrow \\ \psi_L \uparrow \\ \psi_S \downarrow \\ \psi_S \downarrow \end{bmatrix} \tag{1.57}$$

However, the regular four-component eigenvalue equation is not only computationally expensive but also has problems such as variational collapse. Even the non-regular two-component eigenvalue equation which is obtained by a transformation from the regular four-component eigenvalue equation turns out to be difficult to solve.

Many different approximations have been developed to overcome these problems. One of the popular approximations is the zeroth-order regular approximation (ZORA)[59,60]. As a two-component spinor approach for approximately solving the Dirac equation, ZORA is based upon regularizing the wave equation by ignoring the energy dependence of the effective mass of the electron.[61] Only the large components will be calculate in ZORA due to it being a two-component method.

The two-component ZORA equation is given by

$$\left[\frac{1}{2}(\sigma\cdot\hat{p})\kappa(\sigma\cdot\hat{p})+V\right]\psi_n=\varepsilon_n^Z\psi_n \tag{1.58}$$

With

$$\kappa=\frac{2c^2}{2c^2-V} \tag{1.59}$$

In Equation 1.58, ε_n^Z can be improved by scaling the ZORA energy.[62,63]

$$\varepsilon_i^{scaled}=\frac{\varepsilon_i^Z}{1+\langle\varphi_i|\sigma\cdot\hat{p}\frac{\kappa^2}{4c^2}\sigma\cdot\hat{p}|\varphi_i\rangle} \tag{1.60}$$

The total scaled ZORA energy at the DFT level can be written as

$$E_n^{scaled}=\sum_{i=1}^{N}[\langle\varphi_i\left|\sigma\cdot\hat{p}\frac{\kappa}{2}\sigma\cdot\hat{p}\right|\varphi_i\rangle-\varepsilon_i^{scaled}\langle\varphi_i\left|\sigma\cdot\hat{p}\frac{\kappa^2}{4c^2}\sigma\cdot\hat{p}\right|\varphi_i\rangle]$$
$$+E_{ne}+E_H+E_{xc}+E_{nn} \tag{1.61}$$

Where the summation adds up all the occupied orbitals. Equation 1.61 is identical to the non-relativistic total energy functional except for the kinetic energy contribution, which includes the ZORA correction.

The large number of electrons with significant correlations and relativistic effects make calculations challenging in heavy elements studies. One possible way to overcome these difficulties is using the effective core potential (ECP) approach. The idea of effective core potentials (ECPs) is replacing electrons in the inner shells by a suitably parametrized one-electron operator which acts on the remaining valence electrons and which also can include relativistic effects.[64] Take actinides for example, 'large-core' ECPs (LC-ECPs) include everything but the valence shell. Recently, 'small-core' ECP (SC-ECP), which only parameterize 60 electrons as core, have shown good agreement with experimental data such as geometries[65,66], frequencies[65, 66] , ligand NMR chemical shifts[67-69] and dissociation energies[70]. Shamov et al.[71,72] showed that the current SC-ECP is clearly superior to the older 'large core' ECP (LC-ECP) for geometries, frequencies, and reduction potentials.

1.7. Solvation Effects

The effect of solvent can be significant for actinide complexes, especially for spectra and reaction energies, due to the real environment in nature which is usually in solvent. For example, in aqueous solution, the meta-stable U(V) complexes can be oxidized, thus obstructing the isolation and characterization of them.[73-78]

Basically, there are two choices for describing the effect of the solvent environment, which are explicit and implicit/continuum solvation models. The former adds a number of solvent molecules around the solute molecule that one is interested in. The computational cost of the explicit approach will become extremely high when the size of the (super-)molecule is

increased due to the huge number of solvent molecules. On the other hand, after adding solvent molecules, the search for global minima becomes very difficult. A continuum model can be defined as a model with a number of the degrees of freedom of the constituent particles that are described in a continuous way, usually by a distribution function.[79] These models were originally developed by Born[80], Onsager[81], and Kirkwood[82] over 80 years ago. There are two widely used implicit models: the polarized continuum model (PCM)[83-87] and the conductor -like screening model (COSMO)[88-91]. In PCM models, the solvent is treated as a polarizable continuum instead of individual solvent molecules. There are two types of PCMs: (i) The dielectric PCM (D-PCM), which uses polarizable continuum. (ii) Another is conductor-like PCM (C-PCM) which is similar to COSMO that the continuum is conductor-like. COSMO assumes that the surrounding medium is well modeled as a conductor. The problem for continuum models is that the specific interactions between solute and solvent molecules has been neglected.[92] When solvent molecules are close to the solute they perform different from the bulk, which is known as cybotactic behavior[93]. This problem can be fixed by including the first solvation shell which contains a number of explicit solvent molecules.

1.8. Organization of this Thesis

The aim of this thesis is to provide thorough systematic benchmarking studies to evaluate the performance of modern DFT applied to actinide systems. It is expected to contribute to better selection of DFT methods in the study of actinide chemistry.

The work in Chapter 2 is a part of the actinide spectroscopy Round-Robin test (RRT). The goal of the theory cluster within the RRT is the evaluation and comparison of the performance of DFT using different quantum chemistry programs with identical DFT functionals. There are five complexes that were studied in the theory cluster. The data from

different groups that participated in RRT are summarized in this chapter. There are five complexes that were studied in the theory cluster. The task of our group was calculating the properties of specific U(VI) acetate complexes using the ADF program with different DFT functionals, which include GGA, Hybrid GGA, Meta GGA and Hybrid Meta GGA. Besides the theory cluster, several experimental clusters, such as IR, XAS, NMR etc., are available to provide data as reference for the quantum chemical calculations.

In Chapter 3, the performance of different DFT functionals had been further investigated. A total of 22 different functionals have been chosen. These functionals are compared by calculating geometries, vibrational frequencies, and reaction enthalpies. We used several gas phase uranium halides as well as uranium oxides, oxy-halides and oxy-hydroxides are selected as samples in this study. The experimental vibrational frequencies data[94–97] as well as gas phase reactions enthalpies,[98,99] are available. High level *ab initio* CCSD(T) calculations have been performed as reference due to the lack of experimental data for bond lengths[100–105].

Finally, in chapter 4, a brief summary of the thesis is provided as well as an outlook for future studies.

1.9. References

[1] Caley, E. R., *Isis*, **1948**, *38*, 190.
[2] Mellor, J. W. *Comprehensive Treatise on Inorganic and Theoretical Chemistry, vol. XII*,, Longmans, Green and Co., London. (**1932**)
[3] Betti, M., *J. Environ. Radioactiv*. **2003**, *64*, 113.
[4] Grenthe, I.; Drozdzynski, J.; Fujino, T.; Buck, E. C.; Albrecht‐Schmitt, T. E.; Wolf, S. F., *Computational Methods in Lanthanide and Actinide Chemistry, CHAPTER FIVE URANIUM,* John Wiley & Sons, Ltd, (**2015**)
[5] Hahn, O.; Strassmann, F., *Am. J. Phys.*, **1939**, 27, 11.
[6] http://www.world-nuclear.org/info/inf01.html Accessed May 10th, 2016.
[7] http://atom.kaeri.re.kr/nuchart/?zlv=1 Accessed August 23rd, 2016
[8] Ewing, R. C.; Runde, W.; Albrecht-Schmitt, T. E., *Mrs Bulletin* **2010**, *35*, 859.
[9] Graves, C. R.; Kiplinger, J. L., *Chem. Commun.* **2009**, *26*, 3831.
[10] Runde, W., *Los Alamos Science* **2000**, *26*, 338.
[11] Shamov, G. A.; Schreckenbach, G.; Vo, T. N., *Chem-Eur. J.* **2007,** *13,* 4932.
[12] Batista, E. R.; Martin, R. L.; Hay, P. J., *J. Chem. Phys.* **2004,** *121,* 11104.

[13] Seip, H. M. *Acta. Chem. Scand.* **1965**, *19*, 1955.
[14] Kimura, M.; Schomaker, V.; Smith, D.W.; Weinstock, B., *J. Chem. Phys.* **1967**, *48*, 4001.
[15] Zachariasen, W. H.; *Acta Crystallogr*. **1948**, *1*, 285.
[16] Brown, D., *Halides of the Transition Elements* Wiley, New York, **1968.**
[17] Haaland, A.; Martinsen, K.-G.; Swang, O.; Volden, H. V.; Booij, A. S.; Konings, R. J. M., *J. Chem. Soc. Dalton Trans.* **1995**, *2*, 185.
[18] Bazhanov,V. I.; Ezhov, Y. S.; Komarov, S. A., *J. Struct. Chem.* **1990**, *31*, 986.
[19] Han, Y. K., *J. Comput. Chem.* **2001,** *22,* 2010.
[20] Odoh, S. O.; Schreckenbach, G., *J. Phys. Chem. A* **2010,** *114,* 1957.
[21] Schrödinger, E. *Phys. Rev*. **1926**, *28*, 1049.
[22] Born, M.; Oppenheimer, R., Annalen Der *Physik* **1927**, *84*,04
[23] Gordon, A.; Avron, J. E., *Phys. Rev. Lett.* **2000**, *85*, 34.
[24] Waschewsky, G. C. G.; Kash, P. W.; Myers, T. L.; Kitchen, D. C.; Butler, L. J., *J. Chem. Soc., Faraday Trans.*, **1994**, *90*, 1581.
[25] Cramer, C. J.; *Essentials of Computational Chemistry* John Wiley & Sons Ltd, (**2004**)
[26] Levine, I. N., *Quantum Chemistry*, Pearson Education, Inc. (**2014**)
[27] http://cccbdb.nist.gov/vibnotes.asp Accessed May 10th, 2016.
[28] Sinha, P.; Boesch, S. E.; Gu, C.; Wheeler, R. A.; Wilson, A. K., *J. Phys. Chem. A* **2004**, *108*, 9213.
[29] Slater, J. C., *Phys. Rev.*, **1930**, *36*, 57.
[30] Boys, S. F., *Proc. R. Soc. London Ser. A* **1950**, *200*, 542.
[31] Hehre, W. J., Stewart, R. F., and Pople, J. A., *J. Chem. Phys*., **1969**, *51*, 2657.
[32] Velde G.te; Bickelhaupt F.M.; Baerends E.J.; Fonseca Guerra C.; van Gisbergen S.J.A.; Snijders J.G.; Ziegler T. *J. Comput. Chem*. **2001**, *22*, 931.
[33] Hartree, D. R., P. *Camb. Philos. Soc.,* **1928**, *24*, 89.
[34] Hartree, D. R., P. *Camb. Philos. Soc.,* **1928**, *24*, 111.
[35] Roothaan, C. C. J., *Rev. Mod. Phys.*, **1951**, 23, 69.
[36] Moller, C.; Plesset, M. S., *Phys. Rev.,* **1934**, *46*, 0618.
[37] Pople, J. A.; Binkley, J. S.; Seeger, R., *Int. J. Quantum Chem.,* **1976**, 1.
[38] Purvis, G. D.; Bartlett, R. J., *J. Chem. Phys.,* **1982**, *76*, 1910.
[39] Kendall, R. A.; Dunning, T. H.; Harrison, R. J., *J. Chem. Phys*., **1992**, *96*, 6796.
[40] Thomas, L. H., P. *Camb. Philos. Soc.,* **1927**, *23*, 542.
[41] Slater, J. C., *Phys. Rev.,* **1951**, *81*, 385.
[42] Slater, J. C., *Adv. Quantum Chem.,* **1972**, *6*, 1.
[43] Hohenberg, P.; Kohn, W., *Phys. Rev. B*, **1964**, *136*, B864.
[44] Perdew, J. P.; Ruzsinszky, A.; Tao, J.; Staroverov, V. N.; Scuseria, G. E.; Csonka, G. I.; *J. Chem. Phys.*, **2005**, *123*, 062201.
[45] Perdew, J. P.; Schmidt, K., *AIP Conf. Proc.*, **2001**, *577*, 1.
[46] Sabbe, M. K.; Reyniersa, M.-F.; Reuter, K., *Catal. Sci. Technol.*, **2012**, *2*, 2010.
[47] Perdew, J. P.; Burke, K.; Ernzerhof, M. *Phys. Rev. Lett.* **1996**, *77*, 3865.
[48] Perdew, J. P.; Burke, K.; Ernzerhof, M. *Phys. Rev. Lett*. **1997**, *78*, 1396.
[49] Becke, A. D. *Phys. Rev. A* **1988**, *38*, 3098.
[50] Lee, C.; Yang, W.; Parr, R. G. *Phys. Rev. B* **1988**, *37*, 785.
[51] Tao, J. M.; Perdew, J. P.; Staroverov, V. N.; Scuseria, G. E., *Phys. Rev. Lett.*, **2003**, *91*, 146401.
[52] Zhao, Y.; Truhlar, D. G. *J. Chem. Phys.* **2006**, *125*, 194101.
[53] Perdew, J. P.; Chevary, J. A.; Vosko, S. H.; Jackson, K. A.; Pederson, M. R.; Singh, D. J.;Fiolhais, C., *Phys. Rev. B*, **1992**, 46, 6671.
[54] Perdew, J. P.; Wang, Y., *Phys. Rev. B*, **1992**, *45*, 13244.
[55] Adamo, C.; Barone, V. *J. Chem. Phys.* **1999**, *110*, 6158.
[56] Becke, A. D. *J. Chem. Phys.* **1993**, *98*, 1372.
[57] Lee, C.; Yang, W.; Parr, R. G. *Phys. Rev. B* **1988**, *37*, 785.
[58] Atkins, P.W., *Quanta: A handbook of concepts.* Oxford University Press. p. 52. **1974**
[59] van Lenthe, E.; Ehlers, A.; Baerends, E. J., *J. Chem. Phys.*, **1999**, *110*, 8943.
[60] Dyall, K. G.; van Lenthe, E., *J. Chem. Phys.*, **1999**, *111*, 1366.

[61] Autschbach, J.; Govind, N.; Atta-Fynn, R.; Bylaska, E. J.; Weare, J. W.; de Jong, W. A., *Computational Methods in Lanthanide and Actinide Chemistry vol. 12 Computational Tools for Predictive Modeling of Properties in Complex Actinide Systems* John Wiley & Sons, Ltd (**2005**)
[62] van Lenthe, E.; Baerends, E. J.; Snijders, J. G., *J. Chem. Phys.*, **1994,** *101*, 9783.
[63] van Lenthe, E.; Snijders, J.; Baerends, E., *J. Chem. Phys*., **1996**, *105*, 6505.
[64] Cao, X.; Dolg, M., *Relativistic pseudopotentials, in M. Barysz and Y. Ishikawa (Eds.), Relativistic methods for chemists. Challenges and advances in computational physics*, vol. 10, Springer, Berlin, pp. 215–278 (**2010**).
[65] Han, Y.-K.; Hirao, K., *J. Chem. Phys*.; **2000**, *113*, 7345.
[66] Han, Y. K., *J. Comput. Chem*., **2001**, *22*, 2010.
[67] Schreckenbach, G.; Wolff, S. K.; Ziegler, T., *J. Phys. Chem. A*, **2000**, *104*, 8244.
[68] Schreckenbach, G. *Int. J. Quantum Chem.*, **2005**, *101*, 372.
[69] Straka, M.; Kaupp, M. *Chem. Phys*., **2005**, *311*, 45.
[70] Batista, E. R.; Martin, R. L.; Hay, P. J.; Peralta, J. E.; Scuseria, G. E., *J. Chem. Phys*., **2004**, *121*, 2144.
[71] Odoh, S.O.; Schreckenbach G., *J. Phys. Chem. A,* **2010**, *114*, 1957.
[72] Shamov, A. G.; Schreckenbach, G., *J. Phys. Chem. A* **2005**, *109*, 10961.
[73] Graves, C. R.; Kiplinger, J. L., *Chem. Commun.* **2009,** *26*, 3831.
[74] Arnold, P. L.; Pecharman, A. F.; Love, J. B., *Angew. Chem. Int. Edit.* **2011,** *50*, 9456.
[75] Fortier, S.; Hayton, T. W., *Coordin. Chem. Rev.* **2010,** *254*, 197.
[76] Ikeda, A.; Hennig, C.; Tsushima, S.; Takao, K.; Ikeda, Y.; Scheinost, A. C.; Bernhard, G., *Inorg. Chem.* **2007,** *46*, 4212.
[77] Mizuoka, K.; Grenthe, I.; Ikeda, Y., *Inorg. Chem.* **2005,** *44*, 4472.
[78] Mizuoka, K.; Ikeda, Y., *Inorg. Chem.* **2003,** *42*, 3396.
[79] Tomasi, J.; Mennucci, B.; Cammi, R., Chem. Rev. **2005,** 105, 2999.
[80] Born, M. Z., *Physik* **1920**, *1*, 45.
[81] Onsager , L. *J . Am. Chem. Soc.* **1936**, *58*, 1486.
[82] Kirkwood, J., G. *J. Chem. Phys*. **1939**, *7*, 911.
[83] Toma si, J.; Per sico, M. *Chem. Rev.* **1994**, *94*, 2027.
[84] Mier tus, S.; Scr occo, E.; Toma si, J. *Chem. Phys.* **1981**, *55*, 117.
[85] Cammi, R.; Tomasi, J., *J. Com put. Chem.* **1995**, *16*, 1449.
[86] Cossi, M.; Barone, V.; Cammi, R.; Tomasi, J., *Chem. Phys. Lett.* **1996**, *255*, 327.
[87] Amovilli, C.; Barone, V.; Cammi, R.; Cancès, E.; Cossi, M.; Menucci, B.; Pommelli, C. S., *Adv. Quantum Chem.* **1998**, *32*, 227.
[88] Klamt, A.; Schüürmann, G., *J. Chem. Soc., Perkin Trans. 2* **1993**, 799.
[89] Andzelm, J.; Kölmel, C.; Klamt, A. *J . Chem. Phys.* **1995**, *103*, 9312.
[90] Klamt, A. *J. Phys. Chem.* **1995**, *99*, 2224.
[91] Klamt, A.; Jonas, V. J. *Chem. Phys.* **1996**, *105*, 9972.
[92] Cramer, C. J.; Truhlar, D. G., *Chem. Rev.* **1999,** *99,* 2161.
[93] Tapia , O. In *Molecular Interactions*; Ra t a jczak, H., Orville-Thoma s, J . W., Eds.;J ohn Wiley & Sons: Chichest er , **1982**; Vol. 3, p 47.
[94] Shamov, G. A.; Schreckenbach, G.; Vo, T. N., *Chem-Eur. J.* **2007,** *13,* 4932.
[95] Batista, E. R.; Martin, R. L.; Hay, P. J., *J. Chem. Phys.* **2004,** *121,* 11104.
[96] Han, Y. K., *J. Comput. Chem.* **2001,** *22,* 2010.
[97] Odoh, S. O.; Schreckenbach, G., *J. Phys. Chem. A* **2010,** *114,* 1957.
[98] Privalov, T.; Schimmelpfennig, B.; Wahlgren, U.; Grenthe, I., *J. Phys. Chem. A* **2002,** *106,* 11277.
[99] Bross, D. H.; Peterson, K. A., *J. Chem. Phys.* **2014**, *141*, 244308.
[100] Seip, H. M. *Acta. Chem. Scand.* **1965**, *19*, 1955.
[101] Kimura, M.; Schomaker, V.; Smith, D.W.; Weinstock, B., *J. Chem. Phys.* **1967**, *48*, 4001.
[102] Zachariasen, W. H.; *Acta Crystallogr*. **1948**, *1*, 285.
[103] Brown, D., *Halides of the Transition Elements* Wiley, New York, **1968.**
[104] Haaland, A.; Martinsen, K.-G.; Swang, O.; Volden, H. V.; Booij, A. S.; Konings, R. J. M., *J. Chem. Soc. Dalton Trans.* **1995**, *2*, 185.
[105] Bazhanov,V. I.; Ezhov, Y. S.; Komarov, S. A., *J. Struct. Chem.* **1990**, *31*, 986.

Chapter 2 : Theoretical study within the Round-Robin test of actinide spectroscopy

2.1. Introduction

The interactions between uranium(VI) and natural organic matter (NOM) are one of the key parameters to understand the activity of uranium in the environment such as sorption and transport behaviors of uranium(VI) in aqueous surrounding. [1] Simple organic acids can be treated as basic models to study these behaviors thus furthering understanding the reactions of NOM with more complicated carboxylic functionalities. In this study, acetic acid (ac) was chosen as model substance not only because it is the smallest organic acid with a carbon chain and its behavior is similar to most of the larger carboxylic acids but also because it will give geometries with exclusively acetate binding which reduces the number of possible isomers.

In the past, a variety of methods has been used to investigate the aqueous U-ac system, such as Extended X-ray Absorption Fine Structure (EXAFS)[2,3], Infrared absorption (IR)[4-6], Raman scattering[4,7] and Ultraviolet−visible absorption (UV−vis) spectroscopies. However these studies disagree with each other in stoichiometry, structure and speciation. The reason for this significant disagreement might due to the purity of the samples.[1] There are four U(VI) complexes that are predicted by thermodynamic speciation calculations in the U(VI)-acetate system: the uranyl aquo complex $UO_2(H_2O)_5^{2+}$, as well as the acetate complex UO_2ac^+, $UO_2ac_2^0$, and $UO_2ac_3^-$. However, only the aquo complex $UO_2(H_2O)_5^{2+}$ (at pH 0) and $UO_2ac_3^-$ (at pH 4) are experimentally accessible in pure form.[7] In their recent study, Lucks et al.[7] showed that bidentate coordination of the carboxylic groups to the equatorial plane of the uranyl moiety is preferred for

all uranyl ligand complexes except for the newly detected 1:3 U(VI)-acetate complex (RR5 in **Figure 2.2**). This will be the basic model for all theoretical benchmarking studies in this chapter.

There are two fundamentally different modern methods that have been used for relativistic effects in this study. These are the all–electron zeroth-order regular approximation (ZORA) [8-11]approach and small-core effective core potential (SC-ECP)[12]. The large amount of electrons in *f* elements make calculations become a challenge. The idea of effective core potentials (ECPs) is replacing electrons in the inner shells by a suitably parameterized one-electron operator which acts on the remaining valence electrons and which also can including relativistic effects.[13] Recently, "small-core" ECP (SC-ECP), which only parameterize 60 electrons as core, have shown good agreement with experimental data such as geometries[14,15], frequencies[17,18], ligand NMR chemical shifts[16-18] and dissociation energies[19]. Shamov et al.[20]and Odoh et al.[21] proved that the current SC-ECP is clearly superior to the older "large core" ECP (LC-ECP) for geometries, frequencies, and reduction potentials. They further pointed out that these two methods, ZORA and SC-ECP, can yield similar results for a wide range of properties.

Solvation effects also play an important role in the aqueous actinide chemistry.[22,23] The most common models are cluster models and continuum models. Moskaleva et al.[24] show that the first coordination sphere of uranyl has to be included in the continuum model approach in order to yield reasonable hydration energies.

The data from different groups that participated in RRT are summarized in this chapter. There are five complexes that were studied in the quantum chemistry (QC) cluster. The task of our group was calculating the properties of specific U(VI) acetate complexes using the ADF program with different DFT functionals, which include GGA, Hybrid GGA, Meta GGA as well as Hybrid Meta GGA.

2.2. Aims of the Round-Robin Test of actinide spectroscopy

The inter-laboratory Round Robin Test (RRT) is a unique comparison of molecular information which is obtained from the different spectroscopic [time-resolved laser fluorescence spectroscopy (TRLFS), vibrational spectroscopy (IR/Raman spectroscopy), extended X-ray absorption fine structure (EXAFS), nuclear magnetic resonance (NMR), electron spray ionization-mass spectrometry (ESI-MS)] and theoretical methods (Quantum-Chemical calculations, QC). This actinide spectroscopy RRT aims at comprehensive analysis of the actinide complex system U(VI)-acetate in aqueous solution independently investigated by different chemical methods applied by leading laboratories in geochemical research. In this test concordance as well as the source of discrepancies between the results from different methods will be evaluated. Based on this foundation, it illuminates the potentials and limitations of coupling of different spectroscopic and theoretical approaches in order to better use them as tools for the comprehensive molecular study of actinide complexes. This test does not aim at a competitive exercise between the different labs within the actinide community, but is understood to stimulate scientific discussions.

2.3. Clusters and participating institutions.

The RRT was initiated in late 2013 at Helmholtz-Zentrum Dresden-Rossendorf (HZDR). After the acceptance of the participating institutions, six clusters were formed according to the respective approach, namely TRLFS, IR/Raman spectroscopy, NMR, ESI-MS, EXAFS, and QC. For each cluster a representative speaker was nominated. The overall organization chart of the RRT and the list of participating institutions are given in **Figure 2.1**, **Table 2.1.1** and **Table 2.1.2**, respectively.

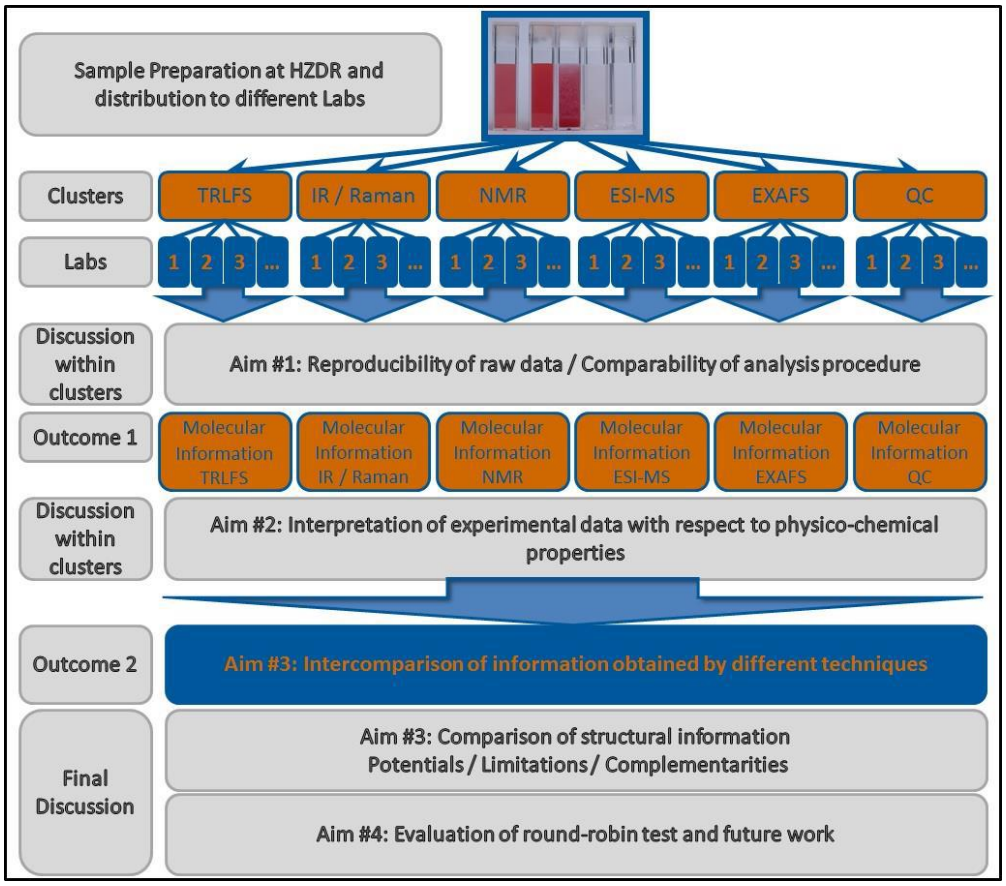

Figure 2.1 General procedure and expected discussion topics of the RRT

Table 2.1.1 Clusters and participating institutions of the RRT.

CLUSTER	CONTRIBUTING INSTITUTION	COUNTRY
TRLFS (Speaker: M.U. Kumke, University of Potsdam, Germany)	French Alternative Energies and Atomic EnergyCommission	France
	French Institute for Radioprotection and NuclearSafety	France
	Helmholtz-Zentrum Dresden-Rossendorf	Germany
	Karlsruhe Institute of Technology	Germany
	Pacific Northwest National Laboratory	U.S.A.
	Trinity College Dublin	Ireland
	University of Heidelberg	Germany
	Heidelberg Germany	Germany
	Université de Toulon	France
IR / Raman (Speaker: G. Lefèvre, École nationale supérieure de chimie de Paris, France)	École Nationale Supérieure de Chimie de Paris	France
	Clemson University	U.S.A.
	Helmholtz-Zentrum Dresden-Rossendorf	Germany
	Pacific Northwest National Laboratory	U.S.A.
	University of Potsdam	Germany
NMR (Speaker: Z. Szabò, Royal Institute of Technology, Stockholm, Sweden)	Helmholtz-Zentrum Dresden-Rossendorf	Germany
	Karlsruhe Institute of Technology	Germany
	Lawrence Livermore National Laboratory	U.S.A.
	Pacific Northwest National Laboratory	U.S.A.
	Royal Institute of Technology	Sweden
ESI-MS (Speaker: C. Walther, University of Hannover, Germany)	University of Hannover	Germany
XAS (Speaker: J. Rothe, Institute for Nuclear Waste Disposal, Karlsruhe, Germany)	Helmholtz-Zentrum Dresden-Rossendorf	Germany
	Karlsruhe Institute of Technology	Germany
	Université de Nice Sophia Antipolis	France
QC (Speaker: P. Yang, Pacific Northwest National Laboratory, Richland, U.S.A.)	Cardiff University	U.K.
	Helmholtz-Zentrum Dresden-Rossendorf	Germany
	Karlsruhe Institute of Technology	Germany
	Pacific Northwest National Laboratory	U.S.A.
	University Manitoba	Canada

Table 2.1.2 Institutions and groups participated the QC cluster of the RRT.

	Country	Institution	Name
1	Germany	Karlsruhe Institute of Technology	Bernd Schimmelpfennig Robert Polly Michael Trumm
2	Germany	Technische Universität München	Alena Kremleva Sven Krüger
3	Germany	Helmholtz-Zentrum Dresden-Rossendorf	Satoru Tsushima
4	Canada	University of Manitoba	Georg Schreckenbach Xiaobin Zhang
5	U.K.	Cardiff University	Jamie Platts
6	U.S.A.	Pacific Northwest National Laboratory	Ping Yang

2.4. System selection.

There are four U(VI) acetate samples at distinct metal and ligand concentrations in different pH values. The concentration of U(VI) was 0.025M. The impact of metal and ligand concentration, ionic strength and temperature were not included in this test. The details of the samples are listed in **Table 2.2**.

Table 2.2 Samples used for round-robin test.

Sample	$c(UO_2^{2+})$ / M	c(Acetate) / M	Ionic strength / M	pH
U1	0.025	0.095	1	1.0
U2	0.025	0.095	1	2.0
U3	0.025	0.095	1	2.5
U4	0.025	0.095	1	3.5
B1	-	0.095	1	1.0
B2	-	0.095	1	2.0
B3	-	0.095	1	2.5
B4	-	0.095	1	3.5

For the theory cluster, the five complexes given below in **Figure 2.2** were studied. It can be assumed that acetate binds exclusively in bidentate fashion to uranyl.[7] Note that, only data of RR1 and RR5 have been collected for experimental and theoretical data because they are chemically accessible in pure form in experiment.

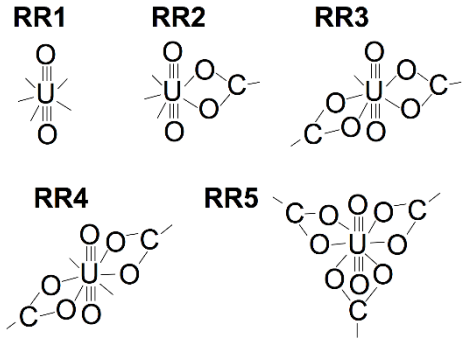

Figure 2.2 Five complexes that were studied: $[UO_2(H2O)_5]^{2+}$ (Complex RR1), $[UO_2(Ac)(H_2O)_3]^{+}$ (Complex RR2), $[UO_2(Ac)_2(H_2O)]^{0}$ (Complex RR3), $[UO_2(Ac)_2(H2O)_2]^{0}$ (Complex RR4) and $[UO_2(Ac)_3]^{-1}$ (Complex RR5). The unlabeled ligands are water.

2.5. Computational details

2.5.1. Gaussian Type Basis sets

All the calculations were performed using identical basis sets but with different programs (TURBOMOLE[25], Gaussian 09[26] and ParaGauss[27]) and different DFT functionals including GGAs (BP86[28-30], PBE[31,32]), Hybrid GGAs (PBE0[34-33], B3LYP[34,35]) and Meta GGAs (M06[36], M06L[37], TPSSh[38]). The common basis set employed includes the SDD (Stuttgart-Dresden) SC-ECP and corresponding basis set[39] on U and cc-pvtz[40] on other elements (C, O, H). Different solvation models have been used depending on the different programs.

2.5.2. Slater Type Basis sets (our group's contribution)

The systems were investigated using different functionals, including GGA (BLYP[31,38], OLYP[41,38] and PBE[34,35]), Hybrid GGA (B3LYP[37,38], O3LYP[42] and PBE0[34-36]), Meta GGA (M06[39] and M06L[40]), without frozen core approximation using the ADF2013 program[43]. All five complexes were investigated both in gas phase and with the COSMO Solvation Model[44,45]. All geometry optimizations and vibrational frequency calculations were done at the scalar ZORA[8-11] level using the ZORA-TZ2P basis set. All excited states and NMR calculations are at the scalar ZORA level and spin-orbit ZORA level and used the ZORA-QZ4P basis set for GGA calculations. For Hybrid GGA and Meta GGA, the ZORA-TZ2P basis set has been used in excited states and NMR calculations at both the Scalar ZORA level and Spin-orbit ZORA levels.

2.6. Results and Discussion

Table 2.3 and **Table 2.4** show the summarized calculated and experimental bond lengths and uranyl frequencies.

Table 2.3 Average U-O/U-C bond distances (Å) and O=U=O v_1 and v_3 vibrational frequency (cm^{-1}) of $UO_2(H_2O)_5^{2+}$ and $UO_2(CH_3COO)_3^-$ in gas phase using the identical DFT functionals and basis sets but different QC program and corresponding experimental data.

		RR1 ($UO_2(H_2O)_5^{2+}$)								RR5 ($UO_2(Ac)_3^-$)										
		cal.		exp.		cal.		exp.		cal.			exp.			cal.		exp.		Reaction Energy
theory		U-O_{ax}	U-O_w	U-O_{ax}	U-O_w	*v1*	*v3*	*v1*	*v3*	U-O_{ax}	U-O_{ac}	U-C_{car}	U-O_{ax}	U-O_{ac}	U-C_{car}	*v1*	*v3*	*v1*	*v3*	delta G
MP2	T	1.761	2.462			887	995			1.803	2.472	2.828				826	928			-386.27
BP86	T	1.767	2.476			888	978			1.804	2.506	2.871				813	897			-381.70
BP86	G	1.765	2.487			901	993			1.802	2.513	2.878				821	906			-394.73
BP86	P	1.767	2.480			890	983			1.798	2.513	2.879				820	904			-391.86
PBE	T	1.765	2.476			893	983			1.801	2.513	2.868				819	903			-378.70
PBE	P	1.764	2.480			895	988			1.795	2.512	2.876				825	909			-390.31
PBE	A	1.768	2.491			892	984			1.805	2.514	2.878				817	903			-410.57
PBE0	T	1.728	2.469			988	1068			1.760	2.484	2.846				904	982			-
PBE0	P	1.727	2.472			992	1075			1.756	2.493	2.854				913	992			-388.11
PBE0	G	1.726	2.475			991	1075			1.758	2.491	2.853				912	993			-391.23
PBE0	A	1.734	2.477			981	1064			1.766	2.492	2.852				898	977			-410.27
B3LYP	T	1.745	2.493			947	1032			1.780	2.512	2.879				-	-			-
B3LYP	G	1.744	2.498	1.76;	2.41;	952	1040	870;	962;	1.777	2.518	2.885	1.773;	2.44; 2.46;	2.88;	875	959	845-	924-	-384.23
B3LYP	A	1.753	2.497	1.78; 1.763-1.766	2.403-2.408	937	1024	870-873	961; 961-963	1.787	2.519	2.884	1.780	2.464; 2.472;	2.887;	860	942	849	926	-407.45
BLYP	A	1.785	2.520			865	957			1.825	2.539	2.910				787	871			-406.48
O3LYP	A	1.731	2.375			965	1052			1.760	2.407	2.763				895	976			-406.89
OLYP	A	1.750	2.542			915	1010			1.787	2.550	2.917				832	923			-412.28
TPSSh	T	1.746	2.469			940	1026			1.782	2.485	2.851				-	-			-
M06L	P	1.739	2.497			945	1039			1.772	2.520	2.881				862	948			-399.15
M06L	G	1.738	2.503			954	1045			1.774	2.518	2.878				863	952			-393.81
M06L	A	1.740	2.507			948	1036			1.779	2.515	2.873				850	937			-414.04
M06	P	1.722	2.491			1017	1096			1.749	2.514	2.872				933	1010			-387.14
M06	G	1.721	2.491			1003	1083			1.750	2.515	2.874				932	1010			-386.71
M06	A	1.727	2.492			998	1078			1.759	2.510	2.866				914	991			-407.47

1) T: TURBOMOLE, G: Gaussian 09, P: ParaGauss, A: ADF 2) For reaction $UO_2(H_2O)_5^{2+} + 3\ CH_3COO^- \rightarrow UO_2(CH_3COO)_3^- + 5\ H_2O$

3) O_{ax} and O_w for oxygen in urania and water, respectively. 4) C_{car} and C_{me} for the carbon in the carboxyl and methyl, respectively.

Table 2.4 Average U-O/U-C bond distances (Å) and O=U=O ν_1 and ν_3 vibrational frequency (cm^{-1}) of $UO_2(H_2O)_5^{2+}$ and $UO_2(CH_3COO)_3^-$ in solvent model using the identical DFT functionals and basis sets but different QC program and corresponding experimental data.

		RR1 (UO2(H2O)52+)								RR5 (UO2(Ac)3-)										
		cal.		exp.		cal.		exp.		cal.			exp.			cal.		exp.		Reaction Energy
theory		U-O_{ax}	U-O_w	U-O_{ax}	U-O_w	v1	v3	v1	v3	U-O_{ax}	U-O_{ac}	U-C_{car}	U-O_{ax}	U-O_{ac}	U-C_{car}	v1	v3	v1	v3	delta G
MP2	G	1.767	2.420			896	988			1.796	2.450	2.832				833	922			
BP86	G	1.774	2.467			880	951			1.811	2.492	2.879				799	863			-98.95
BP86	P	1.780	2.444			857	923			1.809	2.482	2.874				795	852			-85.65
PBE	P	1.777	2.443			863	929			1.806	2.482	2.872				801	857			-83.82
PBE	A	1.779	2.453			865	921			1.818	2.482	2.877				784	829			-92.25
PBE0	G	1.734	2.454			967	1026			1.765	2.471	2.853				894	949			-94.54
PBE0	P	1.739	2.431			956	1004			1.764	2.464	2.851				890	935			-82.27
PBE0	A	1.742	2.444			953	991			1.775	2.465	2.852				869	901			-87.56
B3LYP	G	1.752	2.474	1.76;	2.41;	930	994	870;	962;	1.785	2.497	2.884		2.44;		856	915			-92.27
B3LYP	A	1.762	2.460	1.78;	2.403-	912	954	870-	961;	1.797	2.490	2.883	1.773;	2.46;	2.88;	832	866	845-	924-	-86.38
				1.763-	2.408			873	961-				1.780	2.464;	2.887			849	926	
BLYP	A	1.768	2.490	1.766		891	952		963	1.838	2.510	2.909		2.472		758	801			-93.86
O3LYP	A	1.741	2.345			938	982			1.772	2.381	2.766				862	901			-82.91
OLYP	A	1.759	2.496			887	946			1.797	2.520	2.915				802	854			-93.63
M06L	G	1.747	2.477			926	995			1.782	2.496	2.877				840	906			-97.10
M06L	P	1.752	2.458			902	962			1.781	2.490	2.875				836	891			-90.74
M06L	A	1.750	2.464			916	958			1.790	2.486	2.871				816	855			-92.11
M06	G	1.728	2.470			980	1034			1.756	2.497	2.876				916	968			-86.64
M06	P	1.733	2.451			983	1026			1.755	2.490	2.874				909	950			-80.99
M06	A	1.736	2.454			971	1002			1.766	2.484	2.867				886	916			-86.18

1) T: TURBOMOLE, G: Gaussian 09, P: ParaGauss, A: ADF
2) For reaction $UO_2(H_2O)_5^{2+} + 3\ CH_3COO^- \rightarrow UO_2(CH_3COO)_3^- + 5\ H_2O$
3) O_{ax} and O_w for oxygen in urania and water, respectively.
4) C_{car} and C_{me} for the carbon in the carboxyl and methyl, respectively.

The calculations in gas phase (**Table 2.3**) give U-O_{ax} distances of 1.721 – 1.785 Å and 1.749 – 1.825 Å for RR1 and RR5 respectively. These results show that, when acetic acid molecules replace waters, the uranyl bond becomes weaker, which is confirmed by the experimental data. Note that the BLYP results are significantly larger than those of other functionals. By contrast, M06 gives the shortest U-O_{ax} bond length. The commonly used pure GGA functionals, BP86 and PBE, give very similar results in both RR1 and RR5. All hybrid GGAs and Meta GGAs tend to give shorter U-O_{ax} distances compared with pure GGAs. MP2, PB86 and PBE give very good results for predicting U-O_{ax} in RR1 distances against experimental data. B3LYP and TPSSh give the best result amongst Hybrid GGAs and Meta GGAs, respectively. In case of RR5, the PBE, B3LYP, TPSSh, M06L and MP2 show good agreements with experiment. Again, B3LYP gives the best result in the Hybrid GGA group. Due to the shorter U-O_{ax} distances, the Hybrid GGAs and Meta GGAs tend to give higher frequencies in both RR1 and RR5. The results from pure GGAs and MP2 agree very well with the experimental data in RR1. BLYP gives the best result in pure GGA. All other functionals (Hybrid GGAs and Meta GGAs) result in frequencies that are higher than the experiment values. B3LYP and TPSSh give the best result in Hybrid GGAs and Meta GGAs, respectively, which may be due to the better bond distances given by them. Although, they are still significantly larger than the experimental data compared with pure GGA. In RR5, pure GGAs tend to predict lower and other functionals tend to give higher frequencies compared with the experimental data as well as RR1. B3LYP, OLYP and M06L give the best results in each group. As a wavefunction theory method, in RR5, MP2 is still better than DFT methods against experimental data. OLYP and O3LYP give the longest and shortest U-O_w bond lengths respectively. All methods other than O3LYP give significantly longer bond distances compared with experimental data. The

calculated gas phase U-O_{ac} bond distances in RR5 in are 2.407 – 2.550 Å. MP2 and TPSSh give the best results in all the methods. All other methods except O3LYP gives much longer bond distances than experiment. The calculations in gas phase give the U-C_{car} distances of 2.763 – 2.917 Å. B3LYP gives the best result in all methods. Again, OLYP gives the longest bond length and O3LYP gives the shortest distance compared with the other methods that are relatively close to each other.

The results of calculations using solvation models are summarized in **Table 2.4**. When the calculations include a solvation model, the U-O_{ax} bond lengths in both RR1 and RR5 for all functionals become longer then the gas phase ones by 0.006 Å to 0.013 Å except for BLYP in RR1. Which is not a surprise because BLYP already gives a very large U-O_{ax} bond length in RR1 in the gas phase. On the other hand, the U-O_w bond lengths in both RR1 and RR5 become shorter compared to the gas phase, with changes of 0.020 – 0.046 Å (RR1) and 0.018 – 0.032 Å (RR5), respectively. These changes make most of the functionals perform better since in gas phase most of them underestimate the U-O_{ax} bond length and overestimate the U-O_w bond length. The calculations give U-O_{ax} distances of 1.728 – 1.780 Å and 1.755 – 1.838 Å for RR1 and RR5 respectively. M06 gives the shortest bond lengths both in RR1 and RR5 as well as in gas phase. In RR1, MP2, BLYP, B3LYP and M06L show the best results compared with the experimental data. Similar to the gas phase calculations, all hybrid GGAs and Meta GGAs tend to give shorter U-O_{ax} distances than pure GGAs. Then in RR5, only M06 gives a significantly shorter U-O_{ax} bond length. MP2, M06L and all three Hybrid GGAs give very good U-O_{ax} bond lengths against experimental values. By contrast, pure GGAs tend predict longer U-O_{ax} bonds than experimental data. The corresponding O=U=O ν1 and ν3 stretching vibrational frequencies are 857 – 983 cm^{-1} and 921 – 1034 cm^{-1} in RR1 and 758 – 916 cm^{-1} and 801 – 968 cm^{-1} in

RR5, respectively, which are lower than those of the gas phase calculations. Very similar to the gas phase calculations, in RR1, the results of pure GGAs and MP2 are better than those of the Hybrid GGAs and Meta GGAs. The results of Hybrid GGAs and Meta GGAs are still higher than the experimental data but better than gas phase calculations. B3LYP and M06L give the best results in Hybrid GGAs and Meta GGAs. For RR5, MP2 and B3LYP show the best result over all other methods. All other methods tend to give lower frequencies except for PBE0, O3LYP and M06. M06 and BLYP give the largest and smallest frequencies respectively. For the $U\text{-}O_w$ bonds in RR1, the MP2 method provides the best result, 0.010 – 0.017 Å higher than the experimental data. All other methods tend to predict longer bond lengths except O3LYP which gives bonds of ~0.060 Å shorter than experimental values. For the $U\text{-}O_{ac}$ bonds in RR5, MP2 still give the good results as well as PBE0. BP86 and PBE give slightly longer bond lengths, however, BLYP and OLYP tend to give significantly longer bond lengths. All Meta /GGAs and B3LYP tend to result in longer $U\text{-}O_{ac}$ bond length. Similar to the gas phase calculations, OLYP and O3LYP give the longest and shortest $U\text{-}O_w$ and $U\text{-}O_{ac}$ bond lengths respectively.

The deviations among the calculations using identical DFT functionals and basis set, but different codes, are generally small. Over all, there is excellent agreement between Gaussian 09 and ParaGauss; the differences in bond lengths and frequencies are in many cases only within 0.002 Å and 2 cm^{-1}, respectively. TURBOMOLE, on the other hand, tends to give slightly weaker $U\text{-}O_{ax}$ and stronger $U\text{-}O_{eq}$ bonds. These may be due to its resolution of identity (RI) approximation. But these differences are still small in a relative sense when compared to Gaussian 09 and ParaGauss. ADF, using the Slater type basis sets, gives longer bond lengths for $U\text{-}O_{ax}$ and $U\text{-}O_{eq}$. However, the results from ADF are very close to the results from QC programs discussed above that are using Gaussian type basis sets. The reproducibility of the results appears

to be generally high. The largest deviations among the programs are 0.011 Å for the bond distances and 15 cm^{-1} for the frequencies. The former comes from weak U-O_{eq} bonds in $UO_2(H_2O)_5^{2+}$ using the PBE functional. This is understandable since the U-O_{eq} bonds of uranyl hydrate can be very flexible here. For these weakly bound ligands, the different starting structures and geometry optimize schemes may converge to different potential minima with similar energies. By contrast, in the case of $UO_2(CH_3COO)_3^-$), bidentate acetates are rigidly bound to uranyl with little flexibility in binding, which results in smaller differences for most functionals. When it comes to the case of aqueous phase calculations, the largest deviations for the bond lengths and frequencies are 0.023 Å and 33 cm^{-1}, respectively. These are almost twice as large as those of the corresponding gas phase calculations. This is presumably due to different solvation models and corresponding settings in different programs, which can further interact with starting different starting structures and geometry optimize schemes. However, we should bear in mind that the experimental errors for the EXAFS measurements are in the order of 0.02 Å. Thus, we can conclude that the deviations among different quantum chemistry programs are at the level of the experimental errors.

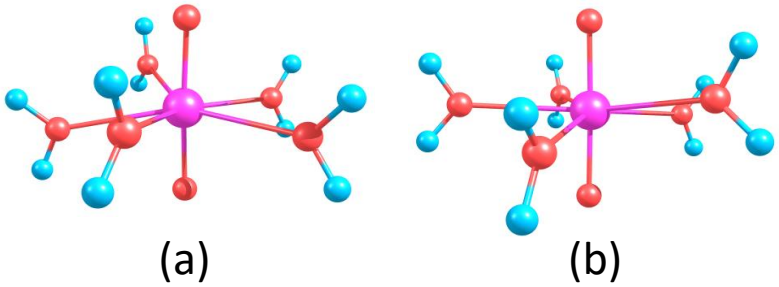

Figure 2.3 Optimized structures (ADF/TZ2P/BLYP) of RR1. (a) in gas phase and (b) in solvent.

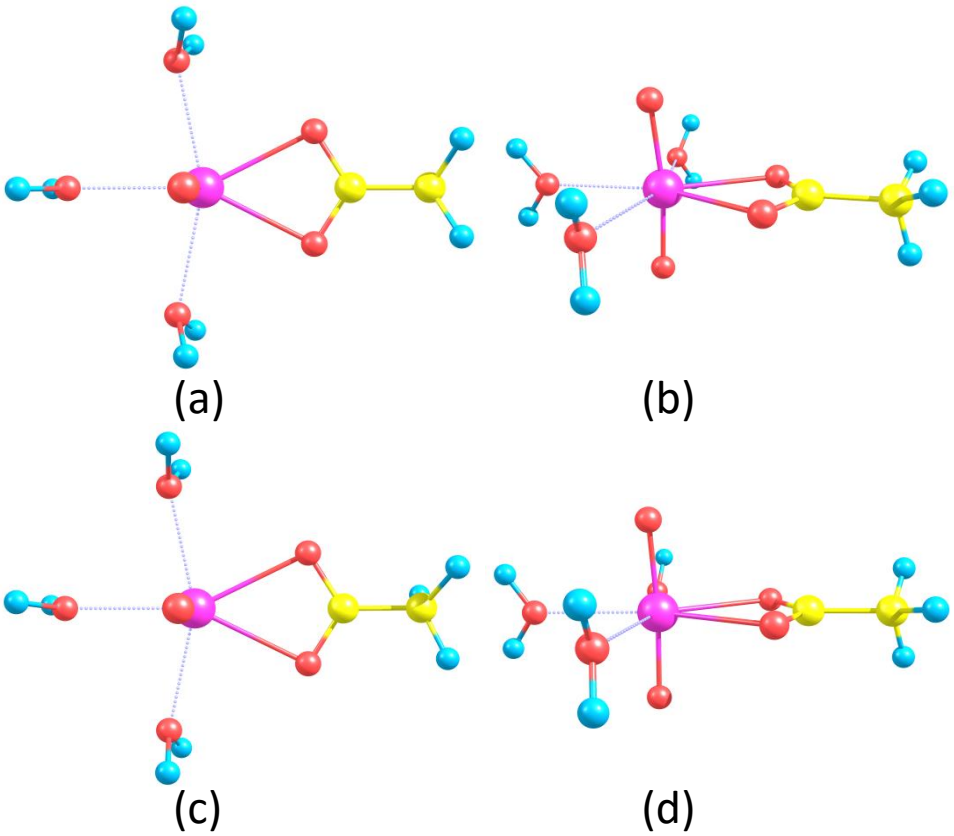

Figure 2.4 Optimized structures (ADF/TZ2P/BLYP) of RR2. (a) top view in gas phase, (b) side view in gas phase, (c) top view in in solvent, and (c) side view in in solvent.

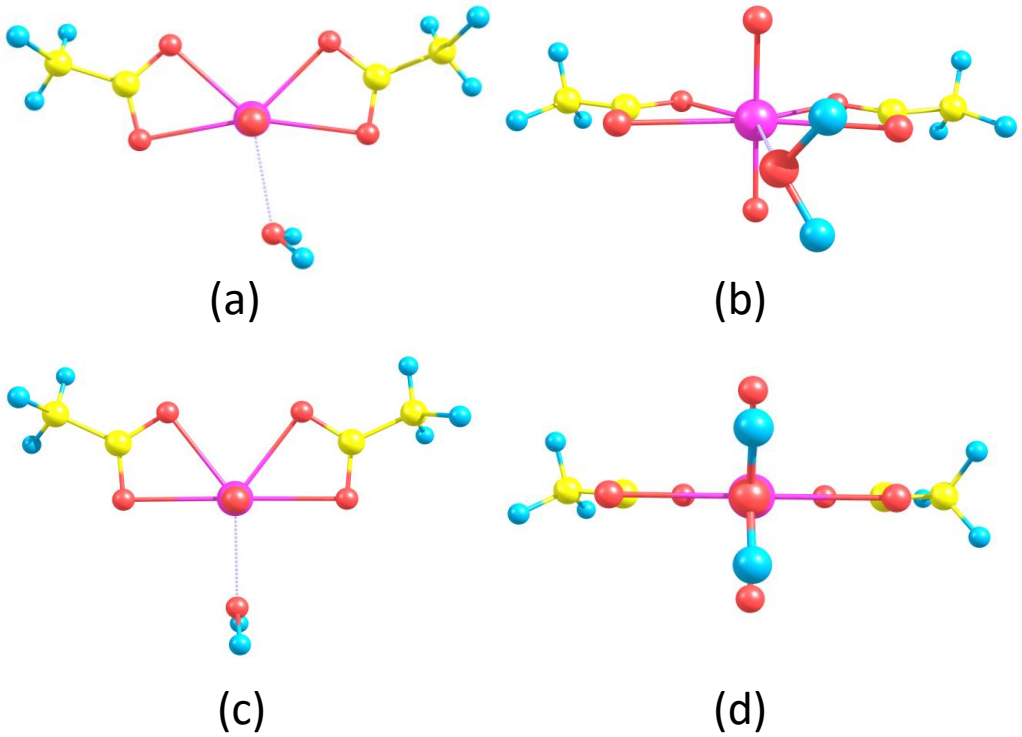

Figure 2.5 Optimized structures (ADF/TZ2P/BLYP) of RR3. (a) top view in gas phase, (b) side view in gas phase, (c) top view in in solvent, and (c) side view in in solvent.

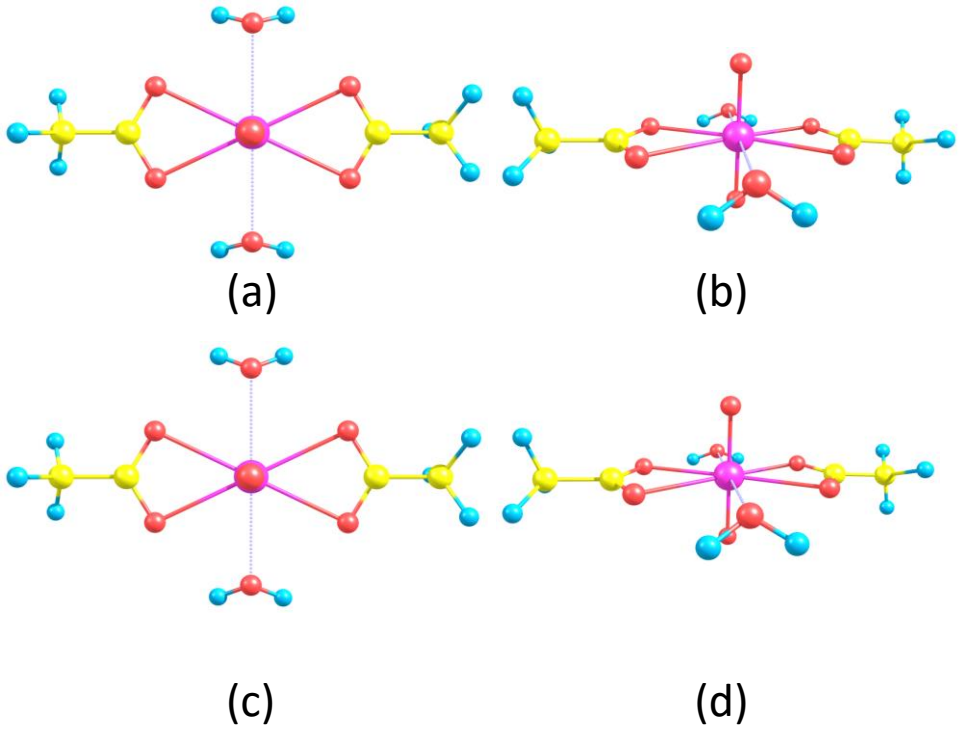

Figure 2.6 Optimized structures (ADF/TZ2P/BLYP) of RR4. (a) top view in gas phase, (b) side view in gas phase, (c) top view in in solvent, and (c) side view in in solvent.

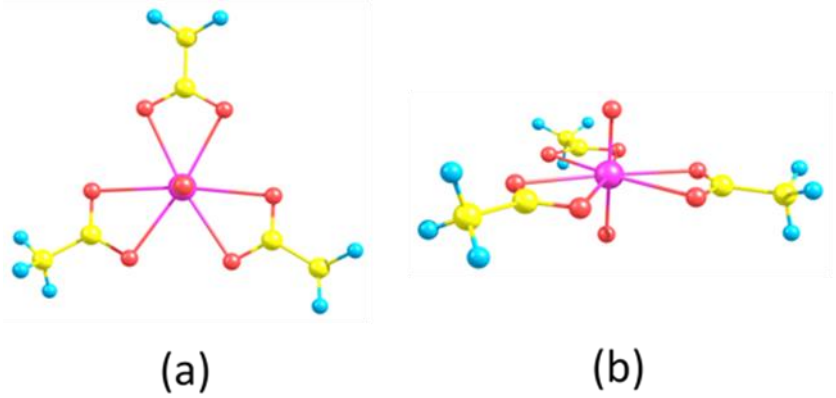

Figure 2.7 Optimized structures (ADF/TZ2P/BLYP) of RR5. (a) top view in gas phase, (b) side view in gas phase

Figure 2.3 to **Figure 2.7** show optimized structures (ADF/TZ2P/BLYP) from RR1 to RR5. As in an earlier study[25], the penta-aquo complex RR1 shows a structure that is slightly distorted from C_5 symmetry both in gas phase and solvent model. RR2 replaces two water molecules by one acetic acid ligand, which forms geometries very close to C_s symmetry both in gas phase and solvent model. When we continue to replace waters by acetic acid, we get RR3. Interestingly, in solvent model RR3 tends to keep C_s symmetry, however in gas phase the single water molecule is distorted and forms hydrogen bonds [RR3(a) in **Figure 2.5**]. All functionals except B3LYP result in uneven O=U=O bond lengths in gas phase. By contrast, all structures in solvent model give equal (even) O=U=O bond lengths. RR4 has one more water molecule then RR3, and the ligand environment around uranyl becomes crowded. The two water molecules tend to generate hydrogen bonds to acetic acid ligands and form a structure of C_s or C_{2v} symmetry. Similar to RR3, we find uneven O=U=O bond lengths in the gas phase and even O=U=O bond lengths in solvent model except for O3LYP that gives a 0.001Å difference. The structures of RR5 only have three bidentate acetates which are close to C_3 symmetry.

Tables 2.5 to **2.9** show the summarized calculated bond lengths from RR1 to RR5 both in gas phase and solvent model by ADF which may help us to better investigate the performance of different functionals. The calculated U-O_{ax} and U-O_{ac} bond lengths show an increasing trend from RR1 to RR5. The corresponding O=U=O $\nu 1$ and $\nu 3$ stretching vibrational frequencies show a decreasing trend due to the change of the U-O_{ax} bond lengths. However, it is very difficult to obtain a clear trend of the U-O_w bond lengths due to different bonding models and convergence to different minima on the potential energy surface as discussed above. **Tables 2.5** to **2.9** clearly show that pure GGAs tend to give longer bonds; on the contrary, Hybrid GGAs and Hybrid Meta

Table 2.5 Average U-O/U-C bond distances (Å) and O=U=O ν_1 and ν_3 vibrational frequency (cm^{-1}) of $UO_2(H_2O)_5^{2+}$ in both gas phase and solvent model using the identical DFT functionals and basis sets.

RR1 ($UO_2(H_2O)_5^{2+}$)					
		distance		frequency	
	theory	U-O_{ax}	U-O_w	sym	asym
Gas	PBE	1.768	2.491	892	984
	BLYP	1.785	2.520	865	957
	OLYP	1.750	2.542	915	1010
	PBE0	1.734	2.477	981	1064
	B3LYP	1.753	2.497	937	1024
	O3LYP	1.731	2.375	965	1052
	M06	1.727	2.492	998	1078
	M06L	1.740	2.507	948	1036
Sol	PBE	1.779	2.453	865	921
	BLYP	1.768	2.490	891	952
	OLYP	1.741	2.345	938	982
	PBE0	1.742	2.444	953	991
	B3LYP	1.762	2.460	912	954
	O3LYP	1.759	2.496	887	946
	M06	1.736	2.454	971	1002
	M06L	1.750	2.464	916	958

1) O_{ax} and O_w for oxygen in urania and water, respectively.
2) C_{car} and C_{me} for the carbon in the carboxyl and methyl, respectively.

Table 2.6 Average U-O/U-C bond distances (Å) and O=U=O ν_1 and ν_3 vibrational frequency (cm^{-1}) of $UO_2(H_2O)_3(Ac)_1^+$ in both gas phase and solvent model using the identical DFT functionals and basis sets.

RR2 ($UO_2(H_2O)_3(Ac)_1^+$)									
		distance						frequency	
	theory	U-O_{ax}	U-O_{w1}	U-O_{w2}	U-O_{ac}	U-C_{car}	U-C_{me}	sym	asym
Gas	PBE	1.787	2.524	2.534	2.3553	2.760	4.249	857	943
	BLYP	1.805	2.552	2.562	2.383	2.793	4.290	830	915
	OLYP	1.769	2.607	2.624	2.3548	2.761	4.253	876	966
	PBE0	1.751	2.502	2.522	2.339	2.732	4.214	940	1021
	B3LYP	1.771	2.525	2.546	2.360	2.760	4.249	900	983
	O3LYP	1.745	2.393	2.402	2.292	2.684	4.133	938	1021
Sol	PBE	1.794	2.457	2.459	2.403	2.805	4.295	832	884
	BLYP	1.813	2.479	2.478	2.430	2.838	4.338	803	854
	OLYP	1.775	2.517	2.536	2.408	2.811	4.305	851	908
	PBE0	1.755	2.436	2.450	2.391	2.782	4.267	919	955
	B3LYP	1.776	2.459	2.461	2.415	2.813	4.305	879	919
	O3LYP	1.751	2.342	2.346	2.326	2.718	4.169	912	955

1) O_{ax}, O_{ac}, and O_w for oxygen in urania , carboxyl and water, respectively.
2) C_{car} and C_{me} for the carbon in the carboxyl and methyl, respectively.

Table 2.7 Average U-O/U-C bond distances (Å) and O=U=O ν_1 and ν_3 vibrational frequency (cm^{-1}) of $UO_2(H_2O)_1(Ac)_2$ in both gas phase and solvent model using the identical DFT functionals and basis sets.

RR3 ($UO_2(H_2O)(Ac)_2$)										
		distance							frequency	
	theory	U-O_{ax}	U-O_{ac}	U-O_{ac1}	U-O_{ac2}	U-O_w	U-C_{car}	U-C_{me}	sym	asym
Gas	PBE	1.794	2.424	2.389	2.459	2.569	2.802	4.303	841	927
	BLYP	1.816	2.444	2.405	2.484	2.598	2.829	4.339	807	891
	OLYP	1.780	2.533	2.672	2.395	2.471	2.813	4.319	850	940
	PBE0	1.756	2.408	2.377	2.439	2.518	2.778	4.271	923	1004
	B3LYP	1.780	2.426	2.392	2.461	2.567	2.801	4.302	879	961
	O3LYP	1.749	2.350	2.321	2.379	2.448	2.725	4.184	921	1006
Sol	PBE	1.806	2.423	2.430	2.416	2.445	2.817	4.313	809	857
	BLYP	1.825	2.464	2.470	2.459	2.442	2.850	4.354	779	827
	OLYP	1.787	2.481	2.517	2.445	2.436	2.835	4.334	824	879
	PBE0	1.765	2.406	2.409	2.403	2.426	2.792	4.279	894	928
	B3LYP	1.786	2.432	2.437	2.427	2.447	2.823	4.318	854	893
	O3LYP	1.760	2.340	2.345	2.334	2.344	2.724	4.177	889	930

1) O_{ax}, O_{ac}, and O_w for oxygen in urania , carboxyl and water, respectively.
2) C_{car} and C_{me} for the carbon in the carboxyl and methyl, respectively.

Table 2.8 Average U-O/U-C bond distances (Å) and O=U=O ν_1 and ν_3 vibrational frequency (cm^{-1}) of $UO_2(H_2O)_2(Ac)_2$ in both gas phase and solvent model using the identical DFT functionals and basis sets.

RR4 ($UO_2(H_2O)_2(Ac)_2$)								
		distance					frequency	
	theory	U-O_{ax}	U-O_{ac}	U-O_w	U-C_{car}	U-C_{me}	sym	asym
Gas	PBE	1.796	2.472	2.580	2.855	4.360	837	925
	BLYP	1.813	2.500	2.607	2.887	4.402	810	897
	OLYP	1.777	2.487	2.697	2.872	4.380	855	947
	PBE0	1.758	2.454	2.548	2.830	4.326	920	1001
	B3LYP	1.778	2.479	2.575	2.860	4.364	882	965
	O3LYP	1.752	2.385	2.425	2.758	4.219	917	1000
Sol	PBE	1.808	2.463	2.556	2.862	4.358	802	850
	BLYP	1.827	2.491	2.586	2.894	4.399	774	822
	OLYP	1.787	2.484	2.670	2.883	4.384	822	877
	PBE0	1.767	2.451	2.525	2.842	4.329	888	920
	B3LYP	1.788	2.475	2.552	2.871	4.366	849	886
	O3LYP	1.764	2.371	2.407	2.759	4.212	879	918

1) O_{ax}, O_{ac}, and O_w for oxygen in urania , carboxyl and water, respectively.
2) C_{car} and C_{me} for the carbon in the carboxyl and methyl, respectively.

Table 2.9 Average U-O/U-C bond distances (Å) and O=U=O ν_1 and ν_3 vibrational frequency (cm^{-1}) of $UO_2(Ac)_3^-$ in both gas phase and solvent model using the identical DFT functionals and basis sets.

RR5 ($UO_2(Ac)_3^-$)							
		distance				frequency	
	theory	U-O_{ax}	U-O_{ac}	U-C_{car}	U-C_{me}	sym	asym
Gas	PBE	1.805	2.514	2.878	4.397	817	903
	BLYP	1.825	2.539	2.910	4.438	787	871
	OLYP	1.787	2.550	2.917	4.440	832	923
	PBE0	1.766	2.492	2.852	4.361	898	977
	B3LYP	1.787	2.519	2.884	4.401	860	942
	O3LYP	1.760	2.407	2.763	4.239	895	976
	M06	1.759	2.510	2.866	4.371	914	991
	M06L	1.779	2.515	2.873	4.381	850	937
Sol	PBE	1.818	2.482	2.877	4.377	784	829
	BLYP	1.838	2.510	2.909	4.418	758	801
	OLYP	1.797	2.520	2.915	4.421	802	854
	PBE0	1.775	2.465	2.852	4.344	869	901
	B3LYP	1.797	2.490	2.883	4.382	832	866
	O3LYP	1.772	2.381	2.766	4.224	862	901
	M06	1.766	2.484	2.867	4.356	886	916
	M06L	1.790	2.486	2.871	4.361	816	855

3) O_{ax} and O_{ac} for oxygen in urania and carboxyl, respectively.

1) C_{car} and C_{me} for the carbon in the carboxyl and methyl, respectively.

GGA tend to give shorter bonds. The COSMO solvent model tends to provide shorter bonds and lower frequencies compared with gas phase calculations. These observations confirm the trends discussed above. All the U-O_{ax} bonds except in RR1 are both in gas phase and solvent model following the same trend which is OLYP < PBE < BLYP. Interestingly, their corresponding Hybrid GGAs follow the same trend,i.e. O3LYP<PBE0<B3LYP from RR2 to RR5. Moreover, for U-O_{ac} and U-O_w in RR2 to RR5, Hybrid GGAs also follow the same trend. On the other hand, for the U-O_{ac} and U-O_w in RR2 to RR5, pure GGAs follow the trend of OLYP<BLYP< PBE except for U-O_{ac} in RR4. This counterexample may be due to hydrogen bonds and steric effects. The difference between pure GGAs and Hybrid GGAs can be explained by the HF exchange helping the hybrid functionals to describe weak bonds better.

For the reaction

$$UO_2(H_2O)_5^{2+} + 3\ CH_3COO^- \rightarrow UO_2(CH_3COO)_3^- + 5\ H_2O \qquad (2.1)$$

we calculated the reaction energies (ΔG) using different functionals in both gas phase and solvent model. The results are shown in **Tables 2.3** and **2.4**. The reaction was calculated to be exothermic by 378.70 – 414.04 kcal·mol^{-1} and 80.99 – 98.95 kcal·mol^{-1} for gas phase and solvent model respectively. Reproducibility of the results of ParaGauss and Gaussian 09 is relatively good. Gaussian 09's results are slightly higher than those of ParaGauss except for the Meta GGA. Turbomole and ADF give the lowest and highest reaction energies respectively. Generally speaking, pure GGAs tend to give higher reaction energies compare with Hybrid GGA as well as M06L (Meta GGA) gives higher reaction energies then M06 (Hybrid Meta GGA). Hybrid GGAs tend to follow the trends like PBE0>B3LYP> O3LYP. The differences between different programs in gas phase are relatively small. However, for solvent models, the deviations are further exaggerated, similarly to the bond lengths effects discussed above. When we look into

the ADF results, the differences between different functionals in gas phase are very small. But these differences become more significant after applied solvent effect.

Table 2.10 Calculated NMR shift (vs TMS) of the ^{1}H and ^{13}C in complexes RR1 to RR5 using ADF.

			NMR(ppm)							
			H_w	$H_{w\text{-}so}$	H_{me}	$H_{me\text{-}so}$	C_{car}	$C_{car\text{-}so}$	C_{me}	$C_{me\text{-}so}$
RR1	Gas	PBE	7.3	7.8	-	-	-	-	-	-
		BLYP	7.5	7.9	-	-	-	-	-	-
		OLYP	7.1	7.5	-	-	-	-	-	-
	Sol	PBE	7.6	8.0	-	-	-	-	-	-
		BLYP	7.7	8.2	-	-	-	-	-	-
		OLYP	8.0	8.5	-	-	-	-	-	-
RR2	Gas	PBE	5.9	6.0	2.9	3.7	212.6	213.7	24.4	27.3
		BLYP	6.0	6.1	2.9	3.8	217.4	219.1	25.0	28.9
		OLYP	5.2	5.2	2.9	3.8	206.8	207.7	23.8	26.3
	Sol	PBE	7.3	8.0	2.7	3.4	212.5	213.6	26.1	29.5
		BLYP	7.4	8.2	2.7	3.6	217.1	218.4	26.9	30.3
		OLYP	6.6	7.2	2.7	3.6	206.2	207.5	25.8	28.8
RR3	Gas	PBE	4.5	4.4	2.5	2.8	200.9	201.1	24.1	28.3
		BLYP	5.2	5.1	2.5	2.8	206.0	206.9	24.9	29.1
		OLYP	4.1	4.0	2.4	2.8	196.4	197.0	24.3	28.1
	Sol	PBE	7.4	7.9	2.6	3.0	208.9	210.0	25.4	29.6
		BLYP	7.8	7.9	3.0	3.1	213.6	214.3	29.4	30.2
		OLYP	6.5	6.8	2.6	3.0	202.8	204.1	25.6	29.5
RR4	Gas	PBE	4.4	4.3	2.4	2.7	201.4	202.2	24.9	28.6
		BLYP	4.4	4.5	2.4	2.5	205.3	206.0	25.6	26.4
		OLYP	3.5	3.3	2.4	2.8	196.0	196.9	24.8	28.3
	Sol	PBE	4.2	4.0	2.5	3.1	202.4	203.5	26.1	29.6
		BLYP	5.1	5.0	2.5	3.1	212.8	214.0	27.0	30.9
		OLYP	5.0	4.9	2.5	3.0	208.7	209.8	26.2	30.0
RR5	Gas	PBE	-	-	2.1	2.3	195.6	196.3	24.2	29.0
		BLYP	-	-	2.1	2.3	199.2	199.9	24.9	29.9
		OLYP	-	-	2.1	2.3	190.3	191.2	24.1	28.7
	Sol	PBE	-	-	2.5	2.8	208.2	209.3	26.0	30.2
		BLYP	-	-	2.5	2.9	212.1	213.3	26.7	31.1
		OLYP	-	-	2.4	2.8	201.5	202.7	25.9	29.9

1) H_w and H_{me} for hydrogen in water and methyl.
2) C_{car} and C_{me} for the carbon in the carboxyl and methyl, respectively
3) Subscript SO for including Spin-Orbit.

Table 2.10 shows the calculated NMR chemical shifts by ADF in both gas phase and solvent model at the scalar ZORA and spin-orbital ZORA level. Spin-orbit effects make a positive contribution to the NMR chemical shifts except for the water ^{1}H shift in RR4 and RR3 in gas phase. The large downfield shifts in the water ^{1}H NMR chemical shift of RR4 and RR3 in gas phase due to hydrogen bonds are formed, as discussed above. Calculations show that there are very small spin-orbit contributions in all complexes, due to the low s bonding character at the U(VI) center. Interestingly, in the calculations, the methyl groups have relative large spin-orbit contributions which indicates that there are some long-range spin-spin coupling effects here. The NMR chemical shifts tend to shift upfield after applied solvent effect. **Table 2.11** compares Gaussian 09 and ADF data as well as pure GGAs and corresponding Hybrid GGAs. From **Table 2.11**, the Gaussian 09 and ADF results are very similar, although ADF tends to give slightly larger values. There is no significantly different between Hybrid GGAs and pure GGAs. Comparing with experimental chemical shifts in this study, **Figures 2.8** and **2.9**, we found all methods can give reasonable results. Pure GGAs tend to give good results in gas phase at the scalar ZORA level, which may due to better error cancelation. M06L gives very good agreement with experiment both in gas phase and solvent model using SC-ECP.

Table 2.11 Calculated NMR chemical shift (vs TMS) by different programs of the ^{1}H and ^{13}C in complexes RR1 and RR5.

			RR1				RR5			
			ppm				ppm			
	theory		H_w	$H_{w\text{-}so}$	H_{me}	$H_{me\text{-}so}$	C_{car}	$C_{car\text{-}so}$	C_{me}	$C_{me\text{-}so}$
	BP86	G	7.3		2.0		187.6		23.8	
	PBE	A	7.3	7.8	2.1	2.3	195.6	196.3	24.2	29.0
	PBE0	G	6.7		2.2		189.5		24.1	
	PBE0	A	6.9	7.2	2.2	2.2	194.8	194.0	25.1	28.8
	BLYP	A	7.5	7.9	2.1	2.3	199.2	199.9	24.9	29.9
gas	B3LYP	G	6.9		2.1		191.9		24.6	
	B3LYP	A	7.2	7.6	2.2	2.2	197.8	197.1	25.4	29.4
	OLYP	A	7.1	7.5	2.1	2.3	190.3	191.2	24.1	28.7
	O3LYP	A	7.9	8.4	2.2	2.3	196.0	195.9	23.6	28.1
	M06L	G	7.0		2.1		179.2		23.5	
	M06	G	7.0		2.2		190.7		24.4	
	BP86	G	7.2		2.3		194.1		25.9	
	PBE	A	7.6	8.0	2.5	2.8	208.2	209.3	26.0	30.2
	PBE0	G	6.6		2.5		197.7		24.8	
	PBE0	A	7.2	7.5	2.6	2.6	206.6	206.1	26.7	29.8
	BLYP	A	7.7	8.2	2.5	2.9	212.1	213.3	26.7	31.1
sol	B3LYP	G	6.8		2.4		200.4		25.3	
	B3LYP	A	7.4	7.8	2.6	2.7	209.8	209.4	27.1	30.4
	OLYP	A	7.3	7.5	2.4	2.8	201.5	202.7	25.9	29.9
	O3LYP	A	8.0	8.5	2.6	2.8	208.5	208.7	25.2	29.0
	M06L	G	7.0		2.4		188.1		24.8	
	M06	G	6.9		2.4		198.7		23.8	

1) G: Gaussian 09, A: ADF.
2) H_w for hydrogen in water.
3) C_{car} and C_{me} for the carbon in the carboxyl and methyl, respectively
4) Subscript SO for including Spin-Orbit.

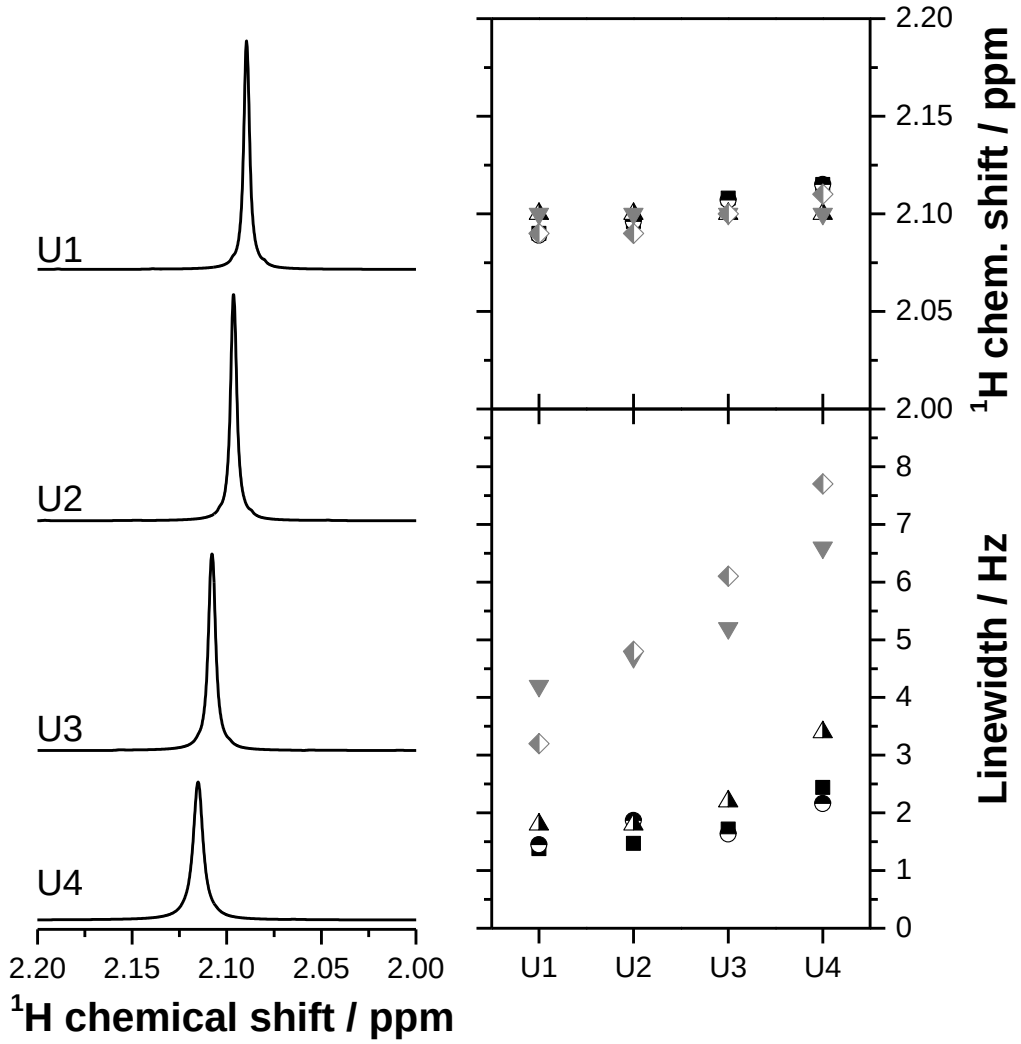

Figure 2.8 ^{1}H NMR spectroscopic data. Representative data of the methyl spectral region of samples U1-U4 (left). Comparison of chemical shift (right, top) and linewidths (right, below) for samples U1–U4 obtained by different RRT participants.

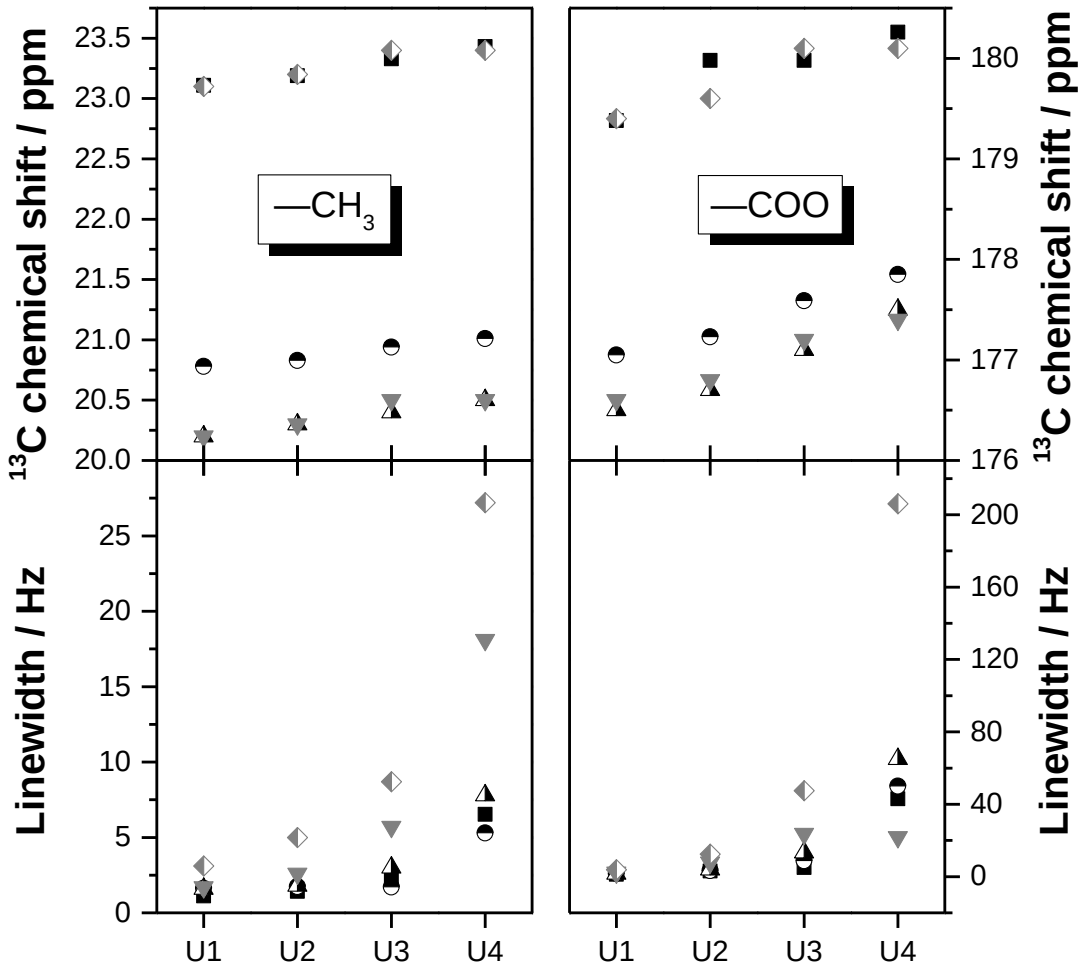

Figure 2.9 ^{13}C NMR spectroscopic data of the methyl (left) and carboxyl region (right). Comparison of chemical shift (top) and linewidths (below) for samples U1–U4 obtained by different RRT participants. For the chemical shift of U4 a deprotonation correction was done according to the spectra obtained for blank samples at equal conditions.

Table 2.12 summarizes the calculated lowest excitation energies from ADF in both gas phase and solvent model at the scalar ZORA and spin-orbital ZORA level. From Table 2.12, we can tell that Hybrid GGAs tend to give higher excitation energies then pure GGAs. When including spin-orbital effects, all methods tend to give lower excitation energies. Solvent effects, on the other hand, tend to increase the lowest energies compared to gas phase calculations. For pure GGAs, PBE always give highest excitation energies compared to BLYP and OLYP. PBE's corresponding Hybrid GGA, PBE0, also give the highest energies among the Hybrid GGAs. The calculated excitation energies of Hybrid GGAs follow the trend B3LYP<O3LYP<PBE0, except for the lowest triplet excitations for which B3LYP and O3LYP are very close to each other. **Table 2.13** compares Gaussian 09, Turbomole and ADF data as well as pure GGAs and the corresponding Hybrid GGAs. In the gas phase, Turbomole and Gaussian 09 give almost the same energies, but not for the BP86 functional. ADF, however, tends to give slightly larger values. Generally speaking, Meta GGAs and Hybrid GGAs give similar results. By contrast, pure GGA tend to give lower energies than Meta GGAs and Hybrid GGAs. This also can be found in ADF's data from RR1 to RR5 in **Table 2.12**. **Figure 2.10** shows the lowest 40 excitations calculated with pure GGAs in this study. These diagrams show strong spin-orbital effects on the excitation energies. Since the lowest excitation energy may not be the lowest one that can be observed in experiment, we look into the strongest peak in **Figure 2.10**. Comparing with the experimental data, **Figure 2.11**, we note that PBE in solvent model at spin-orbital ZORA level shows the best result.

Table 2.12 Calculated excitation energies by ADF of complexes RR1 to RR5

			excitation		
			eV		
			lowest singlet	lowest triplet	SO
RR1	Gas	PBE	2.96	2.52	2.12
		BLYP	2.74	2.46	2.02
		OLYP	2.50	2.47	2.06
	Sol	PBE	2.89	2.61	2.26
		BLYP	2.70	2.64	2.26
		OLYP	3.61	2.79	2.46
RR2	Gas	PBE	2.56	2.51	2.12
		BLYP	2.35	2.30	1.97
		OLYP	2.40	2.35	2.00
	Sol	PBE	2.65	2.59	2.21
		BLYP	2.46	2.42	2.07
		OLYP	2.47	2.43	2.06
RR3	Gas	PBE	2.64	2.52	2.12
		BLYP	2.59	2.51	2.04
		OLYP	2.52	2.47	2.03
	Sol	PBE	2.64	2.57	2.19
		BLYP	2.49	2.43	2.07
		OLYP	2.50	2.43	2.05
RR4	Gas	PBE	2.59	2.51	2.15
		BLYP	2.50	2.42	2.03
		OLYP	2.43	2.35	2.02
	Sol	PBE	2.53	2.46	2.12
		BLYP	2.44	2.38	2.08
		OLYP	2.34	2.27	1.97
RR5	Gas	PBE	2.60	2.54	2.19
		BLYP	2.44	2.39	2.07
		OLYP	2.31	2.26	1.95
	Sol	PBE	2.52	2.46	2.12
		BLYP	2.36	2.31	1.99
		OLYP	2.28	2.24	1.92

1) Subscript SO for including Spin-Orbit.

Table 2.13 Calculated excitation energies by different programs of complexes RR1 and RR5

			RR1			RR5		
			eV			eV		
	theory		lowest singlet	lowest triplet	SO	lowest singlet	lowest triplet	SO
gas	BP86	T	2.95	2.23		2.65	2.44	
	BP86	G	2.75	2.25		2.63	2.49	
	PBE	T	2.96	2.24		2.66	2.44	
	PBE	A	2.96	2.52	2.12	2.60	2.54	2.19
	PBE0	T	3.58	2.50		3.57	2.68	
	PBE0	G	3.58	2.55		3.58	2.73	
	PBE0	A	3.67	2.77	2.46	3.64	2.93	2.57
	B3LYP	T	3.35	2.47		3.38	2.66	
	B3LYP	G	3.36	2.51		3.71	2.70	
	B3LYP	A	3.47	2.70	2.39	3.45	2.85	2.49
	BLYP	A	2.74	2.46	2.02	2.44	2.39	2.07
	O3LYP	A	3.60	2.76	2.44	3.56	2.97	2.56
	OLYP	A	2.50	2.47	2.06	2.31	2.26	1.95
	TPSSh	T	3.26	2.25		3.30	2.48	
	M06L	G	3.04	2.31		2.87	2.55	
	M06L	A	3.22	2.93	2.64	3.03	3.00	2.64
	M06	G	3.15	2.39		3.24	2.54	
	M06	A	3.81	2.83	2.52	3.89	2.98	2.62
aq.	BP86	G	2.86	2.25		2.48	2.41	
	PBE	A	2.89	2.61	2.26	2.52	2.46	2.12
	PBE0	G	3.50	2.55		3.62	2.75	
	PBE0	A	3.80	2.84	2.52	3.69	2.97	2.59
	B3LYP	G				3.44	2.70	
	B3LYP	A	3.61	2.77	2.44	3.50	2.89	2.50
	BLYP	A	2.70	2.64	2.26	2.36	2.31	1.99
	O3LYP	A	3.61	2.79	2.46	3.55	3.01	2.56
	OLYP	A	2.81	2.50	2.10	2.28	2.24	1.92
	M06L	G	2.99	2.31		2.79	2.57	
	M06L	A	3.45	2.99	2.68	2.93	2.89	2.57
	M06	G	3.09	2.37		3.28	2.54	
	M06	A	3.87	2.88	2.56	3.93	3.01	2.63

1) G: Gaussian 09, A: ADF
2) Subscript SO for including Spin-Orbit.

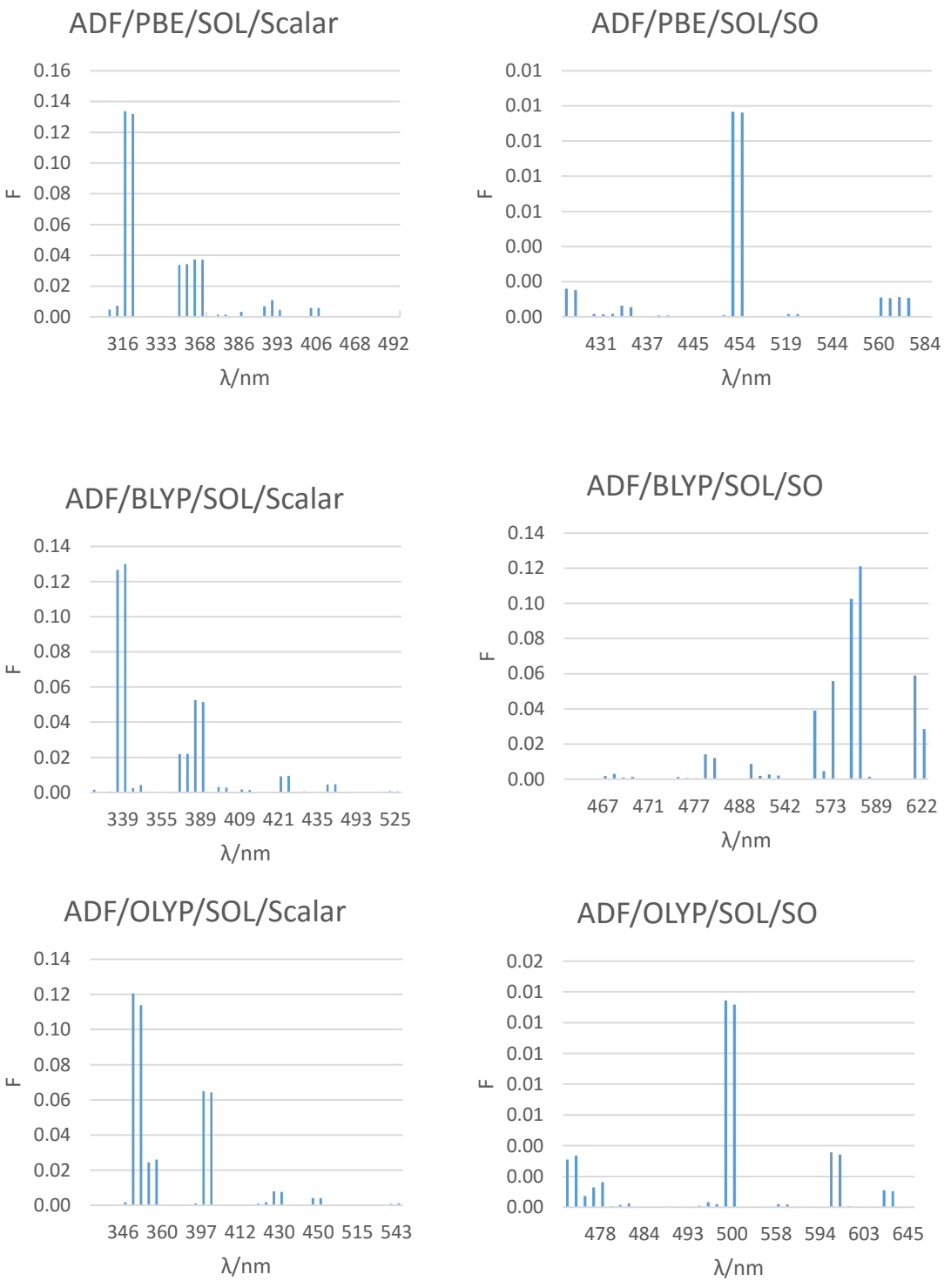

Figure 2.10 Calculated UV spectrum of RR5 by different functionals in solvent model.

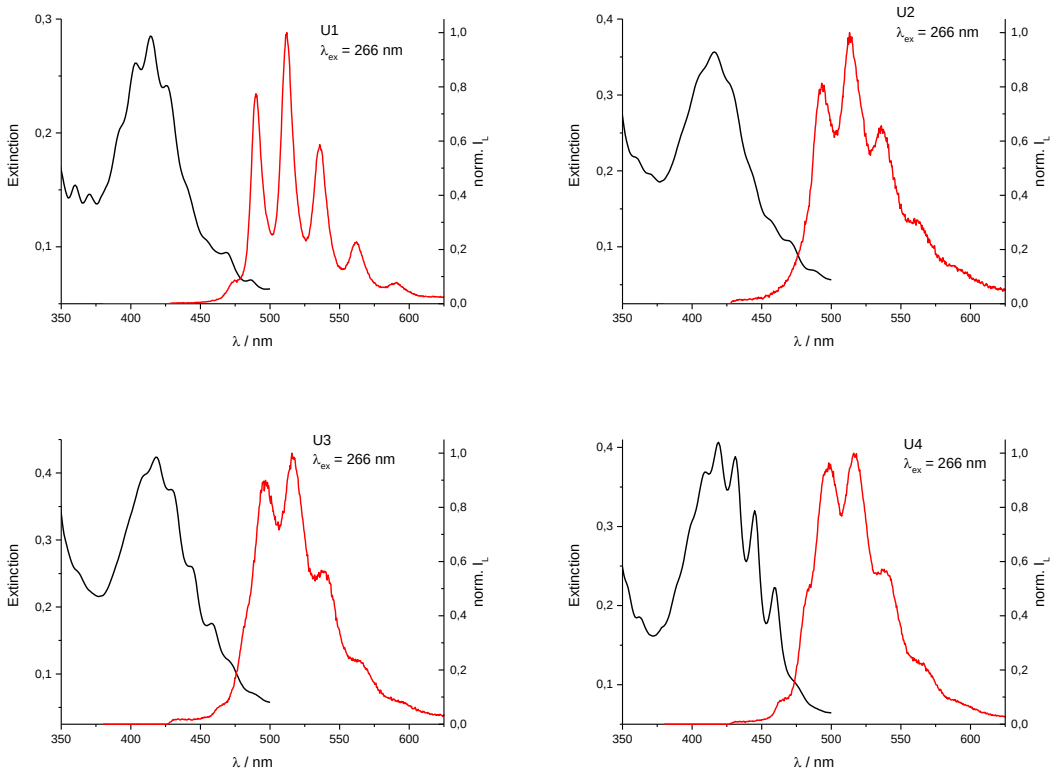

Figure 2.11 Absorption (black) and normalized emission (red) spectra of samples U1 – U4. The emission spectra were recorded at room temperature with λ_{ex} = 266 nm and with a delay of δt = 125 ns after the laser pulse using a gate width of Δt = 1.5 µs.

2.7. Conclusions

In this study, we have investigated the mixed uranyl water and acetic acid complexes from RR1 to RR5 by different DFT methods in order to evaluate their performance with various sets of methodology and programs.

We used two modern methods including the SC-ECP and all–electron ZORA approach for relativistic effects. For the latter, we also included spin-orbit effects by using the spin-orbit ZORA approach for properties like NMR chemical shifts and excitation energies. The calculations show that these two fundamentally different relativistic methods give essentially

similar results for a wide range of properties. Some exceptions may be due to convergence to different local minima. So we can draw a conclusion that both of these relativistic methods are valid for systems like U(VI) with a $5f^0$ electronic configuration and therefore spin-orbit effects can be neglected when deep-core effects are not included.

For the properties like NMR chemical shifts and excitation energies, spin-orbit effects become important. Comparing the results of scalar ZORA and spin-orbit ZORA, the spin-orbit contributions in the NMR chemicals shift are relative small. It is noteworthy that, after applying spin-orbit ZORA, the results become worse compared with the experimental data. This may be due to error cancelations. On the other hand, for excitation energies, there are significantly differences between scalar ZORA and spin-orbit ZORA. The latter shows better results when compared with experimental data. Thus, it is necessary to include spin-orbit effects for excitation calculations.

We compared the uranyl species including first solvation sphere in gas phase as well as in continuum solvation models such as COSMO, PCM etc. These continuum solvation models give results with the deviations between the different methods and codes becoming larger in aqueous phase calculations. This can be explained by different solvation models as well as different optimization schemes in the solvation models which finally yields different minima especially for RR1. The solvent environment strongly influences most of the properties in this study. For example, the solvent models improve the performances of most functionals for predicting bond lengths in this study. What's more, solvation effects stabilize the left hand side of the formation reaction Eq. (1.1), which has smaller size and usually larger charges, thus reducing the reaction energies by almost one order of magnitude.

10 different widely used DFT methods as well as the MP2 method have been compared in this study. It is hard to give a clear answer for the best method in this case due to relative small sample size and experimental errors, as well as the fact that there are many factors that can affect the results. However, we can still draw a few qualitative conclusions. Hybrid and Meta GGAs tend to give shorter bond lengths, lower reaction energies and higher excitation energies. By contrast, pure GGAs tend to give longer bond lengths, higher reaction energies and lower excitation energies. MP2 and B3LYP are good to predict bond lengths, especially after applying solvent models at the latter. On the other hand, BLYP, OLYP and O3LYP usually give larger deviations of bond lengths than other functionals.

Overall the calculations using identical DFT functionals and basis set but different quantum chemistry programs yield very small deviations. We obtain particularly high reproducibility of the results especially for structures like RR5, which has less flexibility.

2.8. References

[1] Lucks C.; Rossberg A.; Tsushima, S.; Foerstendorf, H.; Scheinost A. C.; Bernhard G. *Inorg. Chem.* **2012**, *51*, 12288.
[2] Jiang, J.; Rao, L. F.; Di Bernardo, P.; Zanonato, P.; Bismondo, A. *J. Chem. Soc.*, *Dalton Trans.* **2002**, *8*, 1832.
[3] Bailey, E. H.; Mosselmans, J. F. W.; Schofield, P. F. *Geochim. Cosmochim. Acta.* **2004**, *68*, 1711.
[4] Kakihana, M.; Nagumo, T.; Okamoto, M.; Kakihana, H. *J. Phys. Chem.* **1987**, *91*, 6128.
[5] Quiles, F.; Burneau, A. *Vib. Spectrosc*. **1998**, *18*, 61.
[6] Gal, M.; Goggin, P. L.; Mink, *J. Spectrochim. Acta. Part A,* **1992**, *48*,121.
[7] Nguyen-Trung, C.; Begun, G. M.; Palmer, D. A. *Inorg. Chem*.**1992**, *31*, 5280.
[8] van Lenthe, E.; Baerends, E. J.; Snijders, J. G. *J. Chem. Phys.* **1993**, *99*, 4597.
[9] van Lenthe, E.; Baerends, E. J.; Snijders, J. G. *J. Chem. Phys.* **1994**, *101*, 9783.
[10] van Lenthe, E.; van Leeuwen, R.; Baerends, E. *J. Int. Quantum Chem.* **1996**, *57*, 281.
[11] van Lenthe, E.; Ehlers, A.; Baerends, E. J. *J. Chem. Phys.* **1999**, *110*, 8943.
[12] Küchle, W.; Dolg, M.; Stoll, H.; Preuss, H. *J. Chem. Phys.* **1994**, *100*, 7535.
[13] Cao, X.; Dolg, M., Relativistic pseudopotentials, in Barysz, M.; Ishikawa, Y. (Eds.), *Relativistic methods for chemists. Challenges and advances in computational physics*, vol. 10, Springer, Berlin, **2010**, 215.
[14] Han, Y.-K.; Hirao, K. *J. Chem. Phys.* **2000**, *113*, 7345.
[15] Han, Y. -K. *J. Comput. Chem.* **2001**, *22*, 2010.
[16] Schreckenbach, G.; Wolff, S. K.; Ziegler, T. *J. Phys. Chem. A* **2000**, *104*, 8244.
[17] Schreckenbach, G. *Int. J. Quantum Chem.* **2005**, *101*, 372.
[18] Straka, M.; Kaupp, M. *Chem. Phys.* **2005**, *311*, 45.
[19] Batista, E. R.; Martin, R. L.; Hay, P. J.; Peralta, J. E.; Scuseria, G. E. *J. Chem. Phys.* **2004**, *121*, 2144.
[20] Shamov A. G.; Schreckenbach G. *J. Phys. Chem. A* **2005**, *109*, 10961.
[21] Odoh, S. O.; Schreckenbach, G., *J. Phys. Chem. A* **2010**, *114*, 1957.

[22] Hay, P. J.; Martin, R. L.; Schreckenbach, G. *J. Phys. Chem. A* **2000**, *104*, 6259.
[23] Schreckenbach G.; Shamov G. A. *Acc. Chem. Res.* **2010**, *43*, 19.
[24] Moskaleva, L. V.; Kruger, S.; Sporl, A.; Rosch, N. *Inorg. Chem*. **2004**, 43, 4080.
[25] TURBOMOLE, a development of University of Karlsruhe and Forschungszentrum Karlsruhe GmbH, **1989-2007**, TURBOMOLE GmbH, since **2007**; available from http://www.turbomole.com.
[26] Gaussian 09, Revision E.01, M. J. Frisch, G. W. Trucks, H. B. Schlegel, G. E. Scuseria, M. A. Robb, J. R. Cheeseman, G. Scalmani, V. Barone, B. Mennucci, G. A. Petersson, H. Nakatsuji, M. Caricato, X. Li, H. P. Hratchian, A. F. Izmaylov, J. Bloino, G. Zheng, J. L. Sonnenberg, M. Hada, M. Ehara, K. Toyota, R. Fukuda, J. Hasegawa, M. Ishida, T. Nakajima, Y. Honda, O. Kitao, H. Nakai, T. Vreven, J. A. Montgomery, Jr., J. E. Peralta, F. Ogliaro, M. Bearpark, J. J. Heyd, E. Brothers, K. N. Kudin, V. N. Staroverov, R. Kobayashi, J. Normand, K. Raghavachari, A. Rendell, J. C. Burant, S. S. Iyengar, J. Tomasi, M. Cossi, N. Rega, J. M. Millam, M. Klene, J. E. Knox, J. B. Cross, V. Bakken, C. Adamo, J. Jaramillo, R. Gomperts, R. E. Stratmann, O. Yazyev, A. J. Austin, R. Cammi, C. Pomelli, J. W. Ochterski, R. L. Martin, K. Morokuma, V. G. Zakrzewski, G. A. Voth, P. Salvador, J. J. Dannenberg, S. Dapprich, A. D. Daniels, Ö. Farkas, J. B. Foresman, J. V. Ortiz, J. Cioslowski, and D. J. Fox, Gaussian, Inc., Wallingford CT, **2009**.
[27] Belling, Th.; Grauschopf, Th.; Krüger, S.; Nörtemann, F.; Staufer, M.; Mayer, M.; Nasluzov, V. A.; Birkenheuer, U.; Rösch, N., *Scientific Computing in Chemical Engineering II*, pp 66-73, Springer-Verlag Berlin Heidelberg (**1999**)
[28] Becke, A. D. *Phys. Rev. A* **1988**, *38*, 3098.
[29] Perdew, J. P. *Phys. Rev. B* **1986**, *33*, 8822.
[30] Perdew, J. P. *Phys. Rev. B* **1986**, *34*, 7406.
[31] Perdew, J. P.; Burke, K.; Ernzerhof, M. *Phys. Rev. Lett.* **1996**, *77*, 3865.
[32] Perdew, J. P.; Burke, K.; Ernzerhof, M. *Phys. Rev. Lett*. **1997**, *78*, 1396.
[33] Adamo, C.; Barone, V. *J. Chem. Phys.* **1999**, *110*, 6158.
[34] Becke, A. D. *J. Chem. Phys.* **1993**, *98*, 1372.
[35] Lee, C.; Yang, W.; Parr, R. G. *Phys. Rev. B* **1988**, *37*, 785.
[36] Zhao, Y.; Truhlar, D. G. *Theor. Chem. Acc.* **2008**, *120*, 215.
[37] Zhao, Y.; Truhlar, D. G. *J. Chem. Phys.* **2006**, *125*, 194101.
[38] Tao, J. M.; Perdew J. P.; Staroverov V. N.; Scuseria G. E. *Phys. Rev. Lett.* **2003**, *91*, 146401.
[39] Küchle, W.; Dolg, M.; Stoll, H.; Preuss, H. *J. Chem. Phys.* **1994**, *100*, 7535.
[40] Kendall R. A.; Dunning Jr. T. H.; Harrison R. J. *J. Chem. Phys.*, **1992**, *96*, 6796.
[41] Handy, N. C.; Cohen, A. *J. Mol. Phys.* **2001**, *99*, 403.
[42] Hoe, W.-M.; Cohen, A. J.; Handy, N. C. *Chem. Phys. Lett.* **2001**, *341*,319.
[43] Velde G.te; Bickelhaupt F.M.; Baerends E.J.; Fonseca Guerra C.; van Gisbergen S.J.A.; Snijders J.G.; Ziegler T. *J. Comput. Chem.* **2001**, *22*, 931
[44] Klamt, A.; Schüürmann, G. *J. Chem. Soc.*, *Perkin Trans*. **1993**, *2*, 799.
[45] Pye, C. C.; Ziegler, T. *Theor. Chem. Acc.* **1999**, *101*, 396.

Chapter 3 : A Comparative Scalar-Relativistic Study of the Performance of Modern Density Functionals for Uranium Compounds

3.1. Introduction

Density functional theory (DFT)[1] has become a powerful tool in theoretical actinide science. When regarding the size of real experimentally relevant actinide systems, DFT usually is the only practical method among other methods which can describe these systems correctly. The accuracy of DFT calculations can be very good once an appropriate approach of treating relativistic effects is applied. The previous theoretical work of our group shows small-core effective core potential methods (SC-ECP)[2] can give very close results[3,4] compared to the zeroth order regular approximation (ZORA)[5] and all-electron scalar methods[6]. On the other hand, the older large-core ECP (LC-ECP)[7] method is not recommend for use considering its consistently worse performances.[3,8,9] Spin-orbit effects are usually neglected in ECP methods. Clavaguera-Sarrio et al.[10] concluded that DFT, as a single-reference approach, appears to be sufficient for the

structural and vibrational behavior of the ground states of open-shell actinide molecules without including explicit account of spin-orbit coupling. The spin-orbit effects on the thermodynamics of actinide systems general are relatively small (about 4–5 kcal/mol) compared to the experimental error bars and/or divergences between different experimental results.[4] Due to the nature of approximate DFT, there is strong interest in developing new functionals or benchmarking extant functionals.[11, 12, 13] However the most favorite functional choice for theoretic actinide science is still not completely clear. The most widely used functionals in actinide science are B3LYP, PBE and PBE0. [3, 4, 7, 10, 14–26] In recent years, several groups attempted to quantify the performance of various functionals for predicting the properties in the theoretical actinide area. There is evidence[27, 28] that shows the limitations of these popular functionals for calculating actinide systems. On the other hand, the M06 functional shows advantages over B3LYP in the calculations of redox potentials[28], reactions, [29, 30] and geometries.[31] Thus, it is necessary to systematically test the performance of meta GGAs, such as the M06 family, comparing them to other GGAs and hybrid GGAs for actinide complexes.

The closed-shell uranium hexafluoride UF_6 is the one actinide molecule most studied both in experimentally and theoretically. On the other hand, just a few of the rest of the open-shell uranium fluoride UF_n and uranium chloride UCl_n series have been studied.[14] Because of the lack of experimental data, especially for bond lengths[32–37], high level *ab initio* calculations can be an alternative option. Due to MP2 showing somewhat "erratic" results for uranium oxofluoride compounds[38], CCSD(T), as the golden standard in theoretical chemistry, is the best choice here. Experimental vibrational frequency data of several uranium complexes are available. [4,14,18,20] Frequency scale factors are wildly used to yield better results both for vibrations and thermodynamics.[39] The only correction missing here is the error in vibrational

modes due to the harmonic oscillator approximation and the error from the functional itself. Frequency scale factors may help to correct both of them. It is interesting to investigate the performances of these factors in the actinide area since most of them were fitted for molecules with relatively light elements. The enthalpies of several gas-phase reactions of uranium complexes have been studied both experimentally and theoretically.[4,40,41] Note that Bross et al.[41] found thst the spin-orbit effects in CCSD(T) calculations of these gas-phase reactions are small (<1.3 Kcal/mol) compared to the experimental errors (2.9–6.6 Kcal/mol).

We would like to examine exactly how well the Minnesota functionals as well as other meta GGA functional perform in comparison to the B3LYP functional and other relative old GGAs and hybrid GGAs for gas-phase uranium chemistry. In this work, we systematically determine the crucial factors behind the performance of several density functionals in predicting the structure, vibrational frequencies and reaction energetics of actinide species using 22 different functionals as well as the CCSD(T) method.

3.2. Computational Details

All DFT calculations were performed using the NWChem 6[42]suite of programs. A total of 22 different functionals used in this work are listed in **Table 3.1**. The relativistic Stuttgart SC-ECP[2,43] and corresponding basis set were used for the uranium atom. The aug-cc-pVTZ basis was used for the main group elements. In addition, numerical integration of the exchange-correlation potential was specified to employ ultra-fine integration grids. In the *ab initio* Wave Function Theory（WFT) calculations, the coupled cluster with singles, doubles, and perturbative triples [CCSD(T)] method with the same basis sets and ECP as the DFT calculations was used as implemented in the MOLPRO 2012.1 program.[44,45]

Table 3.1 Functional types and corresponding percentage of HF exchange for 22 functionals used in this work.

Functional	*Functional type*	*percentage of HF exchange*	Ref.
PBE	Pure GGA	-	46, 47
PW91	Pure GGA	-	48 - 52
BP86	Pure GGA	-	53 - 55
BPW91	Pure GGA	-	50, 53, 56
BLYP	Pure GGA	-	57, 58
B3LYP	Hybrid GGA	20%	59, 60
PBE0	Hybrid GGA	25%	46, 47, 61
B1LYP	Hybrid GGA	25%	62
X3LYP	Hybrid GGA	21.80%	63
BHLYP	Hybrid GGA	50%	64
BeckeHandH	Hybrid GGA	50%	64
BHandH	Hybrid GGA	50%	64
M06-L	Meta GGA	-	65
M11-L	Meta GGA	-	66
TPSS	Meta GGA	-	67
M06	Hybrid Meta GGA	27%	68
M06-2X	Hybrid Meta GGA	54%	68
M06-HF	Hybrid Meta GGA	100%	69,70
M08-HX	Hybrid Meta GGA	52.23%	71
M08-SO	Hybrid Meta GGA	56.78%	73
M11	Long-Range Corrected Hybrid Meta GGA	42.8% in the short-range 100% in the long-range	72
TPSSh	Hybrid Meta GGA	10%	73

All geometries were fully optimized and subsequent vibrational frequency calculations were performed at the same level of theory in order to verify that the geometries are real minima on the potential energy surfaces and to yield further thermodynamics data. Different scale factors were used in this work for fundamental vibrational frequencies[74–77], zero point energies [76,77], and enthalpies.[76,77] Unfortunately, scaling factor are not available for all functionals. However, the

factors change only weakly with basis set[78] and therefore, the scaling factors for similar basis set can be used. The scaling factors used in this work are summarized in **Table 3.2**.

Table 3.2 Scaling factors used in this work.

From Ref. 74	
	Fundamentals
M08-HX/aug-cc-pVTZ	0.95
M08-SO/aug-cc-pVTZ	0.959
B3LYP/aug-cc-pVTZ	0.959
PBE0/MG3S	0.95
PBE/def2-TZVP	0.985
BP86/ma-TZVP	0.988
BLYP/6-311G(df,p)	0.987
M06/aug-cc-pVTZ	0.958
M06-L/aug-cc-pVTZ	0.955
M06-2X/aug-cc-pVTZ	0.946
M06-HF/aug-cc-pVTZ	0.936
B1LYP/MG3S	0.955
TPSSh/MG3S	0.963
From Ref. 75	
	Fundamentals
TPSS/aug-cc-pV(T+d)Z	0.9819

[a] Higher than 1000 cm^{-1} [b] Lower than 1000 cm^{-1}

Table 3.2 Scaling factors used in this work.

From Ref. 76

	High Frequency[a]	Low Frequency[b]	Zero Point Vibrational Energy	Enthalpy
BLYP/aug-cc-pVTZ	0.9912	1.0329	1.0181	1.0373
PBE/aug-cc-pVTZ	0.9863	1.023	1.0105	1.0257
BP86/aug-cc-pVTZ	0.9894	1.0277	1.0181	1.0303
BPW91/aug-cc-pVTZ	0.9849	1.0249	1.0136	1.0267
PBE0/aug-cc-pVTZ	0.9568	0.9776	0.9774	0.9735
M06/aug-cc-pVTZ	0.969	0.9862	0.9907	1.0288
M06-2X/aug-cc-pVTZ	0.9574	0.9698	0.9741	1.0511

From Ref. 77

	High Frequency[a]	Low Frequency[b]	Zero Point Vibrational Energy	Enthalpy
B3LYP/aug-cc-pVTZ	0.9676	0.9891	0.9867	0.9867

[a] Higher than 1000 cm^{-1} [b] Lower than 1000 cm^{-1}

3.3. Results and Discussion

3.3.1. Structures

Due to the lack of experimental uranium structural data, high-level CCSD(T) calculations have been performed. **Table 3.3** shows selected CCSD(T) results for uranium halides, which agree with the available experimental data very well. Note that the experimental bond length of UCl_6 was obtained in a crystal environment. Thus further CCSD(T) calculations have been performed as reference data since experimental gas-phase data is scarce.

Table 3.3 Optimized bond lengths (Å) of uranium halides at the CCSD(T) level of theory and experimental data.

	UF_6	UCl_6	UF_4	UCl_4	UCl_3
Symmetry	O_h	O_h	D_{2d}	D_2	C_{3v}
Expt.	1.996[a]	2.460[b]	2.059[c]	2.506[d]	2.549[e]
CCSD(T)	1.995	2.451	2.061	2.506	2.568

[a] Reference 32
[b] Reference 35
[c] References 33 and 34
[d] Reference 36
[e] Reference 37

The calculated structural parameters of various gas-phase uranium compounds obtained at the SC-ECP/aug-cc-pVTZ level used in this work with various functionals and CCSD(T) are presented in **Tables 3.4** and **3.5**.

In a large number of cases, hybrid functionals and hybrid meta GGA tend to give slightly shorter bonds than pure GGA functionals and meta GGA. Hybrid GGAs and hybrid meta GGAs usually have shorter bond lengths compared to CCSD(T). On the other hand, pure GGAs give longer bond lengths. The omission or inclusion of the Hartree-Fock exchange (HFX) in the functional results in bond lengths that are in this order: M06-L (0% HFX) > M06 (27%HFX) > M06-2X (54% HFX) > M06-HF (100% HFX), From **Figures 1** to **6**, it can be seen that all the pure GGA except BLYP tend to give similar results. Interestingly, PBE and PW91 gave almost identical bond lengths as well as BP86 and BPW91. BP86 and BPW91 performed slightly better than PBE and PW91. However, BLYP is the worst amongst the pure GGAs. Hybrid GGAs tend to give better mean signed errors (MSE) but worse mean absolute errors (MAE). B1LYP and X3LYP tend to give very close results. Moreover, they perform better than other hybrid GGAs. M11-L is the worst one in the pure meta GGA group. Another two functionals, M06-L and TPSS, have very

small errors when they are compared against the CCSD(T) data. Generally speaking, hybrid meta GGAs gave better results than other groups. However, M06-HF gave very large errors. M08-HX and M08-SO are designed to improve the M06-2X functional form, with performances similar to those of M06-2X but slightly better.

From **Figures 3.1** and **3.2**, we find that TPSSh is the best functional overall for bond lengths. Note that M11 gives 0.00Å MSE for all bond lengths and is still very good when considering the MAE. As mentioned above, B1LYP an X3LYP are better than other hybrid GGAs. **Figures 3.3-3.4** and **Figures 3.5-3.6** show the MSE and MAE for different types of bonds. For U-X bonds (X = F, Cl), TPSSh is still the best functional both for MSE and MAE. M06 and M08-HX performed very well too. PBE0 and BeckeHandH give excellent MSE, which are almost zero. However, they have larger MAE. Considering both MSE and MAE, B1LYP and X3LYP are still better. For U=O/U-OH bonds, B3LYP is the best functional overall, although it is only slightly better than B1LYP and X3LYP. TPSSh is still the best functional in the hybrid meta GGAs group. M06-L and TPSS are good at predict U=O/U-OH bond lengths too.

Table 3.4 Comparison of the calculated DFT and CCSD(T) bond lengths (Å) of several gas-phase uranium compounds.

		Pure GGA					Hybird GGA							CCSD(T)
		PBE	PW91	BP86	BPW91	BLYP	B3LYP	PBE0	B1LYP	X3LYP	BHLYP	BeckeHandH	BHandH	
Uranium Halides														
UF_6	U-F	2.016	2.016	2.018	2.018	2.035	2.007	1.987	2.004	2.004	1.982	1.976	1.961	1.996 [a]
UF_5	U-Fax	2.028	2.028	2.030	2.030	2.046	2.026	2.010	2.048	2.047	2.012	2.006	1.990	2.021 [a]
	U-Feq	2.031	2.030	2.033	2.033	2.050	2.027	2.009	2.029	2.028	2.010	2.003	1.987	2.019 [a]
UF_4	U-F	2.062	2.061	2.064	2.064	2.081	2.065	2.048	2.066	2.064	2.055	2.047	2.029	2.061 [a]
UCl_6	U-F	2.471	2.471	2.476	2.475	2.505	2.471	2.439	2.470	2.468	2.444	2.435	2.411	2.451 [a]
UCl_5	U-Fax	2.496	2.496	2.464	2.464	2.492	2.514	2.491	2.468	2.465	2.512	2.503	2.418	2.453 [a]
	U-Feq	2.574	2.573	2.491	2.490	2.519	2.590	2.559	2.491	2.489	2.579	2.567	2.440	2.475 [a]
UCl_4	U-F	2.503	2.503	2.508	2.507	2.534	2.516	2.491	2.518	2.515	2.510	2.501	2.476	2.506 [a]
Uranium Oxides, Oxy-halides and Oxy-hydroxides														
UOF_4	U=O	1.791	1.792	1.795	1.793	1.810	1.768	1.746	1.762	1.764	1.725	1.723	1.714	1.764 [a]
	U-Fax	1.991	1.991	1.994	1.993	2.012	1.976	1.954	1.973	1.974	1.942	1.936	1.920	1.962 [a]
	U-Feq	2.058	2.058	2.060	2.060	2.076	2.056	2.039	2.055	2.054	2.042	2.035	2.018	2.050 [a]
UO_2F_2	U=O	1.787	1.787	1.791	1.789	1.806	1.767	1.746	1.762	1.764	1.729	1.727	1.717	1.768 [b]
	U-F	2.069	2.069	2.071	2.072	2.089	2.074	2.058	2.076	2.073	2.068	2.060	2.040	2.075 [b]
$UO_2(OH)_2$	U=O	1.797	1.797	1.801	1.799	1.816	1.777	1.757	1.773	1.775	1.740	1.737	1.728	1.778 [b]
	U-OH	2.111	2.110	2.113	2.114	2.132	2.115	2.097	2.116	2.113	2.107	2.099	2.078	2.116 [b]
UO_3	U=O1	1.855	1.855	1.858	1.857	1.873	1.845	1.827	1.843	1.843	1.822	1.819	1.807	1.852 [b]
	U=O2	1.818	1.818	1.822	1.821	1.842	1.800	1.777	1.796	1.797	1.762	1.758	1.746	1.801 [b]
MSE for all bonds		0.018	0.018	0.014	0.014	0.034	0.014	-0.007	0.006	0.005	-0.006	-0.013	-0.039	
MAE for all bonds		0.020	0.020	0.015	0.014	0.034	0.016	0.021	0.009	0.008	0.026	0.029	0.039	
MSE for U-X bonds		0.021	0.021	0.013	0.012	0.034	0.023	0.001	0.012	0.010	0.008	0.000	-0.034	
MAE for U-X bonds		0.023	0.022	0.013	0.013	0.034	0.023	0.021	0.012	0.011	0.022	0.026	0.034	
MSE for U-O/OH bonds		0.013	0.013	0.017	0.016	0.033	-0.001	-0.022	-0.005	-0.004	-0.032	-0.036	-0.048	
MAE for U-O/OH bonds		0.015	0.015	0.018	0.016	0.033	0.003	0.022	0.005	0.004	0.032	0.036	0.048	

[a] This work [b] Reference 40 and references therein.

Table 3.5 Comparison of the calculated DFT and CCSD(T) bond lengths (Å) of several gas-phase uranium compounds.

		Meta GGA			Hybrid Meta GGA							CCSD(T)
		M06-L	M11-L	TPSS	M06	M06-2X	M06-HF	M08-HX	M08-SO	M11	TPSSh	
UF_6	U-F	2.014	1.964	2.013	1.992	1.981	1.968	1.990	1.993	1.999	2.002	1.996 [a]
UF_5	U-Fax	2.024	2.020	2.027	2.012	2.009	2.016	2.043	2.047	2.051	2.019	2.021 [a]
	U-Feq	2.028	1.986	2.028	2.012	2.010	2.001	2.020	2.023	2.030	2.019	2.019 [a]
UF_4	U-F	2.064	2.015	2.061	2.054	2.052	2.048	2.066	2.073	2.077	2.055	2.061 [a]
UCl_6	U-F	2.477	2.436	2.471	2.453	2.437	2.410	2.438	2.444	2.442	2.458	2.451 [a]
UCl_5	U-Fax	2.462	2.435	2.462	2.450	2.439	2.419	2.442	2.448	2.447	2.453	2.453 [a]
	U-Feq	2.491	2.451	2.487	2.472	2.465	2.447	2.468	2.473	2.474	2.477	2.475 [a]
UCl_4	U-F	2.513	2.490	2.508	2.502	2.498	2.484	2.507	2.516	2.512	2.502	2.506 [a]
UOF_4	U=O	1.764	1.695	1.789	1.735	1.737	1.732	1.741	1.739	1.747	1.770	1.764 [a]
	U-Fax	1.982	1.897	1.987	1.950	1.947	1.939	1.955	1.955	1.967	1.972	1.962 [a]
	U-Feq	2.062	2.022	2.055	2.050	2.040	2.025	2.051	2.058	2.061	2.047	2.050 [a]
UO_2F_2	U=O	1.760	1.696	1.784	1.737	1.739	1.735	1.742	1.743	1.750	1.767	1.768 [b]
	U-F	2.079	2.038	2.067	2.072	2.066	2.054	2.080	2.087	2.089	2.062	2.075 [b]
$UO_2(OH)_2$	U=O	1.771	1.705	1.794	1.748	1.750	1.747	1.754	1.755	1.762	1.777	1.778 [b]
	U-OH	2.122	2.090	2.111	2.107	2.103	2.089	2.113	2.118	2.119	2.105	2.116 [b]
UO_3	U=O1	1.839	1.780	1.855	1.821	1.829	1.832	1.833	1.834	1.835	1.843	1.852 [b]
	U=O2	1.795	1.725	1.816	1.770	1.772	1.769	1.778	1.779	1.787	1.798	1.801 [b]
MSE for all bonds		0.006	-0.041	0.010	-0.012	-0.016	-0.025	-0.007	-0.004	0.000	-0.001	
MAE for all bonds		0.010	0.041	0.011	0.013	0.016	0.025	0.012	0.012	0.012	0.005	
MSE for U-X bonds		0.012	-0.029	0.009	-0.005	-0.011	-0.023	-0.001	0.004	0.007	0.000	
MAE for U-X bonds		0.012	0.029	0.010	0.005	0.011	0.023	0.007	0.009	0.010	0.005	
MSE for U-O/OH bonds		-0.005	-0.065	0.012	-0.027	-0.025	-0.029	-0.020	-0.019	-0.013	-0.003	
MAE for U-O/OH bonds		0.007	0.065	0.013	0.027	0.025	0.029	0.020	0.019	0.014	0.005	

[a] This work [b] Reference 40 and references therein

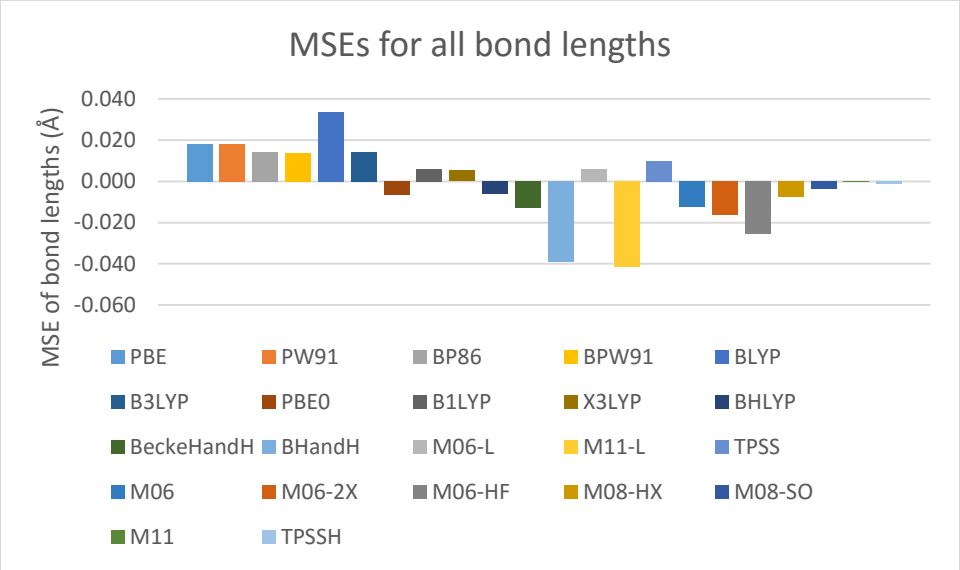

Figure 3.1 The mean signed errors (MSE) of all bond lengths (Å) obtained by comparing to CCSD(T) calculations.

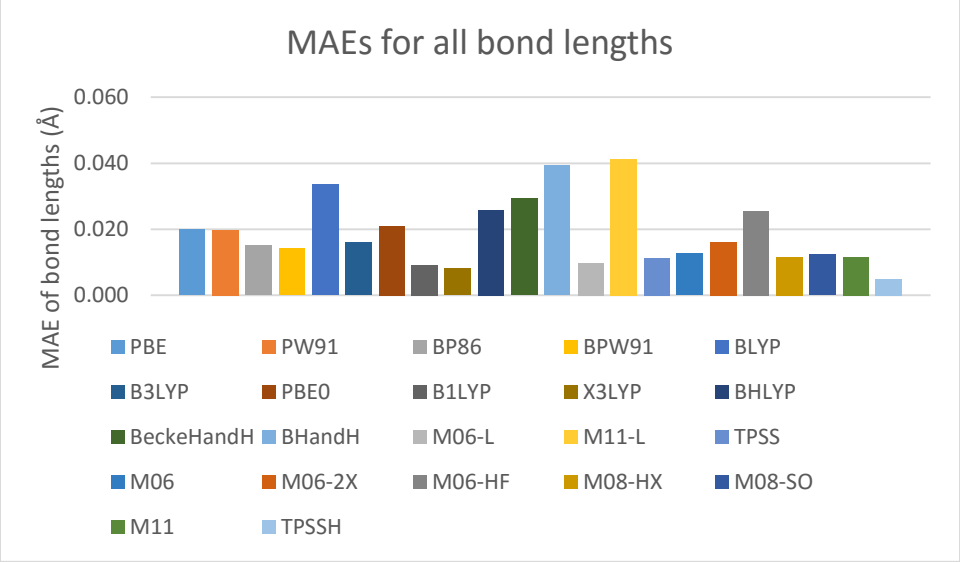

Figure 3.2 The mean absolute errors (MAE) of all bond lengths (Å) obtained by comparing to CCSD(T) calculations.

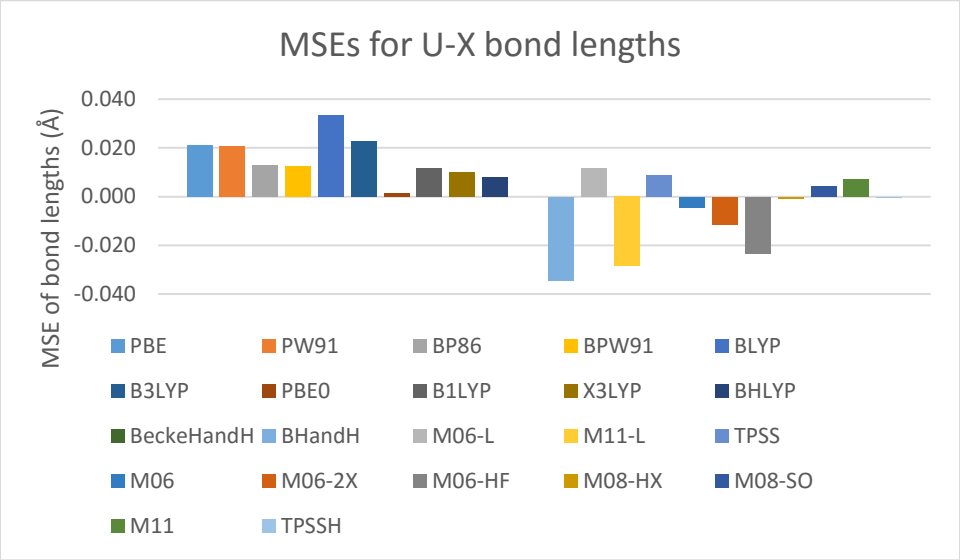

Figure 3.3 The mean signed errors (MSE) of U-X lengths (Å) obtained by comparing to CCSD(T) calculations.

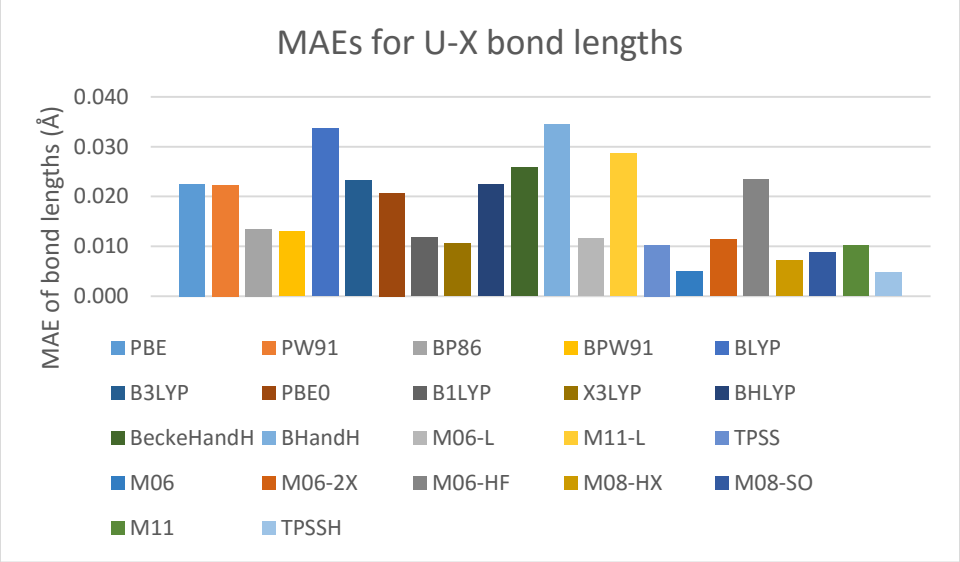

Figure 3.4 The mean absolute errors (MAE) of U-X lengths (Å) obtained by comparing to CCSD(T) calculations.

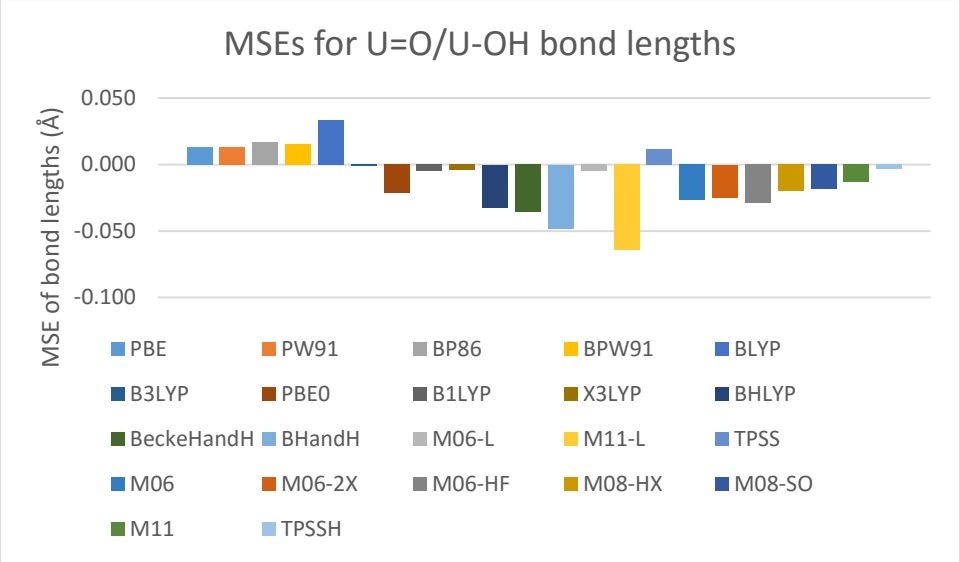

Figure 3.5 The mean errors (MSE) of U=O/U-OH lengths (Å) obtained by comparing to CCSD(T) calculations.

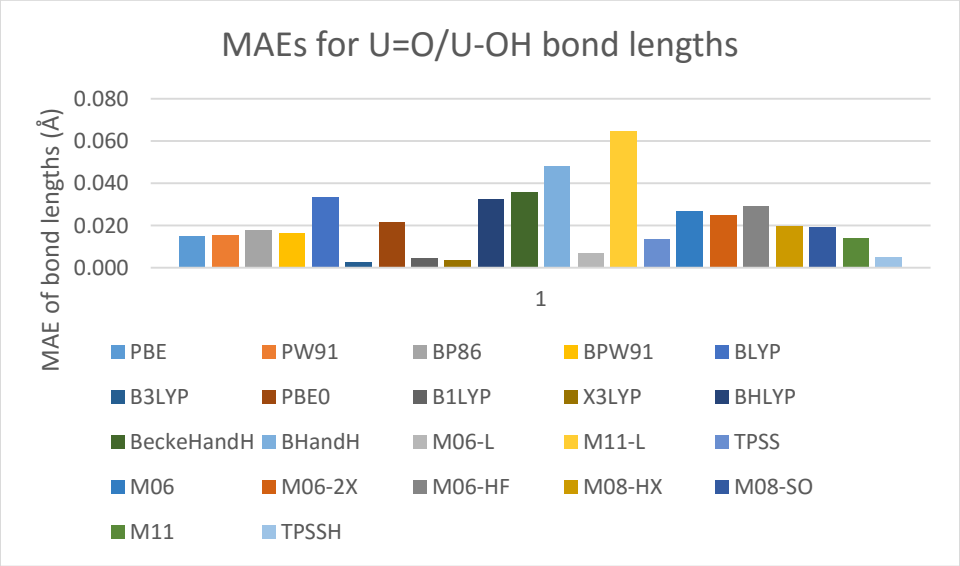

Figure 3.6 The mean absolute errors (MAE) of U=O/U-OH lengths (Å) obtained by comparing to CCSD(T) calculations.

3.3.2. 3.3.2 Vibrational Frequencies.

The calculated vibrational frequencies of several gas-phase uranium complexes are presented in **Tables 3.6** to **3.9**. It is clear that pure GGAs tend to underestimate the vibrational frequencies of these gas-phase uranium complexes. PBE, BP86, PW91 and BPW91 gave similar results due to similar bond lengths. Almost all the vibrational frequencies are lower than 1000 cm^{-1} in **Table 3.6 and 3.7**. From **Table 3.2** we note that Ref. 74 gives scaling factors that are smaller than 1 throughout; however Ref. 76 gives factors for pure GGAs that are larger than 1. The results after applying the scaling factors from Ref. 76 give very good agreement compared with the experimental data. On the other hand, the scaling factors from Ref. 74 make the original data, which already underestimated the vibrational frequencies, become even lower. Hybrid GGAs tend to give higher frequencies than pure GGAs, due to the shorter bond lengths. The frequencies increase following the trend like this: B3LYP < X3LYP ~ B1LYP < PBE0 < BHLYP ~ BeckeHandH ~ BHandH. This is exactly the same trend as the increasing amount of HF exchange in these functionals. B3LYP, B1LYP and X3LYP give good results for uranium halide complexes, which indicates that the best parentage of HF exchange of a functional to describe uranium halide system will be near 20%. Hybrid GGAs overestimate the vibrations of U=O/U-OH bonds. However, unlike pure GGAs, after applying the scaling factors from Ref. 74, B3LYP gives very good results compared to the experimental data. For Meta GGAs, M06-L and TPSS can give reasonable results even without scaling factors. Similar relationship between the amounts of HF exchange and vibrational frequencies as for the hybrid GGAs can be found in the hybrid meta GGAs, i.e. M06, M06-2X and M06-HF. All hybrid meta GGAs can predict the vibrations of uranium halide complexes successful. However, they tend to overestimate the vibrations of U=O/U-OH bonds. Scaling factors can improve the overall results of hybrid meta GGAs, but not

as strongly as for pure GGAs. M06-2X gives very good results after using the scaling factors from Ref. 74 for uranium halide complexes. On the other hand TPSSh performs quite well without scaling factors due to the better bond lengths.

Table 3.6 Comparison of the calculated and experimental vibrational frequencies (cm^{-1}) of several gas-phase uranium compounds.

	Pure GGA					*Expt.*[a]
	PBE	PW91	BP86	BPW91	BLYP	
UF_6	627 592 518 183 173 129 **618 583 510 180 170 127** *641 606 530 187 177 132*	629 594 520 183 170 130	628 593 520 185 174 130 **620 586 514 183 172 128** *645 609 534 190 179 134*	625 592 517 185 177 130 *641 607 530 190 181 133*	611 579 509 185 176 129 **603 571 502 183 174 127** *631 598 526 191 182 133*	667 626 534 200 186 143
UF_5	619 569 552 **610 560 544** *633 582 565*	621 571 553	618 570 553 **611 563 546** *635 586 568*	617 568 551 *632 582 565*	608 556 541 **600 549 534** *628 574 559*	646 584 561
UF_4	537 111 **529 109** *549 114*	539 110	538 111 **532 110** *553 114*	536 112 *549 115*	526 110 **519 109** *543 114*	539 114
UCl_6	344 **339** *347*	344	342 **338** *347*	341 *349*	330 **326** *341*	358
UCl_4	337 62 **332 61** *345 63*	338 61	336 62 **332 61** *345 64*	336 62 *344 64*	326 64 **322 63** *337 66*	337 72
UOF_4	864 **851**[b] *884*[c]	865	859 **849**[b] *883*[c]	861 *882*	832 **821** *859*	835
UO_2F_2	917 **903**[b] *938*[c]	916	909 **898**[b] *934*[c]	914 *937*	883 **872** *912*	941
$UO_2(OH)_2$	3733 899 560 543 **3677 886 552 535** *3682 906 564 547*	3739 899 561 543	3718 895 560 539 **3673 884 553 533**[b] *3679 920 576 554*[c]	3739 896 558 541 *3683 918 572 554*	3699 869 546 529 **3651 858 539 522** *3666 898 564 546*	3670 920 569 547
UO_3	844 841 752 **831 828 741** *863 860 769*	843 841 752	840 836 749 **830 826 740** *863 859 770*	841 838 751 *862 859 770*	817 804 730 **806 794 721** *833 820 744*	853 844 746

[a] Ref. 4, 14, 18, 20 and references therein.

[b] Calculated values in normal font, Ref. 74 scaled values in *italic*, and Ref. 77 scaled in **bold**,

Table 3.7 Comparison of the calculated and experimental vibrational frequencies (cm^{-1}) of several gas-phase uranium compounds.

	Hyir GGA							*Expt.*[a]
	B3LYP	PBE0	B1LYP	X3LYP	BHLYP	BekeHnH	BHnH	
UF6	658 612 531 201 184 143 **631 587 509 193 176 137** *651 605 525 199 182 141*	683 630 541 208 189 148 **649 599 514 198 180 141** *668 616 529 203 185 145*	665 616 531 199 185 141 **635 588 507 190 177 135**	662 614 532 201 184 142	708 645 546 227 204 165	719 653 553 224 205 161	734 671 565 223 198 162	667 626 534 200 186 143
UF5	643 582 564 **617 558 541** *624 564 547*	661 597 576 **628 567 547** *646 584 563*	638 590 572 **609 563 546**	636 589 571	680 608 588	685 612 593	700 630 611	646 584 561
UF4	548 125 **526 120** *542 124*	561 130 **533 124** *548 127*	549 127 **524 121**	550 125	566 141	571 140	589 139	539 114
UCl6	350 **336** *346*	366 **348** *358*	352 **336**	352	369	374	389	358
UCl4	340 76 **326 73** *336 75*	351 75 **333 71** *343 73*	340 78 **325 74**	342 76	350 84	354 83	367 80	337 72
UOF4	917 **879** *907*	959 **911** *938*	932 **890**	923	1012	1019	1037	835
UO2F2	962 **923** *952*	1004 **954** *982*	974 **930**	968	1046	1048	1070	941
UO2OH2	3845 942 570 554 **3687 903 547 531** *3720 932 564 548*	3901 982 586 567 **3706 933 557 539** *3732 960 573 554*	3870 952 573 554 *3696 909 547 529*	3848 947 577 559	4025 1022 593 568	3985 1027 575 565	4012 1041 629 598	3670 920 569 547
UO3	885 880 778 **849 844 746** *875 870 770*	922 920 807 **876 874 767** *901 899 789*	896 889 783 *856 849 748*	890 885 782	961 956 829	966 962 833	988 984 853	853 844 746

[a] Ref. 4, 14, 18, 20 and references therein.

[b] Calculated values in normal font, Ref. 74 scaled values in **bold**, and Ref. 77 scaled in *italic*.

Table 3.8 Comparison of the calculated and experimental vibrational frequencies (cm^{-1}) of several gas-phase uranium compounds.

	Meta GGA			*Expt.*[a]
	M06-L	M11-L	TPSS	
UF_6	630 594 513 185 174 132 **602 567 490 177 166 126**	678 625 503 164 158 110	636 601 524 181 167 128 *624 590 515 178 164 126*	667 626 534 200 186 143
UF_5	627 569 550 **599 543 525**	663 587 584	631 576 557 *620 566 547*	646 584 561
UF_4	538 115 **514 110**	564 136	545 116 *535 114*	539 114
UCl_6	346 **330**	344	347 *341*	358
UCl_4	338 63 **323 60**	330 68	339 62 *333 61*	337 72
UOF_4	899 **859**	998	868 *852*	835
UO_2F_2	958 **915**	1062	921 *904*	941
UO_2OH_2	3879 939 553 537 **3704 897 528 513**	3965 1036 560 537	3746 904 564 552 *3678 888 554 542*	3670 920 569 547
UO_3	870 863 764 **831 824 730**	967 939 824	847 846 753 *832 831 739*	853 844 746

[a] Ref. 4, 14, 18, 20 and references therein.

[b] Calculated values in normal font, Ref. 74 scaled values in **bold**, and Ref. 75 scaled in *italic*.

Table 3.9 Comparison of the calculated and experimental vibrational frequencies (cm^{-1}) of several gas-phase uranium compounds.

	Hyrid Meta GGA							*Expt.*[a]
	M06	M06-2X	M06-HF	M08-HX	M08-SO	M11	TPSSh	
UF_6	670 618 520 200 182 145 **642 592 498 192 174** **139** *661 609 513 197 179* *143*	708 649 552 229 214 169 **670 614 522 217 202** **160** *687 629 535 222 208* *164*	761 684 602 247 218 182 **712 640 563 231 204** **170**	698 641 546 210 190 147 **663 609 519 200 181** **140**	688 627 533 220 196 165 **660 601 511 211 188** **158**	694 631 543 232 210 180	656 615 532 187 175 132 **632 592 512 180 169** **127**	667 626 534 200 186 143
UF_5	658 589 563 **630 564 539** *649 581 555*	681 610 591 **644 577 559** *660 592 573*	636 589 572 **595 551 535**	669 607 579 **636 577 550**	654 597 573 **627 573 550**	652 595 575	643 589 569 **619 567 548**	646 584 561
UF_4	549 120 **526 115** *541 118*	568 138 **537 131** *551 134*	588 134 **550 125**	562 123 **534 117**	555 153 **532 147**	550 131	554 121 **534 117**	539 114
UCl_6	359 **344** *354*	374 **354** *363*	386 **361**	376 **357**	369 **354**	374	356 **343**	358
UCl_4	347 72 **332 69** *342 71*	350 81 **331 77** *339 79*	358 83 **335 78**	342 75 **325 71**	350 90 **336 86**	346 78	344 67 **331 65**	337 72
UOF_4	972 **931** *959*	997 **943** *967*	1040 **973**	986 **937**	994 **953**	987	907 **873**	835
UO_2F_2	1019 **976** *1005*	1034 **978** *1003*	1051 **984**	1026 **984**	1027 **985**	1017	958 **923**	941
UO_2OH_2	3922 994 575 551 **3757 952 551 528** *3800 980 567 543*	3913 1006 590 570 **3702 952 558 539** *3746 976 572 553*	3923 971 610 601 **3672 909 571 563**	3939 996 586 556 **3742 946 557 528**	3901 999 571 545 **3741 958 548 523**	3899 992 589 552	3813 939 578 560 **3672 904 557 539**	3670 920 569 547
UO_3	930 926 812 **891 887 778** *917 913 801*	953 943 827 **902 892 782** *924 915 802*	993 963 840 **929 901 786**	945 931 815 **898 884 774**	946 935 820 **907 897 786**	939 928 819	879 879 776 **846 846 747**	853 844 746

[a] Ref. 4, 14, 18, 20 and references therein.

[b] Calculated values in normal font, Ref. 74 scaled values in **bold**, and Ref. 77 scaled in *italic*.

3.3.3. 3.3.3 Reaction Enthalpies of Uranium (VI) Complexes.

The calculated enthalpies of several gas-phase reactions of uranium complexes are presented in **Table 3.10** and **3.11**. The experimental reaction enthalpies were previously extracted from thermodynamic data by Privalov et al.,[29] Bross et al. [48] and Shamov et al.[15] Bross et al. [41] performed high level CCSD(T) calculations with many corrections including spin-orbit effects. These calculations agree well with the experimental data, which will be good reference data for this section.

The results of the B3LYP, PBE0 and PBE functionals in this work agree well with previously reported works, by our group[4,20] and others.[40,79] All functionals underestimate the enthalpy of reaction 6. For the remaining reactions, all pure GGAs and hybrid GGAs except BHLYP, BeckeHandH, and BHandH overestimate the reaction enthalpies when comparing with the experimental data. M11-L gave a very large error of -43.6 Kcal/mol for reaction 9. Similarly, the error of reaction 5 from M06-HF is 43.0 Kcal/mol. When comparing with the CCSD(T) results, all DFT method overestimate the reaction enthalpies. From Figures 3.7-3.10, we can tell that hybrid GGAs and hybrid meta GGAs are better than pure GGAs and pure meta GGAs. This indicates the important role of HFX in the thermochemistry of U(VI) compounds. Overall, M06 gives the best and excellent agreement with the experimental values and CCSD(T) calculations for both MSE and MAE. TPSSh, however, performed not as well as for predicting bond lengths. The mean absolute errors of enthalpies obtained with the PBE0 and B3LYP functionals are about 3 and 5 times, respectively, larger than the errors obtained with M06. PBE0 is the best functional in the hybrid GGAs group. Although, BHLYP and BeckeHandH have very good MSEs of reaction enthalpies comparing to experimental data. On the other hand, pure GGAs and pure meta GGAs are essentially unsuitable for calculating the gas-phase reactions of U(VI) compounds. The MSE

and MAE of PBE0 (25%HFX), M06 (27%HFX), M06-2X (54% HFX) , BHLYP (50%HFX), BeckeHandH (50%HFX) and M06-HF (100% HFX) indicate that the optimum value of HFX for U(VI) thermochemistry may be around 25-50%.

Table 3.12 shows the results after applied scaling factors. The differences between the results in before and after applied scaling factors for all functionals are minor and can be neglected.

Table 3.10 The calculated and experimental enthalpies (kJ/mol) of several gas-phase reactions of uranium (VI) compounds.

		Pure GGA					Hybird GGA							CCSD(T)	Expt.
		PBE	PW91	BP86	BPW91	BLYP	B3LYP	PBE0	B1LYP	X3LYP	BHLYP	BeckeHandH	BHandH		
1	$UO_3+H_2O \rightarrow UO_2(OH)_2$	-36.1	-37.0	-35.5	-33.3	-34.4	-40.2	-41.8	-41.3	-41.5	-48.7	-50.5	-56.8		-44.0 [b]
2	$UF_6 + 2UO_3 \rightarrow 3UO_2F_2$	-47.5	-47.3	-47.1	-47.8	-46.1	-67.3	-73.0	-72.2	-68.9	-96.5	-94.5	-92.7		-74.3 [b]
3	$UF_6 + 2H_2O \rightarrow 4HF + UO_2F_2$	68.1	70.1	67.3	63.3	68.8	59.8	55.0	57.7	60.6	49.7	51.7	63.5	44.8 [a]	44.7 [b]
4	$UO_2F_2 + 2H_2O \rightarrow 2HF + UO_2(OH)_2$	21.7	21.7	21.7	22.2	23.0	23.3	22.3	23.6	23.2	24.4	22.6	21.3		15.5 [b]
5	$UF_6 + 3H_2O \rightarrow 6HF + UO_3$	126.0	128.8	124.4	118.8	126.2	123.3	119.0	122.7	125.4	122.7	124.8	141.6	108.9 [a]	104.0 [b]
6	$UF_6 + UO_2F_2 \rightarrow 2UOF_4$	4.6	4.5	4.4	4.2	3.1	3.0	4.0	2.6	3.0	0.9	1.6	3.0		7.2 [b]
7	$UF_6 + H_2O \rightarrow 2HF + UOF_4$	36.3	37.3	35.8	33.7	35.9	31.4	29.5	30.2	31.8	25.3	26.7	33.3		25.9 [b]
8	$UOF_4 + UO_3 \rightarrow 2UO_2F_2$	-26.0	-25.9	-25.7	-26.0	-24.6	-35.2	-38.5	-37.4	-36.0	-48.7	-48.1	-47.9		-40.9 [b]
9	$UF_6+SO_3 \rightarrow UO_3+SF_6$	144.9	145.6	147.5	147.5	157.4	145.9	131.0	145.1	144.6	133.9	129.3	117.5	128.9 [a]	126.4 [a]
10	$UF_6+4H_2O \rightarrow UO_2(OH)_2+6HF$	89.9	91.8	88.9	85.5	91.8	83.1	77.3	81.3	83.9	74.0	74.2	84.8	64.6 [a]	61.2 [a]
	MSE for against expt. data	15.6	16.4	15.6	14.2	17.5	10.1	5.9	8.7	10.0	1.1	1.2	4.2		
	MAE for against expt. data	16.2	16.9	16.2	14.8	18.4	11.0	6.6	9.6	10.9	9.4	9.1	14.4		
	MSE for against CCSD(T) data	20.4	22.3	20.2	17.0	24.2	16.2	8.8	14.9	16.8	8.3	8.2	15.0		
	MAE for against CCSD(T) data	20.4	22.3	20.2	17.0	24.2	16.2	8.8	14.9	16.8	8.3	8.2	20.7		

[a] Reference 40 and references therein

[b] Reference 4 and references therein

Table 3.11 The calculated and experimental enthalpies (kJ/mol) of several gas-phase reactions of uranium (VI) compounds.

		Meta GGA			Hybrid Meta GGA							CCSD(T)	Expt.
		M06-L	M11-L	TPSS	M06	M06-2X	M06-HF	M08-HX	M08-SO	M11	TPSSh		
1	$UO_3+H_2O \rightarrow UO_2(OH)_2$	-36.2	-28.2	-36.9	-39.2	-51.2	-66.5	-50.5	-49.5	-47.8	-39.0		-44.0 [b]
2	$UF_6 + 2UO_3 \rightarrow 3UO_2F_2$	-59.1	-71.3	-49.4	-79.2	-90.8	-102.1	-91.6	-97.8	-89.5	-59.5		-74.3 [b]
3	$UF_6 + 2H_2O \rightarrow 4HF + UO_2F_2$	63.0	28.0	70.6	42.5	52.1	63.9	55.0	43.5	54.9	64.8	44.8 [a]	44.7 [b]
4	$UO_2F_2 + 2H_2O \rightarrow 2HF + UO_2(OH)_2$	24.8	21.4	23.1	21.7	20.2	16.5	22.8	21.2	24.4	23.2		15.5 [b]
5	$UF_6 + 3H_2O \rightarrow 6HF + UO_3$	124.1	77.6	130.6	103.4	123.5	146.9	128.4	114.2	127.1	127.0	108.9 [a]	104.0 [b]
6	$UF_6 + UO_2F_2 \rightarrow 2UOF_4$	4.5	2.3	4.0	3.9	4.2	3.0	2.6	0.4	2.8	3.9		7.2 [b]
7	$UF_6 + H_2O \rightarrow 2HF + UOF_4$	33.8	15.1	37.3	23.2	28.1	33.5	28.8	22.0	28.9	34.4		25.9 [b]
8	$UOF_4 + UO_3 \rightarrow 2UO_2F_2$	-31.8	-36.8	-26.7	-41.5	-47.5	-52.5	-47.1	-49.1	-46.2	-31.7		-40.9 [b]
9	$UF_6+SO_3 \rightarrow UO_3+SF_6$	144.9	82.8	146.3	125.5	131.3	137.1	135.3	129.3	138.9	140.5	128.9 [a]	126.4 [a]
10	$UF_6+4H_2O \rightarrow UO_2(OH)_2+6HF$	87.9	49.4	93.7	64.2	72.3	80.5	77.9	64.7	79.2	88.0	64.6 [a]	61.2 [a]
	MSE for against experimental data	13.0	-8.5	16.7	-0.1	1.6	3.5	3.6	-2.7	4.7	12.6		
	MAE for against experimental data	13.6	14.3	17.3	2.9	8.3	16.7	10.5	7.1	10.4	13.2		
	MSE for against CCSD(T) results	18.2	-27.4	23.5	-2.9	8.0	20.3	12.3	1.1	13.2	18.3		
	MAE for against CCSD(T) results	18.2	27.4	23.5	2.9	8.0	20.3	12.3	1.8	13.2	18.3		

[a] Reference 40 and references therein

[b] Reference 4 and references therein

Table 3.12 The experimental and calculated enthalpies after applied scaling factors [a] (kJ/mol) of several gas-phase reactions of uranium (VI) compounds.

		Pure GGA				Hybird GGA		Hybrid Meta GGA		CCSD(T)	Expt.
		PBE	BP86	BPW91	BLYP	B3LYP	PBE0	M06	M06-2X		
						Uranium Halides					
1	$UO_3+H_2O \rightarrow UO_2(OH)_2$	-36.1	-35.5	-33.3	-34.5	-40.3	-41.8	-39.2	-51.3		-44.0 [c]
2	$UF_6 + 2UO_3 \rightarrow 3UO_2F_2$	-47.5	-47.0	-47.8	-46.1	-67.4	-73.1	-78.8	-90.8		-74.3 [c]
3	$UF_6 + 2H_2O \rightarrow 4HF + UO_2F_2$	68.1	67.2	63.3	68.7	59.8	55.1	42.7	52.2	44.8 [b]	44.7 [c]
4	$UO_2F_2 + 2H_2O \rightarrow 2HF + UO_2(OH)_2$	21.7	21.6	22.2	22.9	23.3	22.3	21.6	20.2		15.5 [c]
5	$UF_6 + 3H_2O \rightarrow 6HF + UO_3$	125.9	124.3	118.8	126.1	123.4	119.1	103.5	123.7	108.9 [b]	104.0 [c]
6	$UF_6 + UO_2F_2 \rightarrow 2UOF_4$	4.6	4.4	4.2	3.2	2.9	3.9	3.7	4.4		7.2 [c]
7	$UF_6 + H_2O \rightarrow 2HF + UOF_4$	36.4	35.8	33.7	35.9	31.4	29.5	23.2	28.3		25.9 [c]
8	$UOF_4 + UO_3 \rightarrow 2UO_2F_2$	-26.0	-25.7	-26.0	-24.6	-35.1	-38.5	-41.3	-47.6		-40.9 [c]
9	$UF_6+SO_3 \rightarrow UO_3+SF_6$	144.9	147.5	147.5	157.4	145.8	130.9	125.4	131.2	128.9 [b]	126.4 [b]
10	$UF_6+4H_2O \rightarrow UO_2(OH)_2+6HF$	89.8	88.8	85.4	91.6	83.1	77.4	64.3	72.4	64.6 [b]	61.2 [b]
	MSE for against experimental data	15.6	15.6	14.2	17.5	10.1	5.9	0.0	1.7		
	MUE for against experimental data	16.1	16.1	14.8	18.3	11.0	6.6	2.8	8.4		
	MSE for against CCSD(T) results	20.4	20.2	16.9	24.2	16.2	8.8	-2.8	8.1		
	MUE for against CCSD(T) results	20.4	20.2	16.9	24.2	16.2	8.8	2.8	8.1		

[a] Reference 76, 77 and references therein

[b] Reference 40 and references therein

[c] Reference 4 and references therein

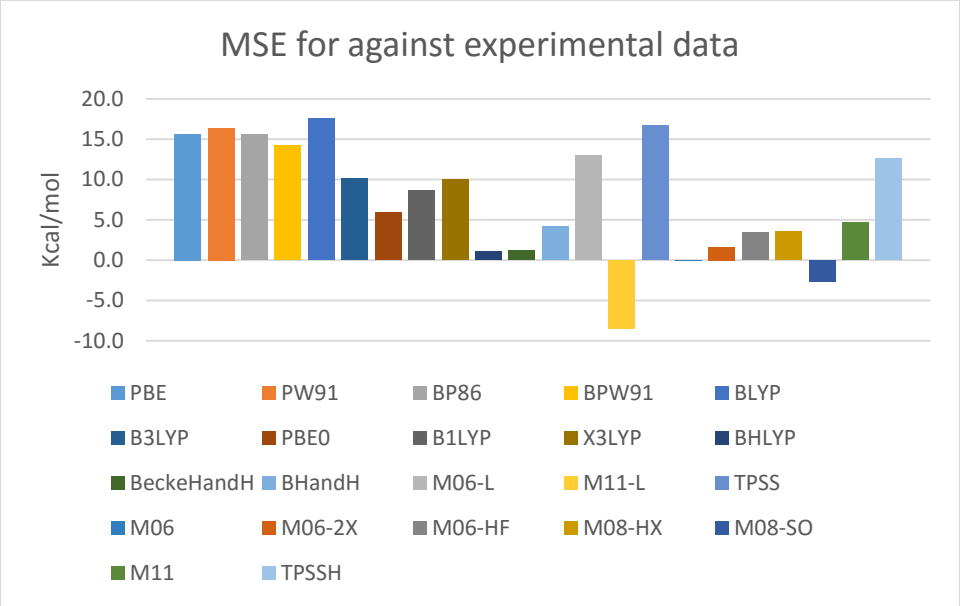

Figure 3.7 The mean signed errors (MSE) of reaction enthalpies obtained by comparing to experimental data.

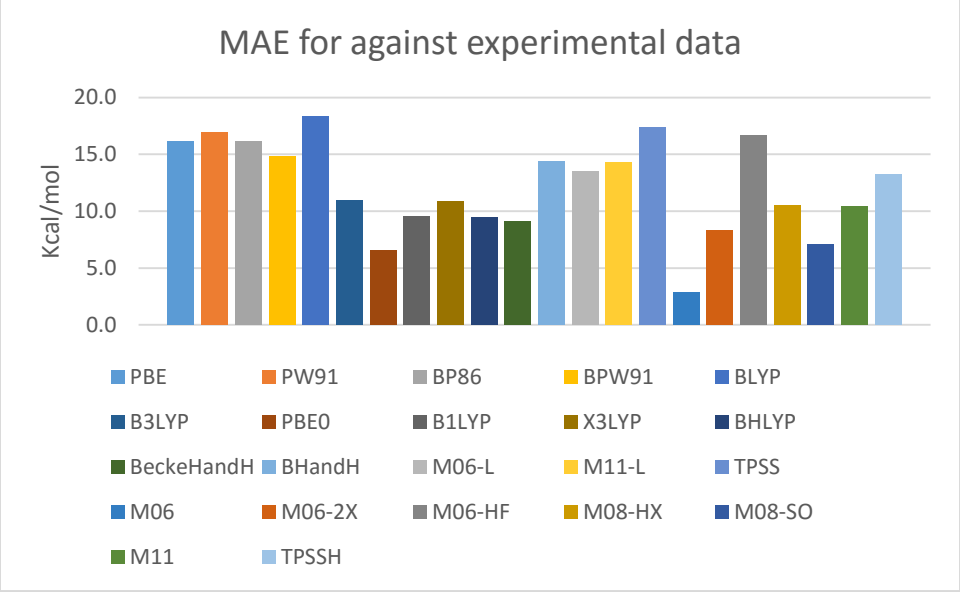

Figure 3.8 The mean absolute errors (MAE) of reaction enthalpies obtained by comparing to experimental data.

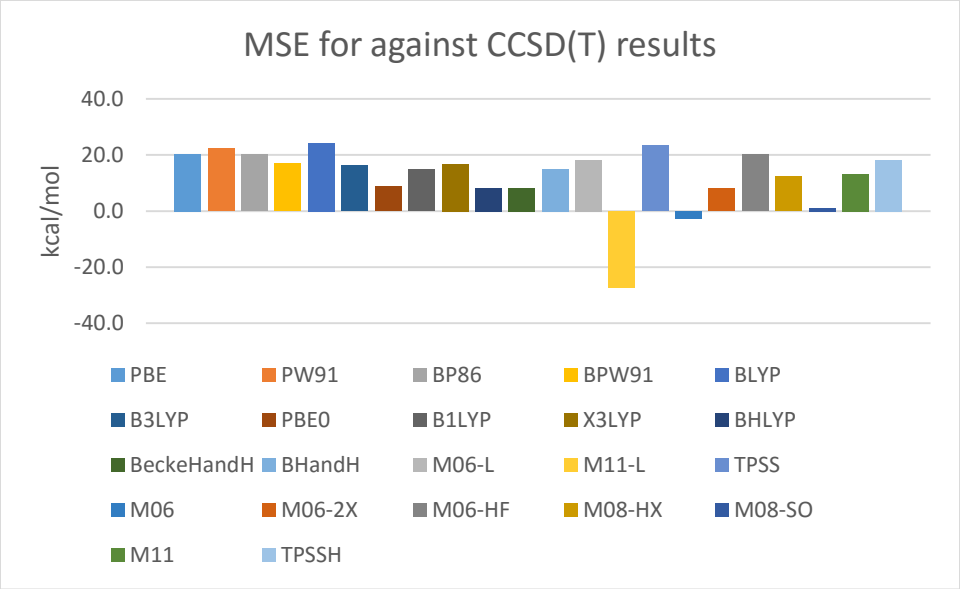

Figure 3.9 The mean signed errors (MSE) of reaction enthalpies obtained by comparing to CCSD(T) data.

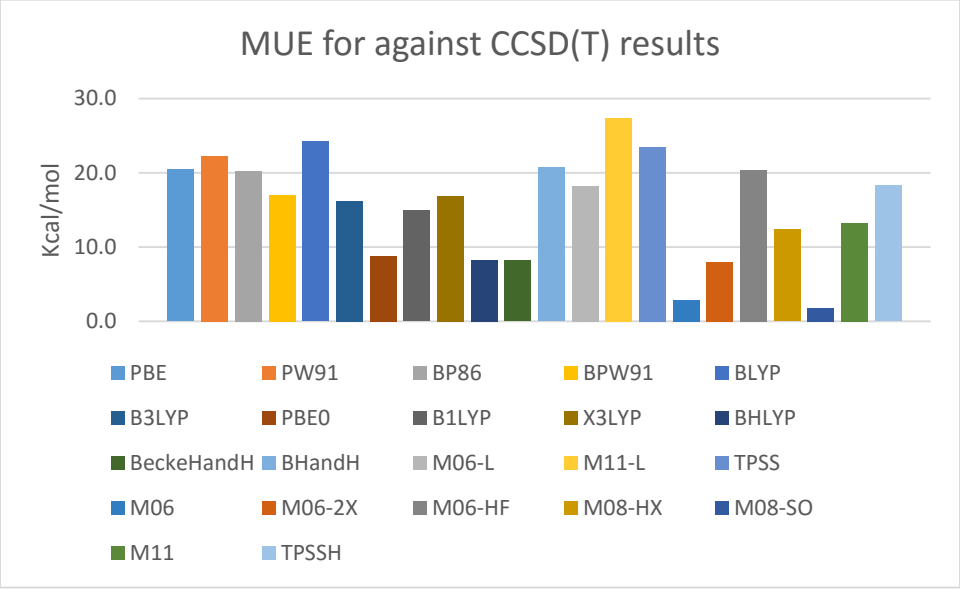

Figure 3.10 The mean absolute errors (MAE) of reaction enthalpies obtained by comparing to CCSD(T) data.

3.4. Conclusions

Structures, vibrations and reaction enthalpies of various gas-phase reactions of small uranium compounds were systemically investigate using 22 different density functionals combined with scalar relativistic small-core pseudopotentials. Some relatively new functionals are compared to the well-used and popular B3LYP, PBE0 and PBE functionals. CCSD(T) data have been used as reference data since experimental gas-phase data is scarce. We found that CCSD(T) calculations of bond lengths and energetics of these gas-phase uranium compounds are quite consistently good compared to the available experimental data. These data that can be useful in future studies in theoretical actinide science such as by providing benchmark data.

The TPSSh functional provides the best agreement with CCSD(T) values for the bond lengths. The MSE and MAE of TPSSh are only -0.001 and 0.005Å. M06-L is also a good choice for balancing accuracy and efficiency. B1LYP and XLYP are the best hybrid GGAs in this study for predicting bond lengths. Pure GGAs generally overestimate the bond lengths compared with the CCSDT(T) data.

Most functionals in this work can successfully predict vibrations of uranium halide complexes. However U=O/U-OH bonds are problematic. Pure GGAs and meta GGAs performing better than Hybrid GGAs and Hybrid meta GGAs. Different scaling factors were tested. The results indicate that applying these scaling factors on actinide systems should be done very carefully since, as mentioned before, these factors were usually fit for light elements. Pure GGAs with their corresponding scaling factors are recommended due to efficiency and accuracy.

For reaction enthalpies of U(VI) compounds, M06 gave excellent agreement with experimental and CCSD(T) data. M06 is superior to other DFT functionals in this study, as it gave

smallest MSE and MAE for -0.1 and 2.9 Kcal/mol, respectively. PBE0 (MSE and MAE of 5.9 and 6.6 Kcal/mol) and M06-2X (MSE and MAE of 1.6 and 8.3 Kcal/mol) also gave good results. On the other hand, TPSSh performed not as good as for predicting bond lengths. Scaling factors of ZPVE and enthalpy did not improve the energetics results at all. In fact, there is almost no difference between the results with and without using scaling factors.

Overall there is not a universal DFT functional for every property in this chapter. Thus, using particular functionals for special purposes of calculations in order to yield better results is recommended. The results and conclusions in this chapter can give suggestions for better choosing DFT functionals in the theoretical actinide field.

3.5. References

[1] Koch, W.; Holthausen, M. C. A Chemist's Guide to Density Functional Theory; Wiley Verlag Chemie: New York, 2000.
[2] Küchle, W.; Dolg, M.; Stoll, H.; Preuss, H. *J. Chem. Phys.* **1994**, *100*, 7535.
[3] Shamov, G. A.; Schreckenbach, G., *J. Phys. Chem. A* **2005,** *109,* 10961. Correction: Shamov, G. A.; Schreckenbach, G. *J. Phys. Chem. A* **2006**, *110*, 12072.
[4] Shamov, G. A.; Schreckenbach, G.; Vo, T. N., *Chem-Eur. J.* **2007,** *13,* 4932.
[5] van Lenthe, E.; Baerends, E. J.; Snijders, J. G., *J. Chem. Phys.* **1993**, *99*, 4597.
[6] Laikov, D. N.; Ustynyuk, Y. A., *Russ. Chem. Bull.* **2005**, 54, 820.
[7] Hay, P. J.; Martin, R. L., *J. Chem. Phys*. **1998**, *109*, 3875.
[8] Hay, P. J.; Martin, R. L.; Schreckenbach, G. *J. Phys. Chem. A* **2000**, *104*, 6259.
[9] Shamov, G. A.; Schreckenbach, G.; Martin, R. L.; Hay, P. J. *Inorg. Chem*. **2008**, 47, 1465.
[10] Clavaguera-Sarrio, C.; Vallet, V.; Maynau, D.; Marsden, C. J., *J. Chem. Phys.* **2004,** *121,* 5312.
[11] Cohen, A. J.; Mori-Sánchez, P.; Yang, W., *Chem. Rev.* **2012**, *112*, 289.
[12] Cramer, C. J.; Truhlar, D. G., *Phys. Chem. Chem. Phys.* **2009**, *11*, 10757.
[13] Grimme, S.; Antony, J.; Ehrlich, S.; Krieg, H., *J. Chem. Phys.* **2010**, *132*.
[14] Batista, E. R.; Martin, R. L.; Hay, P. J., *J. Chem. Phys.* **2004,** *121,* 11104.
[15] Cao, Z. J.; Balasubramanian, K., *J. Chem. Phys.* **2005,** *123*, 12.
[16] Chaudhuri, D.; Balasubramanian, K., *Chem. Phys. Lett.* **2004,** *399,* 67.
[17] Garcia-Hernandez, M.; Lauterbach, C.; Krüger, S.; Matveev, A.; Rösch, N., *J. Comput. Chem.* **2002,** *23,* 834.
[18] Han, Y. K., *J. Comput. Chem.* **2001,** *22,* 2010.
[19] Ismail, N.; Heully, J. L.; Saue, T.; Daudey, J. P.; Marsden, C. J., *Chem. Phys. Lett.* **1999**, *300*, 296.
[20] Odoh, S. O.; Schreckenbach, G., *J. Phys. Chem. A* **2010,** *114,* 1957.
[21] Peralta, J. E.; Batista, E. R.; Scuseria, G. E.; Martin, R. L., *J. Chem. Theory Comput.* **2005,** *1,* 612.
[22] Prestianni, A.; Joubert, L.; Chagnes, A.; Cote, G.; Ohnet, M. N.; Rabbe, C.; Charbonnel, M. C.; Adamo, C., *J. Phys. Chem. A* **2010,** *114,* 10878.
[23] Schreckenbach, G.; Hay, P. J.; Martin, R. L., *J. Comput. Chem.* **1999,** *20,* 70.
[24] Schreckenbach, G.; Shamov, G. A., *Acc. Chem. Res.* **2010,** *43,* 19.

[25] Odoh, S. O.; Schreckenbach, G., *J. Phys. Chem. A* **2011,** *115,* 14110.
[26] Vallet, V.; Macak, P.; Wahlgren, U.; Grenthe, I., *Theor. Chem. Acc.* **2006,** *115,* 145.
[27] Rötzinger, F. P., *J. Phys. Chem. B* **2005,** *109,* 1510.
[28] Austin, J. P.; Burton, N. A.; Hillier, I. H.; Sundararajan, M.; Vincent, M. A., *Phys. Chem. Chem. Phys.* **2009,** *11,* 1143.
[29] Bühl, M.; Schreckenbach, G., *Inorg. Chem.* **2010,** *49,* 3821.
[30] Doudou, S.; Arumugam, K.; Vaughan, D. J.; Livens, F. R.; Burton, N. A., *Phys. Chem. Chem. Phys.* **2011,** *13,* 11402.
[31] Oncak, M.; Schroder, D.; Slavicek, P., *J. Comput. Chem.* **2010,** *31,* 2294.
[32] Seip, H. M. *Acta. Chem. Scand.* **1965**, *19*, 1955.
[33] Kimura, M.; Schomaker, V.; Smith, D.W.; Weinstock, B., *J. Chem. Phys.* **1967**, *48*, 4001.
[34] Zachariasen, W. H.; *Acta Crystallogr*. **1948**, *1*, 285.
[35] Brown, D., *Halides of the Transition Elements* Wiley, New York, **1968.**
[36] Haaland, A.; Martinsen, K.-G.; Swang, O.; Volden, H. V.; Booij, A. S.; Konings, R. J. M., *J. Chem. Soc. Dalton Trans.* **1995**, *2*, 185.
[37] Bazhanov,V. I.; Ezhov, Y. S.; Komarov, S. A., *J. Struct. Chem.* **1990**, *31*, 986.
[38] Schreckenbach, G.; Shamov, G., *Acc. Chem. Res.*, **2010**, *43*, 19.
[39] Cramer, C. J.; *Essentials of Computational Chemistry* John Wiley & Sons Ltd, (**2004**)
[40] Privalov, T.; Schimmelpfennig, B.; Wahlgren, U.; Grenthe, I., *J. Phys. Chem. A* **2002,** *106,* 11277.
[41] Bross, D. H.; Peterson, K. A., *J. Chem. Phys.* **2014**, *141*, 244308.
[42] Valiev, V.; Bylaska, E. J.; Govind, N.; Kowalski, K.; Straatsma, T. P.; van Dam, H. J. J.; Wang, D.; Nieplocha, J.; Apra, E.; Windus, T. L.; de Jong, W. A., *Comput. Phys. Commun.* **2010,** *181,* 1477.
[43] Küchle, W.; Dolg, M.; Stoll, H.; Preuss, H., *Mol. Phys.* **1991,** *74,* 1245.
[44] Werner, H.-J.; Knowles, P. J.; Knizia, G.; Manby, F. R.; Schütz, M., WIREs *Comput. Mol. Sci.* **2012**, *2*, 242.
[45] MOLPRO, version 2012.1, a package of ab initio programs, H.-J. Werner, P. J. Knowles, G. Knizia, F. R. Manby, M. Schütz, and others, see http://www.molpro.net.
[46] Perdew, J. P.; Burke, K.; Ernzerhof, M. *Phys. Rev. Lett.* **1996**, *77*, 3865.
[47] Perdew, J. P.; Burke, K.; Ernzerhof, M. *Phys. Rev. Lett*. **1997**, *78*, 1396.
[48] Perdew, J. P. in Electronic Structure of Solids '91, Ed. P. Ziesche and H. Eschrig (Akademie Verlag, Berlin, **1991**) 11.
[49] Perdew, J. P.; Chevary, J. A.; Vosko, S. H.; Jackson, K. A.; Pederson, M. R.; Singh, D. J.;Fiolhais, C., *Phys. Rev. B*, **1992**, 46, 6671.
[50] Perdew, J. P.; Wang, Y., *Phys. Rev. B*, **1992**, *45*, 13244.
[51] Perdew, J. P.; Burke, K.; Wang, Y., *Phys. Rev. B*, **1996**, *54*, 16533.
[52] Burke, K.; Perdew, J. P.; Wang, Y., in Electronic Density Functional Theory: Recent Progress and New Directions, Ed. J. F. Dobson, G. Vignale, and M. P. Das (Plenum, **1998**).
[53] Becke, A. D. *Phys. Rev. A* **1988**, *38*, 3098.
[54] Perdew, J. P. *Phys. Rev. B* **1986**, *33*, 8822.
[55] Perdew, J. P. *Phys. Rev. B* **1986**, *34*, 7406.
[56] Ceperley, D. M.; Alder, B. *J Phys. Rev. Lett.* **1980**, *45*, 566.
[57] Becke, A. D. *Phys. Rev. A* **1988**, *38*, 3098.
[58] Lee, C.; Yang, W.; Parr, R. G. *Phys. Rev. B* **1988**, *37*, 785.
[59] Becke, A. D. *J. Chem. Phys.* **1993**, *98*, 1372.
[60] Lee, C.; Yang, W.; Parr, R. G. *Phys. Rev. B* **1988**, *37*, 785.
[61] Adamo, C.; Barone, V. *J. Chem. Phys.* **1999**, *110*, 6158.
[62] Becke, A. D. *J. Chem. Phys.*, **1996**, *104*, 1040.
[63] Xu, X.; Goddard III, W. A., *Proc. Natl. Acad. Sci. USA*, **2004**, 101, 2673.
[64] Becke, A. D., *J. Chem. Phys.*, **1993**, *98*, 1372.
[65] Zhao, Y.; Truhlar, D. G. *J. Chem. Phys.* **2006**, *125*, 194101.
[66] Peverati, R.; Truhlar, D. G. *J. Phys. Chem. Lett.* **2012**, *3*, 117.
[67] Tao, J. M.; Perdew, J. P.; Staroverov, V. N.; Scuseria, G. E., *Phys. Rev. Lett.*, **2003**, *91*, 146401.
[68] Zhao, Y.; Truhlar, D. G. *Theor. Chem. Acc.* **2008**, *120*, 215.
[69] Zhao, Y. Truhlar, D. G. *J. Phys. Chem.*, **2006**, *110*, 5121.
[70] Zhao, Y. Truhlar, D. G., *J. Phys. Chem. A*, **2006**, *110*, 13126.
[71] Zhao ,Y. Truhlar, D.G., *J. Chem. Theory Comput.*, **2008**, *4*, 1849.

[72] Peverati, R.; Truhlar, D. G., *J. Phys. Chem. Lett.,* **2011**, *2*, 2810.
[73] Tao, J. M.; Perdew J. P.; Staroverov V. N.; Scuseria G. E. *Phys. Rev. Lett.* **2003**, *91*, 146401.
[74] http://comp.chem.umn.edu/freqscale/version3b2.htm access by May 10th, 2016.
[75] Kesharwani, M. K.; Brauer, B.; Martin, Jan M. L., *J. Phys. Chem. A* **2015**, *119*, 1701.
[76] Sinha, P.; Boesch, S. E.; Gu, C.; Wheeler, R. A.; Wilson, A. K., J. Phys. Chem. A 2004, 108, 9213-9217
[77] Laury, M. L.; Boesch, S. E.; Haken, I.; Sinha, P.; Wheeler, R. A.; Wilson, A. K., *J. Comput. Chem.* **2011**, *32*, 2339.
[78] Irikura, K. K.; Johnson III, R. D.; Kacker, R. N., *J. Phys. Chem. A.*, **2005**, 109, 8430.
[79] Schimmelpfennig, B.; Privalov, T.; Wahlgren, U.; Grenthe, I., *J. Phys. Chem. A* **2003**, *107*, 9705.

Chapter 4: Summary and Future Studies

4.1 Summary

The work presented in this thesis has provided systematic benchmarking studies in order to evaluate the performance of modern DFT on actinide systems. Several aspects of using DFT for studying actinide complexes have been investigated: DFT studies of U(VI) acetate systems for structures, vibrations, reaction energies, NMR as well as UV spectra in both gas phase and solution (Chapter 2); thermodynamics studies of small gas phase uranium compounds using modern DFT for structures, vibrations and reaction energies (Chapter 3).

Chapter 2 is a part of the actinide spectroscopy RRT, which aims at comprehensive analysis of the actinide complex system U(VI) acetate in aqueous solution independently investigated by different chemical methods. In this study, several experimental data, such as IR, XAS, NMR etc., from different experimental clusters are available as reference for quantum chemical calculations. The goal of the theory cluster within the RRT is the evaluation and comparison of the performance of DFT using different quantum chemistry programs with identical DFT functionals, basis sets, solution models, and relativistic approaches. The task of our group was calculating the properties of specific U(VI) acetate complexes using the ADF program with GGA, Hybrid GGA, Meta GGA and Hybrid Meta GGA. There are five complexes given in Figure 2.2 that were studied in the theory cluster. However, finally, only the data of RR1 and RR5 have been collected for the RRT due to the fact that they are chemically accessible in pure form in experiment. However, we still present the rest of our calculations for further investigating the performance of different DFT functionals. This study shows that the calculations using an identical DFT functional, basis set, relativistic approach and solution model

but different quantum chemistry programs yield very small deviations. The deviations between different methods and codes become larger after applying solvation models. This can be explained by different minima yielded from different solvation models and different optimization schemes in different codes. On contrast, the reproducibility of the results of RR5 is high due to its lower flexibility. Applying solvent models can give better bond lengths for most functionals even though the gas phase calculations already include the first solvation sphere. For excitation energies, including spin-orbit effects using spin-orbit ZORA gives better result when comparing with the experimental data. However, for NMR calculations, results of the spin-orbit ZORA are slightly worse than scalar ZORA. This may be due to error cancelations. When it comes to the performances of 10 different DFT functionals in this chapter, it is hard to give a clear answer for the best method in this study due to the small sample size and too many variables such as different codes and basis sets etc. A few qualitative conclusions can still be made: Hybrid and Meta GGAs tend to give shorter bond lengths, lower reaction energies and higher excitation energies. On contrast, pure GGAs tend to give longer bond lengths, higher reaction energies and lower excitation energies. There is some evidence which shows that pure GGAs tend to give better bond lengths and vibrational frequencies. PBE and BP86 predict very close results. On the other hand, B3LYP, M06L, and TPSSh are the best for predicting bond lengths and vibrational frequencies in each group.

In Chapter 3, we further investigated the performance of different DFT functionals. Thus 22 different functionals have been chosen. In order to prevent the problems we met in Chapter 2, the only variable here is the choice of DFT functional. For the relativistic approach, the small-core ECP method (SC-ECP)[1] has been used in this chapter, which can give very close results[2,3] compared to the zeroth order regular approximation (ZORA)[4] and all-electron scalar methods[5].

On the other hand, a lager data set has been chosen. Several gas phase uranium halides as well as uranium oxides, oxy-halides and oxy-hydroxides are selected as samples because experimental vibrational frequencies data[6–9] as well as gas phase reactions enthalpies[,10,11] are available. Due to the lack of experimental data for bond lengths[12–17], high level *ab initio* CCSD(T) calculations have been performed as reference. For structures, the TPSSh functional gives the best results against CCSD(T) calculations. M06L, as in Chapter 2, is very good for predicting bond lengths. B1LYP and X3LYP are also good choices for calculating bond lengths. On the other hand, some functionals are good for specified bond types, for example, B3LYP and M06 performs well for U=O bonds and U-X bonds, respectively. Pure GGAs generally overestimate the bond lengths compared with the CCSDT(T) data. PBE and BP86 as well as PW91 and BPW91 tend to give very similar results. Most functionals in this chapter can successfully predict vibrations of uranium halide complexes. However, pure GGAs and meta GGAs show some advantage over Hybrid GGAs and Hybrid meta GGAs for U=O/U-OH bonds. This confirmed the conclusion in Chapter 1. Different frequency scaling factors were examined. However, the results can be worse after applying these scaling factors on actinide systems. Pure GGAs with their corresponding scaling factors from Laury et al.[18] are recommended due to efficiency and accuracy. For reaction enthalpies of U(VI) compounds, M06 gave excellent agreement with experimental and CCSD(T) data which is superior to other DFT functionals in this study, as it gave the smallest MSE and MAE of -0.1 and 2.9 Kcal/mol, respectively. PBE0 (MSE and MAE of 5.9 and 6.6 Kcal/mol) and M06-2X (MSE and MAE of 1.6 and 8.3 Kcal/mol) also gave good results. On the other hand, TPSSh performed not as good as for predicting bond lengths. The poor performances of scaling factors for reaction energies show that those factors that were fitted for light elements do not work well for actinide complexes. Special scaling factors for actinide

complexes reactions are needed. However, due to the excellent performance of M06, we can obtain very accurate result without applying scaling factors.

Overall, the work in this thesis gives an insight into the performance of DFT in the actinide area. Although DFT is a powerful tool for predicting the properties of actinide complexes, there is not a universal DFT functional for all purposes. Because when approximate DFT functionals have been created, different approaches have been applied and different aspects of data have been used for fitting any empirical parameters. For example, M06 is very good for predicting reaction energies. Thus, we recommend to use different functionals for special purposes of calculations. The results and conclusions in this thesis can give suggestions for better choosing DFT functionals in the theoretical actinide field.

4.2 Future studies of actinide complexes specific to this thesis

The following are possible directions for continuing the computational work on actinide complexes studied in this thesis:

1. The systems in this thesis are relatively small actinide complexes. It is worth to further examine the conclusions made in this work for a larger size of real experimentally relevant actinide systems. The performances of pure GGAs and pure meta GGAs will be of interest due to their relative good accuracy and efficiency. The latter is particularly important for larger system for which hybrid GGAs and hybrid meta GGAs are too expensive.

2. The conclusions for the spin-orbit and multiplicity effects in actinide systems are not completely clear. Further investigations will be interesting because they are important for many properties and growing numbers of studies of low oxidation state or open shell actinide

complexes. Such studies could include comparison of scalar ECPs and spin-orbit ECPs as well as all-electron methods in different areas such as UV, NMR and anion photoelectron spectroscopy. The performance of TDDFT will also be interesting here.

3. Double hybrid GGAs and double hybrid meta GGAs were not included in this work. Because they are more expensive and potential double counting problems, whether can they give better performance especially for reaction energies will be interesting.

4. The results of solvent models are not completely clear. It is necessary to reexamine them systemically. It is also worth to test the relative new SM12 model for actinide systems.

4.3 References

[1] Küchle, W.; Dolg, M.; Stoll, H.; Preuss, H. *J. Chem. Phys.* **1994**, *100*, 7535.
[2] Shamov, G. A.; Schreckenbach, G., *J. Phys. Chem. A* **2005,** *109,* 10961. Correction: Shamov, G. A.; Schreckenbach, G. *J. Phys. Chem. A* **2006**, *110*, 12072.
[3] Shamov, G. A.; Schreckenbach, G.; Vo, T. N., *Chem-Eur. J.* **2007,** *13,* 4932.
[4] van Lenthe, E.; Baerends, E. J.; Snijders, J. G., *J. Chem. Phys.* **1993**, *99*, 4597.
[5] Laikov, D. N.; Ustynyuk, Y. A., *Russ. Chem. Bull.* **2005**, 54, 820.
[6] Shamov, G. A.; Schreckenbach, G.; Vo, T. N., *Chem-Eur. J.* **2007,** *13,* 4932.
[7] Batista, E. R.; Martin, R. L.; Hay, P. J., *J. Chem. Phys.* **2004,** *121,* 11104.
[8] Han, Y. K., *J. Comput. Chem.* **2001,** *22,* 2010.
[9] Odoh, S. O.; Schreckenbach, G., *J. Phys. Chem. A* **2010,** *114,* 1957.
[10] Privalov, T.; Schimmelpfennig, B.; Wahlgren, U.; Grenthe, I., *J. Phys. Chem. A* **2002,** *106,* 11277.
[11] Bross, D. H.; Peterson, K. A., *J. Chem. Phys.* **2014**, *141*, 244308.
[12] Seip, H. M. *Acta. Chem. Scand.* **1965**, *19*, 1955.
[13] Kimura, M.; Schomaker, V.; Smith, D.W.; Weinstock, B., *J. Chem. Phys.* **1967**, *48*, 4001.
[14] Zachariasen, W. H.; *Acta Crystallogr*. **1948**, *1*, 285.
[15] Brown, D., *Halides of the Transition Elements* Wiley, New York, **1968.**
[16] Haaland, A.; Martinsen, K.-G.; Swang, O.; Volden, H. V.; Booij, A. S.; Konings, R. J. M., *J. Chem. Soc. Dalton Trans.* **1995**, *2*, 185.
[17] Bazhanov,V. I.; Ezhov, Y. S.; Komarov, S. A., *J. Struct. Chem.* **1990**, *31*, 986.
[18] Laury, M. L.; Boesch, S. E.; Haken, I.; Sinha, P.; Wheeler, R. A.; Wilson, A. K., *J. Comput. Chem.* **2011**, *32*, 2339.